Réponse des cellules épithéliales pulmonaires à l'exposition au perflurocarbone dans le contexte des applications de la ventilation liquide totale

Sofia Andre Dias

UNIVERSITÉ PARIS-EST

ÉCOLE DOCTORALE UNIVERSITÉ PARIS-EST
Sciences de la Vie et de la Santé

THÈSE

pour obtenir le grade de

Docteur de l'Université Paris Est

Réponse des cellules épithéliales pulmonaires à l'exposition au perfluorocarbone dans le contexte des applications de la ventilation liquide totale

---

Présentée publiquement par

Sofia André Dias

le 27 mars 2017

devant le jury composé de:

Armelle Baeza-Squiban	Professeur, Université Paris Diderot	Rapporteur
Abdul Barakat	Directeur de Recherche CNRS, Ecole Polytechnique	Rapporteur
Atef Asnacios	Professeur, Université Paris Diderot	Examinateur
Arthur Brouillet	Maître de conférences, Université Paris Est	Examinateur
Jean-Christophe Richard	MD-PhD, Hôpital d'Annecy Air Liquide Medical Systems	Examinateur
Luc Lotteau	MD, Bertin Technologies	Co-encadrant
Daniel Isabey	Directeur de Recherche CNRS	Directeur de thèse

Institut Mondor de Recherche Biomédicale

Inserm UPEC, UMR955, Equipe 13- CNRS ERL 7240,

Faculté de Médécine, Créteil, France

bertin TECHNOLOGIES

IMRB INSTITUT MONDOR DE RECHERCHE BIOMÉDICALE

Instituts thématiques Inserm Institut national de la santé et de la recherche médicale

cnrs dépasser les frontières

To Sofia's everywhere

Empower yourself, for by empowering one woman, you empower generations

Hifzha Shaheen

Para ser grande, sê inteiro: nada

Teu exagera ou exclui.

Sê todo em cada coisa. Põe quanto és

No mínimo que fazes.

Assim em cada lago a lua toda

Brilha, porque alta vive.

Ricardo Reis (Fernando Pessoa)

Acknowledgements

To Armelle Baeza-Squiban and Abdul Barakat for so kindly accepting to do the report on my manuscript, and to Jean-Christophe Richard, Arthur Brouillet, and Atef Anascios for being part of the jury.

To Daniel Isabey for being the greatest teacher I have ever had. For his passion for science and the unknown, for his humanity, his effort, his never ending help and support. I would never have accepted doing a PhD with anyone else.

To Emmanuelle Planus for her precious knowledge in biology and the Fibronectin idea that saved the day.

To Bertin Technologies that allowed me to do my PhD, most especially to Luc Lotteau and Sylvain Milleman for their support and help during all this years.

To Bruno Louis for the endless hours of help on MTC, although the (groundless!) accusations of lack of concern for the MTC device.

To Gabriel Pelle and Marcel Filoche for all their valuable help and discussions.

To Patricia Zadigue for sharing her knowledge on biology and laboratory techniques.

To Gilbert Desmarais for the technical help, and his continuous availability.

To Renaud Tissier and his team, that so kindly receiving me on their laboratory, and for showing me the world of liquid ventilation.

To Claude Danan for the surfactant.

To Ngoc-Minh Nguyen, Christelle Angely, Alireza Kazemi, Emilie Bequignon, Kaouther Saihi, and Sarah Bourass, for all their help, ninja qualities and friendship.

To the Erasmus exchange program and the European Union, that allowed me to study abroad, that reflect the true spirit of being a citizen of the world, and without whom I would probably be very different.

To the CIFRE convention that supported this PhD.

To my family, Celina Dias, Noel Dias, Joana Dias Mota, Fábio Mota, Alzira André, Brigida André, Docas and my unborn niece/nephew.

To my second family, Rosa Rocha, Luís Rocha, Rita Rocha and Filipa Campos Silva.

To my loving, Jorge Costa.

To me dearest, Catarina Almeida and Margarida Félix.

To my coolest Ricardo Ribeiro dos Santos, Filipa Romano, Mafalda Correia, Inês Vieira, Teresa Falcão Campos, and Sílvia Martins.

To my Germans, Andreas Mayer, Harry Krüguer, Matthias Kuderer, Eva-Katharina Dietsche, and Agnès Rodenhausen.

And to you, the reader, for taking the time to read my small contribution to science.

Index

Table Index

Equation Index

Figure Index

List of symbols	
α	*Exponent of the power law*
γ_t , γ_a	*Magnification*
β , Φ	*Rotation angles*
Γ	*Euler-Gamma function*
δ	*Capillary length*
η	*Dissipation (loss) modulus*
θ_e	*Contact angle*
μ	*Dynamic viscosity*
μ_0	*Permeability constant*
ρ	*Density*
σ	*Surface tension*
σ_{12} σ_{AB}	*Interfacial energies between 1 and 2, A and B*
σ_c	*Reference stress*
ω	*Pulsation*
A_0	*Prefactor of the power law*
$B(t)$	*Amplitude of bead magnetic moment*
B_0	*Amplitude of the initial bead magnetic moment*
C	*Amplitude of the magnetic torque*
C	*Lung compliance*
$c(t)$	*Creep function*
c	*Bead calibration coefficient*
E	*Young's modulus (rigidity, stiffness, elastic modulus)*
EEP	*End Expiratory Pressure*

F	*Force amplitude*
f^*	*Rupture force of a single bond*
f_β	*Reference force for bond rupture*
g	*Amplitude of gravitational acceleration*
G_e	*Complex storage modulus*
H	*Amplitude of magnetic field*
h	*Height*
I	*Inertance*
k_B	*Boltzmann constant*
k_BT	*Scale for thermal energy*
$k_{off}(f)$	*Dissociation rate of a single bond at force f (de-adhesion)*
$K_{off}(f)$	*Dissociation rate of a multiple bond at force f (de-adhesion)*
k_{off}^0	*Natural dissociation rate at zero force for a single bond*
K_{off}^0	*Natural dissociation rate for a multiple bond (prefactor)*
m	*Bead magnetic moment (magnitude)*
N	*Number of bonds*
n	*Refraction index*
P	*Pressure*
$P(t)$	*Probability of bond survival*
R	*Resistance*
R	*Radius*
r_f	*Force ramp*
S	*spreading coefficient*
T	*Absolute temperature*
T	*Viscoelastic relaxation time*
t	*Time*

t_{off}	*Life-time*
U	*Energy of a single molecular bond*
V	*Volume*
V	*Vergence*
V_R	*Velocity of the retrograde motion of F-actin*
W	*Work of adhesion or adhesion energy*
x	*Distance*
x_β	*Nanometer distance at which appears energy barrier of a bond*

I. INTRODUCTION

Perfluorocarbons (PFCs) are fluorinated organic compounds with a great capacity for dissolving high concentration of oxygen and carbon dioxide, making this liquid of interest to perform liquid ventilation (Clark and Gollan, 1966). Liquid ventilation has been proposed for a wide range of applications such as bronchial lavage after meconium aspiration (Avoine et al., 2011), induction of ultrafast hypothermia after cardiac arrest for brain tissue protection (Darbera et al., 2013; Hutin et al., 2015), and improvement of gas exchanges and lung compliance in adults and infants with acute respiratory distress (Hirschl et al., 1995; Leach et al., 1996; Wolfson and Shaffer, 2005). PFC exhibits specific physical properties namely low surface tension, and high density and viscosity. These last two characteristics are deleterious for frictional resistance. In the frame of an ANR project entitled "*Therapeutic hypothermia by total liquid ventilation for sudden death resuscitated*" (ABYSS) coordinated by Bertin Technologies (01/01/2012-31/12/2014), we have predicted the impact of these properties on airway pressure drop throughout the various generations of the respiratory tract (André Dias et al., 2015). To go further on the evaluation of the impact of PFC, and to validate the technique of Total Liquid Ventilation, Bertin Technologies wanted to access the cellular consequences of this type of ventilation, to help predicting the feasibility of this procedure in a near future. So an exhaustive evaluation of the physical properties of PFC and their relation with cellular and lung responses, was performed during this PhD thesis.

The aim of the present thesis is to evaluate the response of pulmonary cells after PFC exposure by a systematic study of the changes in their mechanical, structural and functional properties in relation with the highly specific physical characteristics of this liquid. We also examine the role of cytoskeleton and glycocalyx layer in the studied cellular regulation. In view of future applications of liquid PFC for Total Liquid Ventilation, we also aim at relating

the changes observed at the cellular level to the changes in lung compliance estimated from *in vivo* data obtained in a separate study performed in large size animals.

The particular airway architecture is such that during liquid ventilation, bronchial epithelial cells will experience shear stress in addition to being exposed to PFC, while alveolar epithelial cells will experience no shear stress since distal airway flow velocity vanishes at the acinar (deep lung) level. So other PFC physical properties, than density and viscosity will play a role at the alveolar level.

From a fluidic point of view, the low surface tension and the high spreading power of PFC enables the fluid to distribute uniformly throughout the lung, and perform an easy liquid migration up to gas exchanges territories, leading to an improvement of ventilation and to a greater compliance in liquid ventilation than in air ventilation (Tooley et al., 1996; Wolfson et al., 1996). By contrast, experiments on excised mammal lungs show that removing surfactant or filling alveoli with aqueous liquid seriously aggravates lung compliance due to an increase in surface tension in alveolar regions (Bachofen and Schurch, 2001).

Across the various applications of PFC, the biological response of cells to PFC exposure is a central question which has rarely been investigated. Some studies suggest potential anti-inflammatory effects at the cellular scale (Nakstad et al., 2001; Varani et al., 1996; Woods et al., 2000a) and a cellular effect through the lipid membrane (Obraztsov et al., 2000; Rüdiger et al., 2003; Wemhöner et al., 2010; Woods et al., 2000b). Yet, to our knowledge, a thorough structural and mechanical assessment of the cell response to PFC exposure is still lacking. It is known that changing either chemical or mechanical properties of basal cellular environment, changes cell response by altering cell migration and modifying cell stiffness (Fereol et al., 2006; Planus et al., 1999). Therefore, one of the main questions

raised by PFC exposure is whether a change in environmental conditions at the apical cell face impacts the cell structure, mechanics and adhesion.

Fluorocarbons are chemically very stable and have no known deleterious biological properties, including toxic, carcinogenic or mutagenic effects (Krafft, 2001). To confirm these innocuous effects, I performed cell viability studies, followed by functional assays of wound healing in double chamber, to assess the functional capability of cells on migration and repair after several days of PFC exposure. Based on these innocuous effects, in the present study, I want to evaluate the early response of alveolar epithelial cells to static PFC exposure, without presuming the effects and the mechanisms susceptible to affect cell physiology. For this we designed a cellular in vitro study in which alveolar epithelial cells are exposed to PFC for various short durations of time ($\leq$ 2 hours), while a systematic evaluation of structural and mechanical properties is performed and compared to the cellular response obtained with a classical culture medium (DMEM), herein defined as control conditions. I also tested the roles of cytoskeleton prestress and glycocalyx layer which are both known to contribute to mechanotransduction, as well as intracellular and transmembrane adaptation to stress (Martins and Abairos, 2002; Thi et al., 2004). The changes in F-actin, focal adhesion and glycocalyx are followed and evaluated using images of fixed and living cells stained after exposure either to PFC (PFC group) or to culture medium (control group). Fluorescence of F-actin and glycocalyx is compared between both groups. Changes in adhesion are monitored by counting the average number of focal adhesions per cell, and the number of focal adhesions per size. We use the multiscale Magnetic Twisting Cytometry (MTC) method, recently upgraded to assess simultaneously cell mechanics and cell adhesion from ligand-coated ferromagnetic microbeads binding integrins (Isabey et al., 2016). The intracellular and interfacial molecular responses to stress was evaluated for limited durations of PFC exposure. The evolutions of cell adhesion and mechanics during the clamping MTC manoeuvre, are modelled using a de-

adhesion probabilistic approach coupled to two alternative microrheological models (a single viscoelastic-solid and a power law).

The response of other lung cell types is also tested to the presence of PFC, such as alveolar macrophages and bronchial epithelial cells. I studied on bronchial cells the long term mechanical stimulation using Magnetic Twisting Stimulation (MTS), which enables to exert a cyclic shear stress on cells, thereby resembling to the cyclic stress imposed by mechanical ventilation (Chen et al., 2001; Wang et al., 2012).

In addition to performing, with a specifically designed capillary pressure method, measurements of surface tension of the different fluids used to study the cell response, we also discuss, using theoretical approach, the direction of evolution of the interfacial energy when exposing the cells to a low surface tension fluid. Noteworthy, although the cell response to the change in surface tension remains in the physiological range, we found a close correlation between the estimated change in interfacial energy and the reported cellular and molecular effects, suggesting that cells are able to sense and adapt to the drastic changes at the cellular surface of apical environmental conditions. Measure of PFC surface tension and theoretical considerations suggest that PFC induces a change in the energy balance at the cellular/alveolar surface, which might be responsible for the reported cellular observations, suggesting a never reported cell sensitivity to apical energetic conditions.

In correlation with the effect of changing cell interfacial energy, we finally discuss the consequences at the lung level of the low surface tension of PFC in terms of the alveolar cell surface, and by contrast we compare the previous situation with an extreme case of increase in surface tension (e.g., in the case of Acute Respiratory Distress Syndrome). On the whole, present results provide new elements on the physiological consequences of using Total Liquid

Ventilation (TLV), notably in terms of respiratory compliance presently evaluated in pigs ventilated with TLV in the acute conditions of resuscitation from cardiac arrest.

II. BIBLIOGRAPHIC STUDY

II.1 Specific physical properties of PFC

Liquid perfluocarbons (PFC) have highly specific physical properties, such as chemical and biological inertness, low surface tension, high spreading coefficient and elevated capacity of dissolving gases, that makes them of high interest for a variety of biomedical applications and most particularly drug and oxygen deliveries (Krafft, 2001).

The peculiar physical properties of PFC are mostly due to fluorine. PFC is highly electronegative and possess a low polarization level along with high ionization potential (Karsa, 1995), resulting in low van der Waals interactions between fluorinated chains as well as low cohesive energy densities in liquid fluorocarbons (Chhatre et al., 2010; Riess, 1994). These reduced interactions make PFC a non-polar liquid of low surface tension, with a high spreading coefficient and high gas solubility (Riess and Krafft, 1997). The connections between fluorine and carbon atoms (C-F) also play a role in PFC properties. These bonds are very stable due to the overlap of electron orbital which increases the bond strength. As a consequence, fluorocarbons are thermally and chemically very stable and have no known deleterious biological properties, including toxic, carcinogenic or mutagenic effects (Krafft, 2001). From a fluidic point of view, the low surface tension and the high spreading power of PFC enables the fluid to distribute uniformly throughout the lung, and an easy liquid migration up to gas exchanges territories, leading to an improvement of ventilation and to a greater compliance in liquid ventilation than in air ventilation (Tooley et al., 1996; Wolfson et al., 1996).

There are several different PFCs, amongst which the most commonly used for biomedical applications are the perfluoro-n-octane (C_8F_{18}), the perfluoro-n-decane ($C_{10}F_{18}$),

and the perfluorobrome ($C_8F_{17}Br$) (see Table 1). Between these different PFC, the physical properties may differ but their range of variations remain somehow limited (Wesseler et al., 1977).

Table 1: Configuration, density and surface tension of the most commonly used PFCs.

PFC	*Configuration*	*ρ (kg/m^3)*	*μ(kg/m.s)×10^{-4}*	*σ(mN/m)*
Perfluoro-n-octane	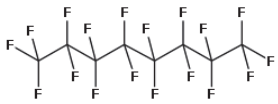	1755	18	14
Perfluoro-n-decane	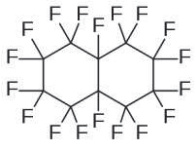	1946	51	16
Perfluorobrome	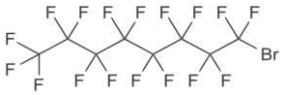	1890	16	16

In the ANR project ABYSS, an animal study compared three different PFCs to observe which one is more suitable to perform a liquid ventilation (Chenoune et al., 2014). The best lung clearance after lavage was obtained with the perfluoro-n-octane (C_8F_{18}). This positive result with perfluoro-n-octane is due its high vapor pressure compared with the other two PFCs, that makes very easy to evaporate and eliminate every PFC residues from the lung after lavage. So for the cellular experiments in the present study, we retained that clinically-selected PFC, i.e., the perfluoro-n-octane: C_8F_{18}, which physical characteristics are summarized below (Table 2) and will be called from now on simply by PFC.

Table 2: Physical properties of PFC compared with air and water. Issued from 2 literature studies (Nishikido et al., 1989; Wesseler et al., 1977), summarizes the characteristics of the liquid perfluocarbon used in our study.

Properties	*Air*	*Water*	*Selected PFC*
Percentage of dissolved oxygen (%)	21	~1	28
Surface tension σ (with air) (mN/m) (25°C)	-	73	14
Density (ρ) (kg/m^3) (25°C)	1.2	997	1755
Dynamic viscosity (μ) (kg/m.s)×10^{-4} (25°C)	0.2	9	18

II.2 Surface tension and spreading properties

Surface tension is the interactional potential raised between two close molecules of the same liquid phase. At the frontier between a liquid phase and air, the attraction between two close liquid molecules is much higher than between liquid molecules and gas. This phenomenon creates, at the interface between liquid and gas, a film whose shape and behavior are governed by surface tension properties. Surface tension σ is defined as free energy per unit of surface area $(\sigma = \partial G/\partial A)$, G: free enthalpy i.e., units of σ are in J/m^2 or equivalently in N/m (more commonly in mN/m) (Israelachvili, 2015). The nature of the interactions between two close liquid particles is going to determine the liquid surface tension. For liquids with weak molecular interactions such as when the sole van der Walls forces exist, surface tension is rather low (e.g., for oil σ=20 mN/m). If interactions are stronger, such as when hydrogen bonding dominates, the surface tension is high (e.g., for water σ=73 mN/m).

Surface tension (i.e., with air) of a given liquid phase "*A*" is the sum of energies involved throughout the different types of interaction: atomic, molecular, dispersive. These interactions are classically divided into a dispersive or non-polar component, and polar component (Owens and Wendt, 1969):

$$\sigma_A = \sigma_A^d + \sigma_A^p \qquad \textbf{Equation 1}$$

PFC possesses a low polarization level resulting in low interactions which make PFC a non-polar liquid of low surface tension $\left(\sigma_{PFC} = \sigma_A^p \approx 0\right)$ (Chhatre et al., 2010). Let us consider the typical case of 3 phases in close interaction: planar solid (*S*), liquid drop (*L*) and gas or vapor (V or G) (Figure 1).

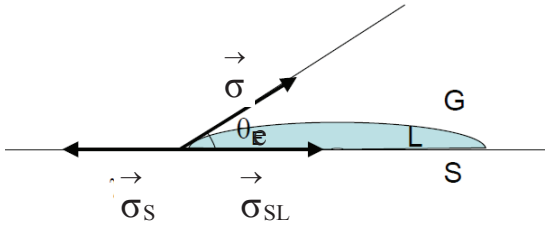

Figure 1: Representation of surface forces equilibrium between a solid surface and a liquid drop.

At contact point, the equilibrium between the 3 phases can be described by the projection of surface tension forces in the plane of the solid phase leading to the Young's equation, that gives the contact angle θ_e (Young, 1805) (S: solid; L: liquid; G,V: gas, vapor):

$$\sigma_{SV} = \sigma_{SL} + \sigma_{LV} \cos\theta_e \qquad \textbf{Equation 2}$$

σ_{SV} is the surface tension in presence of the gaseous phase. The σ_{SL} is called the interfacial energy (or tension) between the solid and the liquid, σ_{LV} is the liquid surface tension in contact with gas between solid and liquid, i.e., $\sigma_{LV} = \sigma_L$. The quantity σ_S is the so called surface energy of the solid phase, i.e., by reference to air phases whose magnitude is not so easy to determine experimentally as the surface energy of liquids, or free energies of liquid/liquid interfaces (Israelachvili, 2015). The projection of surface forces in the direction perpendicular to the solid surface is equilibrated by the solid wall reaction, which can be infinite. In case of a deformable wall, e.g., a cellular layer, the perpendicular component of σ may induce local cellular deformation.

The spreading coefficient (*S*) of a liquid is classically defined by the difference between the solid (dry) surface energy, and the liquid (wetted) surface energies, which can be written with the help of Young's equation:

$$S = \sigma_{SV} - \sigma_{SL} - \sigma_{LV} = \sigma_{LV}\left(\cos\theta - 1\right)$$ **Equation 3**

In the case of a liquid with low surface tension, the spreading coefficient is high (S>0), meaning that a drop of that liquid is able to spread very easily on a solid surface and form a small contact angle θ_e (Figure 2). In the case of a liquid with high surface tension, the contact angle formed with the solid is different from zero, and the drop does not spread and adopt a spherical shape (S<0).

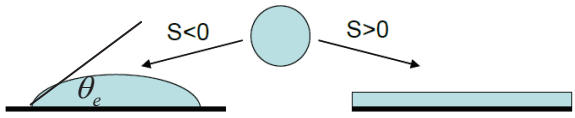

Figure 2: Spreading of two liquids with different spreading coefficients. In the case of a high surface tension liquid (S<0) the drop acquires a spherical shape. In the case of a decrease surface tension the liquid spreads easily through the solid surface.

When there is no solid surface but 3 fluids in contact, there is no privileged direction for projections. The 3-fluid contact angle method can be used, leading to following system of equations obtained by projection on the 3 main axis defined by the direction of fluid surface at equilibrium (red, green and blue axis in Figure 3):

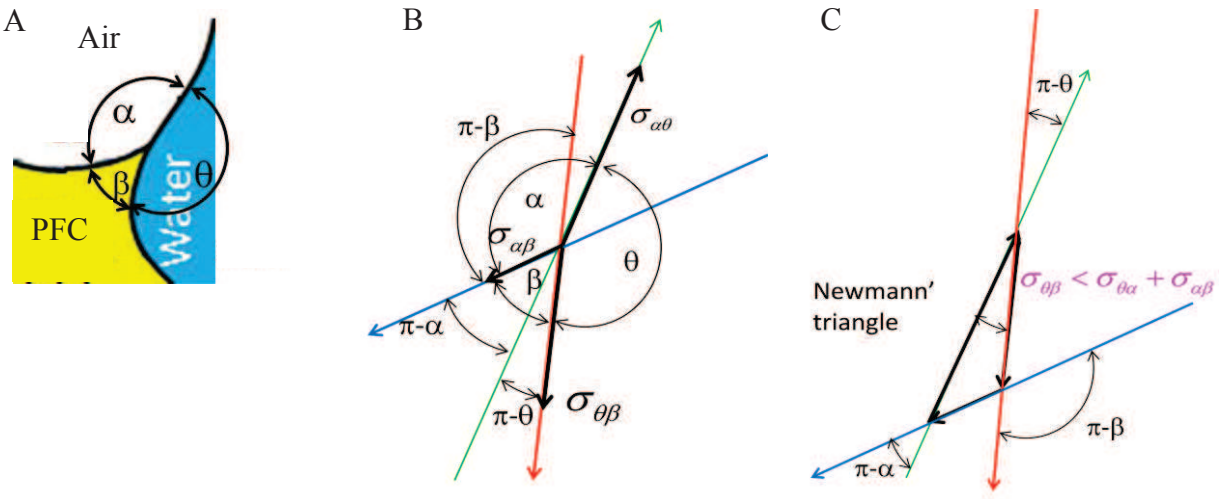

Figure 3: A) Angles of contact for three fluids, Air, PFC and Water (DMEM). B) Representation of the angles. C) Projections of the three different angles.

$$\sigma_{\alpha\beta} - \sigma_{\theta\beta}\cos(\pi-\theta) - \sigma_{\alpha\beta}(\pi-\alpha) = 0$$
$$\sigma_{\theta\beta} - \sigma_{\alpha\beta}\cos(\pi-\theta) + \sigma_{\alpha\beta}\cos(\beta) = 0$$
$$\sigma_{\alpha\beta} - \sigma_{\alpha\theta}\cos(\pi-\alpha) + \sigma_{\theta\beta}\cos(\beta) = 0$$
$$\alpha+\beta+\theta = 0$$

Equation 4

This system of equation governs the equilibrium between 3 non-miscible fluids in contact, e.g., PFC, Water (DMEM) and air.

A solid surface energy may be deeply modified with a surface treatment such as plasma treatment or surfactant application. The plasma treatment effectively reduces the solid surface energy, decreasing the contact angle between the liquid and the solid. As a consequence the spreading coefficient is highly increased: $\sigma_{SG}\uparrow;\sigma_{SL}\downarrow \Rightarrow (\sigma_{SG} > \sigma_{SL} + \sigma_{LV}) \Rightarrow S > 0$, Figure 4.

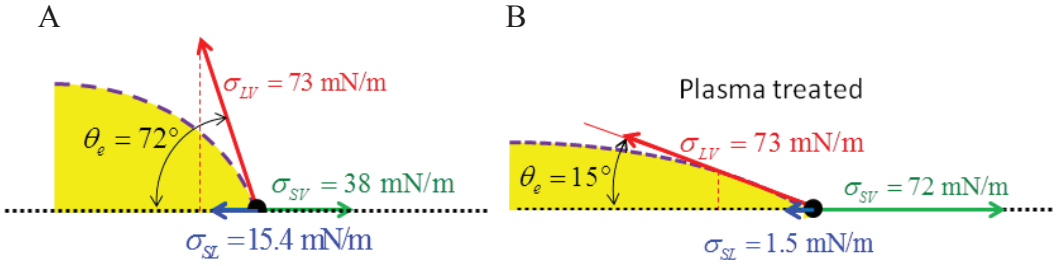

Figure 4: A) Non-treated surface with a water drop. B) Plasma treated surface with a water drop. The plasma treatment effectively reduces the solid surface energy, resulting in an increase of the spreading coefficient.

Another type of surface treatment is the application of a surfactant layer. With an application of a surfactant layer in a solid surface, the surfactant molecules placement is dependent of the polarity of each phase. When putting a surfactant drop on a solid surface, the hydrophobic part of the surfactant (tail) is going to be turned to air, and the hydrophilic (head) to the solid. In the borders of the drop, surfactant molecules are going to displace to the solid

surface, decreasing the surface tension of this area with air, $\sigma_{LV}\downarrow;\sigma_{SL}\downarrow;\sigma_{SV}\uparrow\Rightarrow S=\sigma_{SV}-(\sigma_{SL}+\sigma_{LV})\uparrow$, Figure 5.

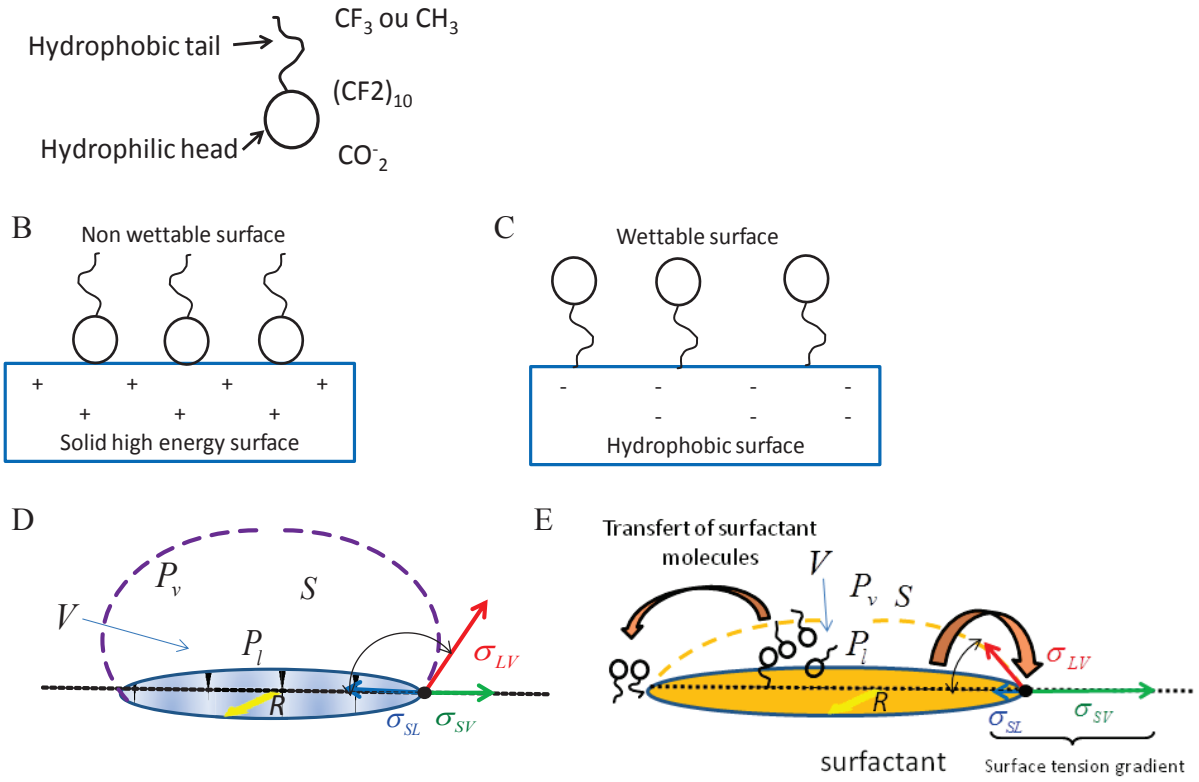

Figure 5: A) Configuration of the surfactant molecule. Displacement of the surfactant depending on the polarity of the surface: B) Hydrophilic surface, surfactant connects using its hydrophilic head; C) Hydrophobic surface, surfactant connects using its hydrophobic tail. D) Water droplet with no treatment. E) Surfactant droplet. The presence of surfactant effectively reduces the solid surface energy.

II.3 Surface tension effects on the lung

II.3.1 Effect of surface tension on lung geometry

The evolution of surface tension at the alveolar interface is of particular physiological significance due to its influence on lung mechanical properties, most particularly on lung compliance and the associated elastic work of breathing (Goerke and Clements, 1986). This assertion is supported by the strong correlation observed between the increase in surface tension in case of surfactant deficiency and pulmonary diseases (Avery and Mead, 1959; Clements et al., 1972; Gruenwald et al., 1962). Therefore several efforts have been made to exogenously control surface tension (Adams et al., 1978; Enhorning and Robertson, 1972). The lung geometry dictates that the fractal division of acinar volume between alveoli and alveolar ducts, is determined by the balance between two types of force: (i) inward-acting tissue forces in the alveolar entrance ring, and (ii) outward-acting forces arising from septal tissue acting in parallel to surface forces at the air-liquid interface (Figure 6) (Butler et al., 2002). Alveolar surface forces exert a molding effect on alveolar tissue elements, and a change in surface tension dramatically alters the recoil pressure of the lung by deforming lung tissue and changing tissue tension (Bachofen and Schurch, 2001). Increasing surface tension by, e.g., rinsing surfactant with a detergent, causes an exaggerated widening of alveolar ducts, and stretching of septal segments and axial fibers leading to a drastic reduction in alveolar surface area (Figure 6). On the other hand, a decrease in surface tension caused by, e.g., filling the lungs with hexadecane solution, results in large alveolar surface area, and a slight stretching of alveolar fiber tension with positive consequences on lung compliance.

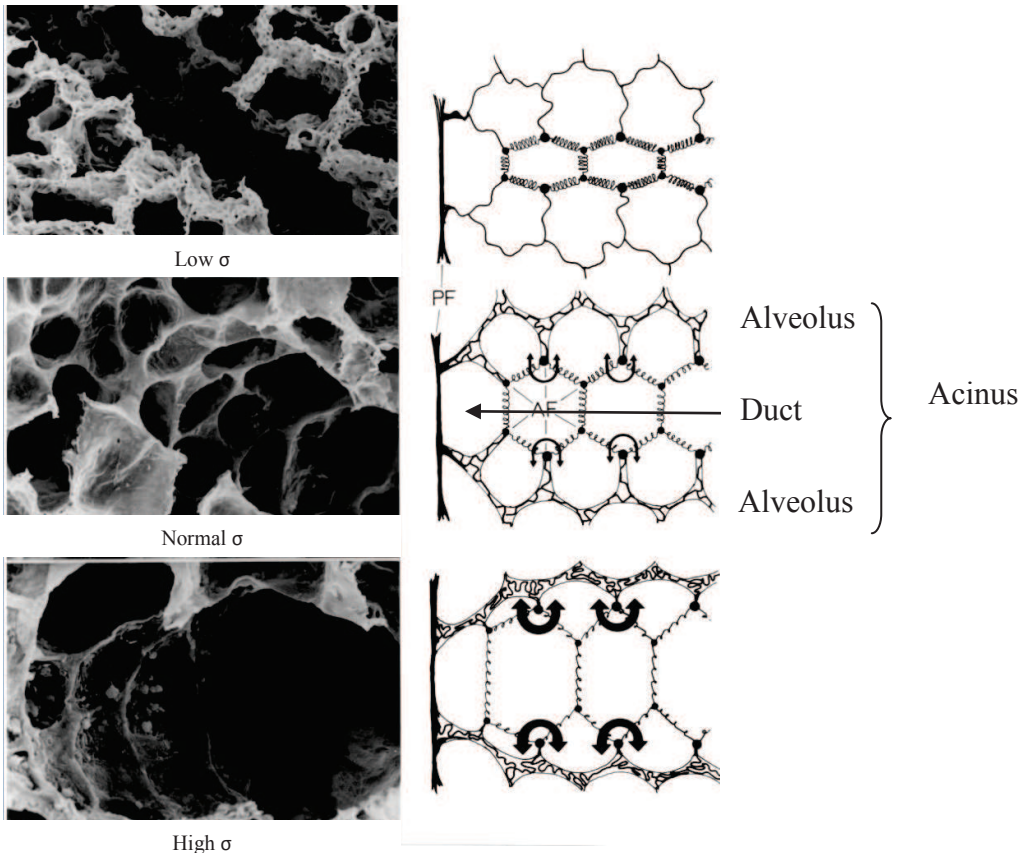

Figure 6: Modified from Bachofen (Bachofen and Schurch, 2001) scanning electron micrographs of alveolar ducts. With the increase in surface tension there is an increase in the duct diameter. The fibers on the image are the force-bearing elements, and the dimensions of the peripheral air spaces are governed by an interplay between tissue and surface tension.

II.3.2 The effect of alveolar surface tension on lung compliance: the case of acute respiratory failure

An increase of surface tension is responsible for altering altogether the lung volume, the alveolar diameter and the lung compliance, causing a severe impact on lung mechanics. As a consequence, pulmonary perfusion and gas exchange are deteriorated and leukocyte sequestration is increased (Topulos et al., 2002). Surface tension increase causes a compressive force on capillaries, decreasing capillary volume and compliance (Weibel, 2011; West, 2000; West et al., 1991). Specifically during ARDS (Acute Respiratory Distress

Syndrome), there is a loss of permeability of the alveolo-capillary barrier, causing a massive flooding of alveoli by blood plasma and a disruption of production and turnover of surfactant, contributing to respiratory deficiency, Figure 7 (Ware and Matthay, 2000). Lack of surfactant causes an increase in surface tension between air and the alveolar liquid lining, causing alveolar collapse and stiff lungs that thereby become difficult to inflate (Filoche et al., 2015). Highly hypoxemic ARDS patients have a typical drop in lung compliance and lung infiltrations, which are evidenced by chest X-ray (Ashbaugh et al., 1967). In addition to plasma infiltrations at the alveolar level, an invasion of different blood cells such as neutrophils, erythrocytes and protein-rich edema fluid has been observed (Bachofen and Weibel, 1982; Pratt et al., 1979). The classical treatment of ARDS consists of mechanical ventilation at low tidal volumes, i.e., typically: 6 ml/kg because ventilating with classical gas volumes (10-15 ml/kg), or at increased lung volumes and pressures further increases lung injury (Dreyfuss et al., 1988). However, the efficacy of such a treatment is somehow limited, and the mortality in a situation remains elevated, i.e., 40-60% (Doyle et al., 1995; Zilberberg and Epstein, 1998). Thereby, decrease in alveolar surface tension has been considered as a potential treatment to increase compliance in a number of pathological situations such as ARDS (Anzueto et al., 1996; Gunther et al., 1996; Ware and Matthay, 2000), infant respiratory distress syndrome (Avery and Mead, 1959) and exposure to toxic aerosols (Glynn and Gale, 1990; Tashiro et al., 1998).

A recently tested treatment for ARDS is surfactant replacement therapy. This technique appears very effective to decrease surface tension in newborns with neonatal respiratory distress syndrome (Long et al., 1991), but showed drastic limitations in adults (Anzueto et al., 1996). This is probably because surfactant failed to reach the alveolar territories in adult size lungs (Filoche et al., 2015; Fulkerson et al., 1996). The idea of reducing alveolar surface tension, in addition to an adapted low tidal volume mechanical

ventilation, remains promising for improving the outcome of ARDS patients from neonates to adults.

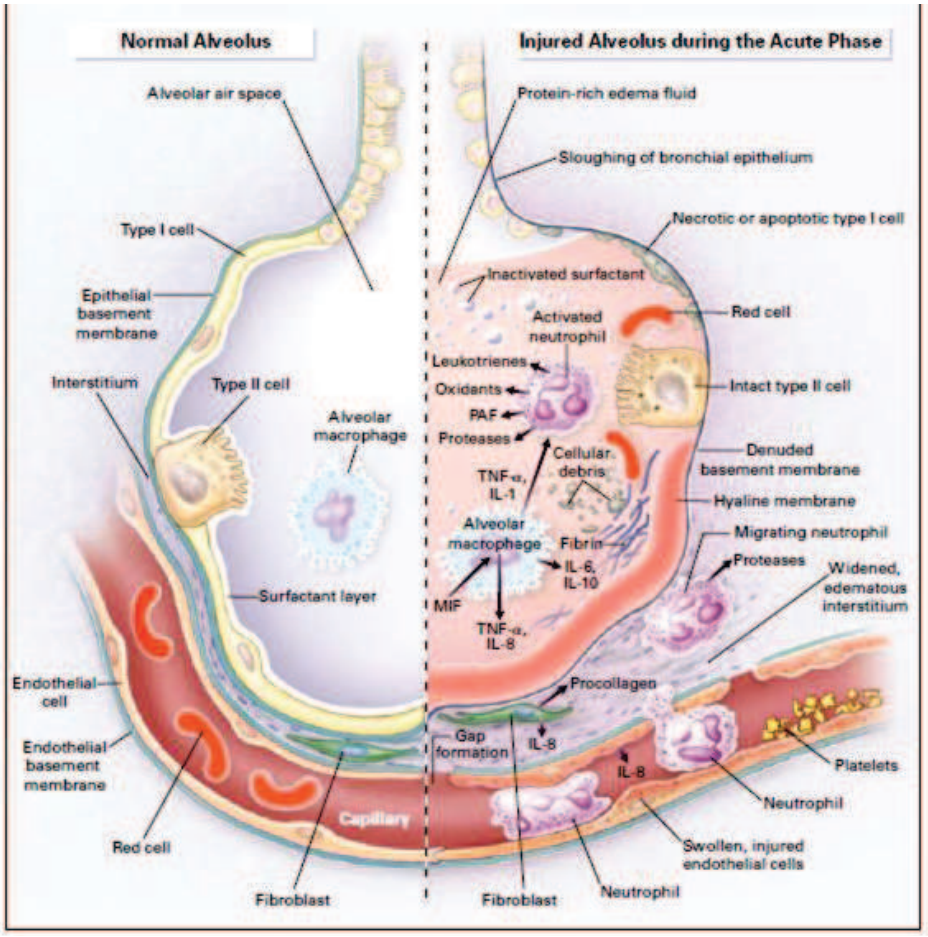

Figure 7: Modified from Ware and Matthay (Ware and Matthay, 2000). Left side, normal alveolus, right side, injured alveolus during ARDS. In the injured alveolus, there is an invasion of air space by blood cells, and an influx of protein rich edema fluid that dramatically dilutes surfactant.

II.3.3 The effect of alveolar surface tension on lung compliance: the case of Total Liquid Ventilation (TLV)

Several studies show that during Total Liquid Ventilation (TLV) with perfluorocarbons (PFC), the reduction of alveolar surface tension tends to decrease elastic recoil, and the amplified density of this liquid causes a reopening of atelectatic alveoli. These PFC-induced

effects contribute to increase pulmonary compliance compared to gas ventilation in normal lungs as well as in surfactant-deficient lungs (Figure 8) (Hirschl et al., 1996; Sage et al., 2016; Tooley et al., 1996). As a matter of fact, during TLV, a liquid interface replaces the gas-liquid interface at alveolar level, eliminating a major cause of high surface tension. Moreover, filling the lungs with a heavy liquid enables recruitment of normally collapsed lung regions, resulting in a decrease of the slope of the pressure-volume curve, (i.e., equivalent to an increase in compliance) (Wolfson and Shaffer, 2004). Lung recruitment is also enhanced by the increase in transmural pressure (p_i–p_e) across the alveolo capillary membrane, creating a "liquid positive-end-expiratory pressure" that helps to raise lung compliance.

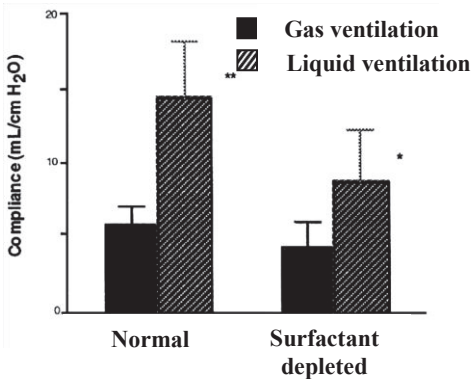

Figure 8: Modified from Hirschl (Hirschl et al., 1996). Lung compliance of pigs during gas ventilation (black) and liquid ventilation (stripped). In a "normal" (with surfactant) lung (right), and in a surfactant depleted lung (left).

However, the complexity of the role of surface tension arises from the discrepancies in patient's outcomes between partial and total liquid ventilations. It seems that the positive effects of total liquid ventilation cannot be simply extrapolated to partial liquid ventilation (Hirschl et al., 1996). Compared to gas ventilation, static compliance was significantly increased in the case of total liquid ventilation but not in the case of partial liquid ventilation. As if the permanence of air in partially liquid filled lungs, caused a surface tension higher than in lungs completely filled with PFC. Another important point to mention to understand the role of surface tension on lung compliance is the presence of surfactant. In a completely

liquid filled and ventilated lungs the compliance is even greater if surfactant remain in the lungs (Figure 8). In the TLV context where gas-liquid interfaces are eliminated, the distal lung is supposed to receive maximal protection because inflation pressures are reduced, recruited lung volume is maximal, compliance is consistently increased, and pulmonary barotrauma is expected to be reduced. However, this difference of compliance in lungs partially filled with PFC, and totally filled lungs with PFC with and without surfactant, shades a light to the possibility of the non-linear role played by surface tension in alveolar response. As if the low surface tension of PFC solo was not a sufficient condition to increase lung compliance, explaining the lack of success in some studies using partial liquid ventilation (Kacmarek et al., 2006). But an optimal surface tension with the alveolar all, without the presence of air and with the presence of surfactant, was necessary to obtain the positive effect of the presence of PFC in lung compliance. The table below (interpreted from Bachofen (Bachofen and Schurch, 2001)) sensitizes the evolution of lung parameters with the change in surface tension (see also Figure 6).

Table 3: Evolution of lung compliance, alveolar surface and alveolar fiber tension with surface tension.

At constant lung volume	*PFC +surfactant*	*PFC*	*Air +surfactant*	*PFC (Partial ventilation)*	*Air (detergent rinsed, no surfactant)*
Surface tension	- - -	- -	-	+	+ +
Lung compliance	+ + +	+ +	+	-	- -
Alveolar surface	+ + +	++	+	-	- -
Alveolar fiber tension	- - -	- -	-	+	+ +

II.3.4 Effect of a change in surface tension at the cellular level

If the lung effects of surface tension have largely been documented, the cellular effect of surface tension have rarely been studied. Although a few studies suggest that surface tension effect is far from being negligible. For instance, in Bachofen (Bachofen and Schurch, 2001) an increase of surface tension causes a drastic change in the shape of bronchial macrophages, suggesting a cell sensitivity to mechanical environment. At low surface tension (~2 mN/m), macrophages adopt a more rounded shape consistent with its migration activity on the apical face of the epithelial cells forming bronchial lumen. At high surface tension (~20 mN/m), bronchial macrophages adopt a flattened shape and become embedded in the bronchial wall which means flattening and firm anchorage to the bronchial epithelium (Figure 9).

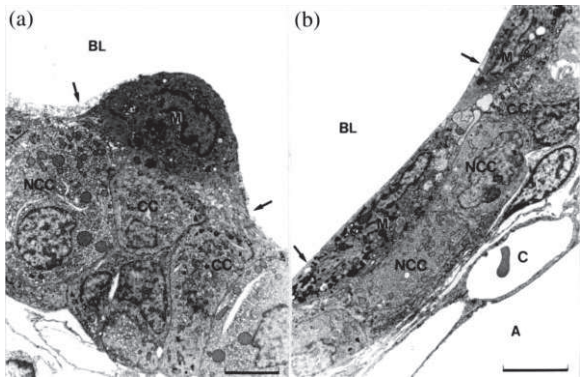

Figure 9: Modified from (Bachofen and Schurch, 2001) BL: bronchiolar lumen. C: capillary. M: bronchiolar macrophages. CC: ciliated epithelial cells. NCC: non-ciliated epithelial cells. Arrows point to surface lining layer. Scale bar 5mm.

The role of surface tension is also thought to be determinant in organogenesis (Discher et al., 2005), most likely because organs or organisms under development are to some extent isolated mechanically from tissue environments, and mostly under the dependence of surface tension. It has been shown that random mixtures of two cell types often lead to shell-core cell aggregates (Figure 10), as initially observed when heart cells segregated into the interior of a mass of retinal cells after only 1 day in culture (Steinberg, 1962). Individual cell clusters form

by segregation from each other (Trinkaus and Lentz, 1964). Quantitative estimates of surface tension for these spherical aggregates, e.g., of cadherin-expressing cells (Foty and Steinberg, 2005) exceed the rate-dependent cohesive strength of lipid bilayers (as low as 2 to 3 mN/m) (Evans et al., 2003), and suggest adhesion energies per cadherin that are orders of magnitude larger than would be expected on individual cadherin bonds. There are many unsolved questions raised by the development of these aggregates, and the role of surface tension as a regulator factor of cell proliferation and organization, remains to be elucidated.

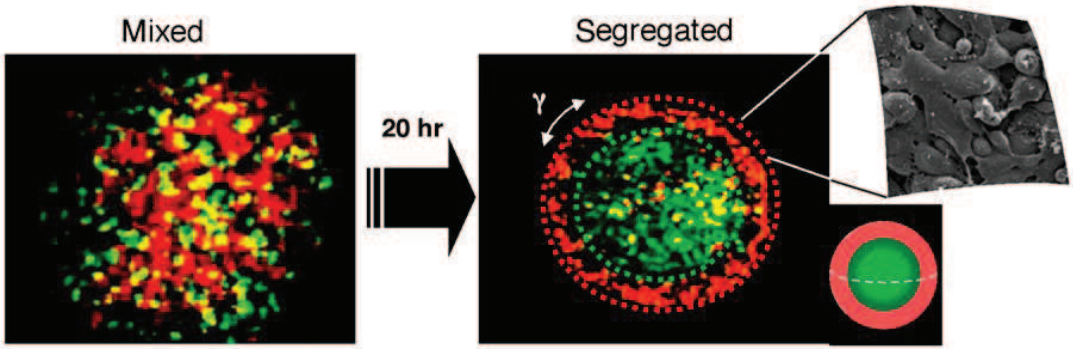

Figure 10: Modified from Discher (Discher et al., 2005). Sorting of two cell types into a 3D shell-core aggregate (~300 mm in diameter) in which low expressers of N-cadherin (labeled in red) surround high expressers of N-cadherin (labeled in green). Scanning electron micrograph of a typical spheroid's surface shows well-spread cells.

To try to fill the lack of data about cell sensitivity to surface tension, we describe in this document a systematic study to determine how cell responds to changes in surface tension, and what are the directions of cellular evolution in response to these changes. First, it is necessary to review the cellular adaptation to mechanical properties environment, and the biological mechanisms that originate a physic-chemical signalization.

II.4 Cellular adaptation to mechanical environment

II.4.1 A broad range of cell sensitivities

Some cells such as the neutrophils have been shown to be insensitive to substrate rigidity, maintaining their shape and ability to spread on either a soft or rigid substrates (Yeung et al., 2005), but most cells have been found to respond to the mechanical environment that surrounds them (Discher et al., 2005). For example alveolar macrophages, muscle cells, stem cells, and normal and pathological, such as cancer cells, have been found to be mechanosensitive. In such cases, mechanical properties of substrate or environment play a role on cell phenotype and cell behavior in a dependent manner. It has been shown that lack of cell-cell contact and cell growth in a confinement space is important for fibroblasts and endothelial cells. In the absence of neighboring cells, these cells recover a migrating phenotype and express a sensitivity to substrate stiffness (Yeung et al., 2005). For many cell types, changing substrate stiffness, e.g., using glass plates, soft or rigid gels of polymers, efficiently modifies the cell structure, cell shape and cell behavior by durotaxis. Durotaxis is a property mainly of tissue cells in which the cell direction of migration is dependent on the gradient of substrate stiffness, precisely the cell moves from low to high substrate stiffness (Lo et al., 2000). In myoblasts cultured on collagen coated polyacrylamide gels, differentiation was optimal for substrate stiffness approaching muscle stiffness, while on very stiff substrates such as glass or on very soft substrates, cells did not striated (Engler et al., 2004). By seeding cells on substrates of various properties, it was found, by measuring contractile function and calcium handling, that cell function is optimal when substrate mechanical conditions is closer from physiological (and thus mechanical) conditions (Tallawi et al., 2015). By studying alveolar macrophages, Féréol et al. found that the rigidity of the substrate modulated cell shape and cellular stiffness. Precisely, macrophages adherent on rigid

substrates adopted a flat shape and increase their stiffness, while they adopted a round shape when cultured on soft substrates (Fereol et al., 2006) Figure 11.

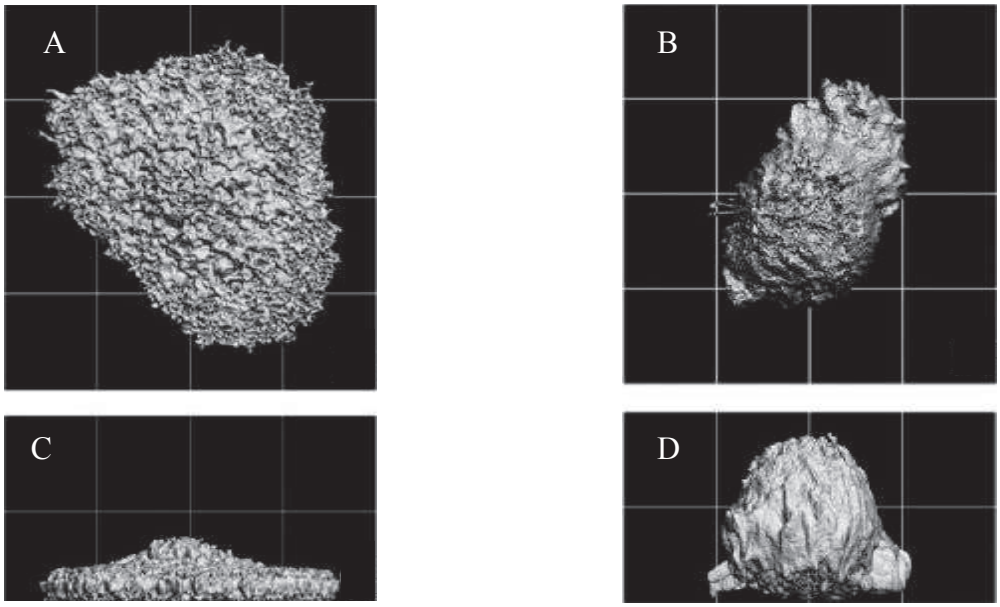

Figure 11: Modified from Féréol 2006 (Fereol et al., 2006). 3D reconstructions of the actin cytoskeleton structure in alveolar macrophages, top and side views. Alveolar macrophage in type I collagen-coated glass substrate A) top view C) side view. Alveolar macrophages in flexible polyacrylamide gel substrate B) top view D) side view. Macrophages in a rigid substrate significantly increase area compatible with an increase of adhesion and rigidity. In a soft substrate they occupy a much smaller area and are less adherent.

For undifferentiated mouse embryonic stem cells, changing the substrate rigidity from stiff to soft has been shown to play an effective role to stop differentiation. Accordingly, soft substrates were found to contain optimal conditions to maintain undifferentiated a cell culture over long periods (Chowdhury et al., 2010). Neuronal cells were also shown to be sensitive to surface energy distribution. By maintaining constant the total free-energy of the substrate while changing the proportion of dispersive and non-dispersive potentials, it was possible to act on neuritogenesis. Similarly, increasing the proportion of dispersive/non-dispersive potentials was shown to enhance efficiently neurite outgrowth (Lamour et al., 2011). Beyond

mechanical properties of substrate and/or environment, cells express sensitivity to the topography of the substrate (Wong et al., 2004). The variety of cellular responses to mechanical and topographical stimulus are multiple and can be related to cell function. The mechanism by which cells transduce a mechanical signal into a chemical signal seems to be common to all cell types, nevertheless many studies provide a fundamental understanding of the mechanisms behind such a cell sensitivity. A common agreement nevertheless exists at this date concerning the capability of (sensitive) cells, to transduce mechanical cues into chemical signals. The molecules specifically incriminated in these mechatransduction processes are the transmembrane receptors of the integrin type.

II.4.2 Mechanotransduction

A transmembrane mechanoreceptor receives mechanical cues from the local environment, and converts this information into a biochemical signal (outside-inside), which is then transmitted within the cell up to the nucleus as a cascade of molecular events susceptible to initiate adapted cellular changes through inside-outside signaling. Cell sensitivity to mechanical environment is actually dependent on: (i) the type of adhesion system used by the cell, e.g., macrophages have dynamic adhesion sites of the podosome type while cells in tissue have more stable focal adhesion sites (Fereol et al., 2009); (ii) the capacity of activation of biomolecules constituting these sites, e.g., phosphorylation leads to molecular unfolding and enables to reveal hidden sites for new molecule recognition and aggregation (Zhu et al., 2000). Astonishingly, these mechanosensitive systems are capable to detect shallow changes in mechanical properties, which necessarily occur at extremely low levels, while the intrinsic mechanical properties of surrounding tissues might be at much higher levels in terms of stiffness or viscosity.

In adherent cells, forces inducing a biological response are transmitted via the cytoskeleton (CSK), a multiscale, interconnected network composed by actin filaments, intermediate filaments and microtubules. CSK is responsible for many cell functions and govern cell shape and spreading (Ingber et al., 1995; Janmey, 1998). The other force sensors are proteins at the membrane-phospholipid interface, elements of the nuclear matrix and the lipid bilayer itself (Janmey, 1998). Prestress is the residual tension observable even in the absence of external force applied. It is sustained by F-actin filaments or stress fibers, in which tension is essentially generated by acto-myosin coupling. Tension in actin network is counterbalanced by compression in the non actinic network and in the substrate, as well described by the tensegrity model (Ingber, 2008). This concept is useful to understand why a force exerted from the mechanical environment to the cell, may affect the internal force equilibrium, changing cell shape and tension within cytoskeleton elements (Wang et al., 1993; Wang and Ingber, 1994; Zhu et al., 2000).

Adherent cells are anchored to the matrix via adhesion sites whose mature form is called focal adhesion (FA), and to neighboring cells via cell junctions. The connection of the cell to the matrix is required for the initiation and reinforcement of integrin-mediated adhesions. FA are constituted by integrins that are connected to actin CSK on the intracellular side, and to the matrix on the extracellular side. Adhesion sites serve as forces transmitter between intracellular structure and extracellular matrix (Bershadsky et al., 2006; Vogel and Sheetz, 2006).

An example of cellular adaptation to the exerted stress is the change in cell stiffness. Most of experimental results reveal a stiffening process, which is consistent with the structural nature of the cell. The application of an external force that elongates the cell, or the activation of intracellular processes results in an increase in intracellular tension, affecting the elastic modulus and resulting in an increase in cell stiffness (Fernandez et al., 2006). On the

contrary, removing the contribution of one component of the CSK such F-actin by, e.g., depolymerizing the actin network by treating the cell with cytochalasin (cytoD), results in a decrease in cell stiffness and a disappearance of the tensed actin structure (Wendling et al., 2000).

Another type of well identified cellular force sensor is the cell-cell connector which implicates intercellular adhesive molecules, such as cadherins (Ko et al., 2001). Some studies demonstrate that cadherins, which are transmembrane proteins, as integrins contribute to mechanical signaling (Ko et al., 2001; Potard et al., 1997). This opens the possibility that the process by which cells convert mechanical stimuli into biochemical responses (mechanotransduction), is not limited to the cell-matrix interactions, but concerns the global cell microenvironment, thus implicating the recruitment of a wide variety of cell attachment, cytoskeleton elements, and signaling proteins. So integrins and cadherins would serve as mediators for mechanotransduction. Both, due to their connection to the CSK, would transmit the forces across the plasma membrane (Huang and Ingber, 1999) and convert physical forces into chemical signals (Schwartz and Assoian, 2001).

II.4.3 Force sensitive cellular elements: Cytoskeleton, adhesion sites and glycocalyx

The CSK is connected to the extracellular matrix via the cell-matrix adhesion system, but mechanotransduction requires the CSK tension generated by actomyosin contraction that enables to transmit and transduce the mechanical cues received at the adhesion site level. The deep component of the cellular structure is formed by focal adhesion and stress fiber system. They are under the control of RhoA-GTPases, which regulate altogether actin assembly and remodeling of adhesion in response to mechanical stimulation (Asparuhova et al., 2009). Cell-matrix adhesions are advantageously located at cell surface and thereby are well positioned to transduce mechanical stress into chemical signal (Bershadsky et al., 2006). The CSK is going

to modulate the cell-matrix adhesion, by activating integrin receptors at its surface. This activation takes place due to inner cell signaling secondary, after ligand binding integrins signal back to the cell (Arnaout et al., 2007). Focal adhesions are firmly attached to actin stress fibers (Zaidel-Bar et al., 2007), their development is going to proportionally depend on the mechanical stress at the site (Tan et al., 2003), and they contain several adaptors and signal components.

The cortical component of the cellular structure system is formed by cortical CSK and a dynamic adhesion structure system, usually formed in the lamellipodium region during cell migration. Focal complexes correspond to weak bonding to the extracellular matrix, a situation encountered when the substrate is soft. This situation corresponds also to low traction forces and CSK links and consequently less strength but more dynamic adhesion sites.

As mechanical stress increases, cellular traction enhances and adhesion structure is reinforced by addition of new junction proteins and clusterisation of new integrin-ligand bonds (Choquet et al., 1997; Tan et al., 2003). Traction forces are dependent on dynamic actin CSK. Rho-family GTPases control actin assembly and contraction, the most relevant are Racl and RhoA (Burridge and Wennerberg, 2004). Racl controls assembly of the cortical actin and formation of new focal complexes (Young and Copeland, 2010). So, through Racl and RhoA activities, adherent cells use cell-matrix interactions constantly sense and adapt to mechanical forces generated intracellularly or extracellularly, and control actin remodeling (Asparuhova et al., 2009). Focal complexes exhibit force sensitivity as well as focal adhesion structures. In cultured cells, focal complexes are going to experience a traction force on the substratum by the cells (Schoenwaelder and Burridge, 1999), causing a maturation of adhesion sites (Figure 12), and a transition from focal complexes to focal adhesions (Galbraith et al., 2002).

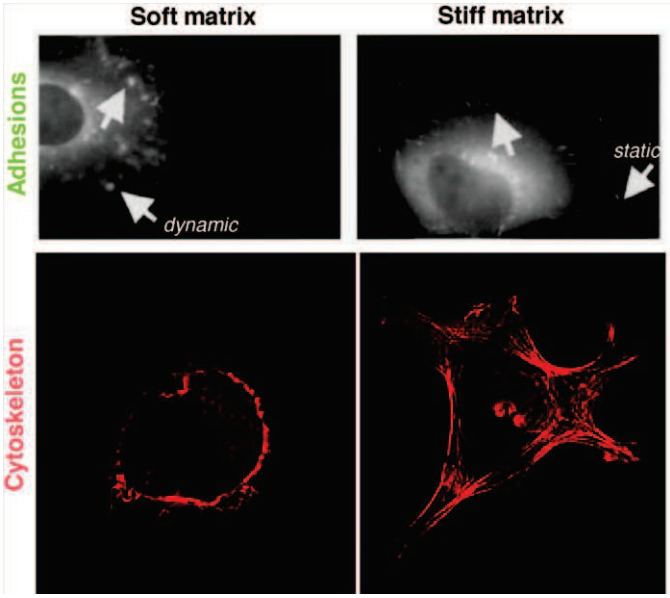

Figure 12: Modified from Discher (Discher et al., 2005). Adhesion and CSK structures on soft matrix and in a stiff matrix.

Although integrins and cadherins are the favorites for mechanoreception at the cell membrane for mediating cell and matrix and cell-cell interactions, there are other mechanoreceptors that have been found to transmit mechanical stimuli from the environment into cellular response. An example of a non-integrin mecanosensor is glycocalyx (Gasparski and Beningo, 2015). Glycocalyx is a sugar chain composed of membrane-bound macromolecules, including glycolipids, glycoproteins and proteoglycans with glycosaminoglycan side chains (Pahakis et al., 2007; Pries et al., 2000). This diversification is because the monosaccharides units can be joined in different combinations of covalent linkages and at multiple points. This variety of sugar polymers enables them to have the highest capacity for carrying information (Bourrillon and Aubery, 1989; Fukuda, 1996). Due to their privileged position on the outer of the plasma membrane, sugar residues covalently bound to membrane proteins or lipids and play a significant role in intracellular and extracellular transport and in cell-cell adhesion and recognition (Bhavanandan, 1995). This molecule has been found to be an important mechanosensor in endothelial cells and in the

response to a shear flow. In this cell type, glycocalyx coats the apical surface in front of the lumen of the blood vessels, serving as interface between blood flow and the cell, sensing the flow and transmitting it to the surrounding intracellular structures (Yao et al., 2007). In normal situation the presence of glycocalyx serves as a modulator to the presence of flow and provides an adaptation mechanism by redistribution of glycocalyx to areas of cell surface that are more sensible to flow effects (Yao et al., 2007) Figure 13.

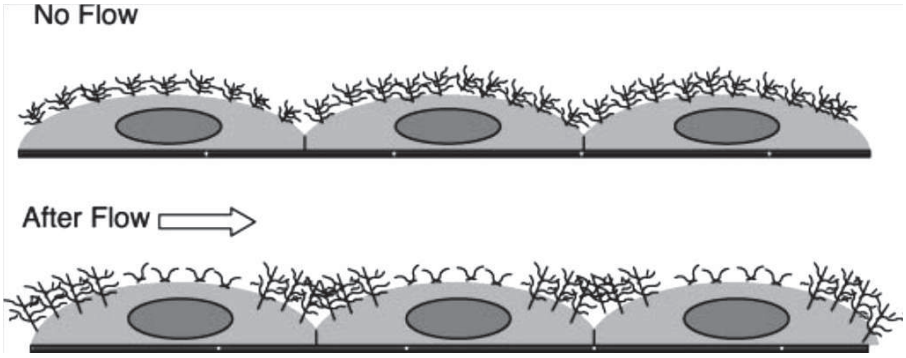

Figure 13: Modified from Yao (Yao et al., 2007). Schematic representation of the displacement of glycocalyx to adapt to the stress of a shear stress.

The contribution of glycocalyx to the cell response of a sheer flow is evidenced by degrading one of the compounds of this receptor. Before degrading the glycosaminoglycans through heparinase III, endothelial cells migrate slowly in the presence of flow and aligned in the same direction as the flow. After glycocalyx degradation, endothelial cells migrate at comparable speed than in the absence of flow (Sill et al., 1995), and do not align in the flow direction (Kang et al., 2011; Yao et al., 2007). So they lose their capacity of adaptation after decomposition of this element, Figure 14.

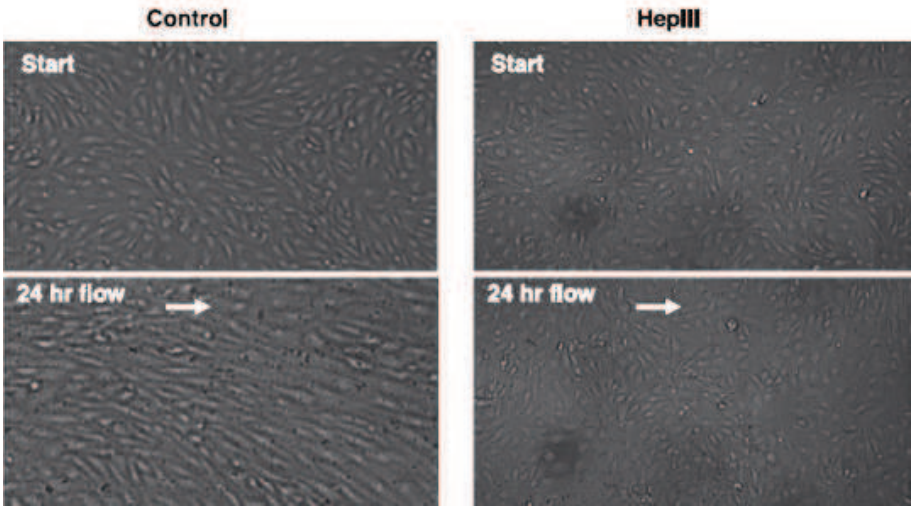

Figure 14: Modified from Yao (Yao et al., 2007). In the presence of a shear stress endothelial cells align in the direction of the flow. After glycocalyx degrading this adaptation process is stopped.

Glycocalyx is also present in lung epithelial cells, and due optimal surfacic position on cell layer, and interesting role in stress adaptation, it might be an key mechanosensor to explore for cells exposed to PFC. For bronchoalveolar cells the main glycocalyx component is the siliac acids, that seems to act as shield protector and to participate in the maintenance and development of lung architecture (Martins and Abairos, 2002). This sugar coating seems to work closely to surfactant due to the fact that besides a large component of mucopolysaccharides, typically present on glycocalyx, where found in alveoli, there was also an important presence of phospholipids, suggesting a close association of the alveolar mucopolysaccharides and phospholipids (Kalifat et al., 1970).

II.4.4 Models of cell adhesion initiation

Cell adhesion is a complex interplay between physics and biochemistry. Historically, at least two strategies have been followed to study the problem of cell adhesion. A first strategy consists on simplifying models which only share some of the fundamental properties with biological systems. This is the case with the adherence-induced deformation studies of lipid vesicles and/or red blood cells (Buxbaum et al., 1982; Evans et al., 1991), or antibody-coated

red blood cells in controlled hydrodynamic flow (Tha et al., 1986). These biologically-inspired simplified models provided some important information about bond formation and intracellular bond rupture in relation with the physics of interface. However, they failed to account for the adhesion complexity which characterizes nucleated cells. Lateral displacement of adhesion molecules depend on cytoskeleton constraints (Tank et al., 1982), and active processes (van Oss, 1991), that fundamentally differ from simplified models. Moreover, whereas the surface of vesicles and red blood cells is generally smooth, the surface of nucleated cells is covered by protrusions, blebs, ruffles, microvillus and lamellipodium with complex mechanical behavior and whose influence on adhesive interactions cannot be neglected (Mege et al., 1987). A recurrent question in understanding cell adhesion is to identify the key parameters influencing this process and how to obtain reliable parameters (Bongrand, 1995). We present below "energetic" approaches which, to our understanding are essential to understand cell-surface interactions: one is the classical surface energy approach which is issued from the physical field of interfaces and has a long standing interest for biologists. Second is the receptor-ligand binding approach controlled by force and bounded by a local mechanical environment.

II.4.4.1 Surface energy approach

The generalization of the cell culture practice has reinforced the interest for studying the mechanisms of interaction between a given cell population and culture dish. The study of cell response to PFC raises an additional question which concerns the apical effect of cell-medium interface.

The interfacial energy between two mediums is the free energy required to create an interface of unit area between the two. The work of adhesion between medium 1 and medium 2 is the work done by the system when two free surfaces of medium 1 and 2 are brought into contact (Bongrand, 1995):

$$W_{12} = \sigma_1 + \sigma_2 - \sigma_{12}$$ **Equation 5**

In cell cultures, adhesion occurs in liquid solutions (usually aqueous) which constitute a third medium, and the new adhesion energy between medium 1-2-3 can be described by (Bongrand, 1995):

$$W_{12}^3 = \sigma_{13} + \sigma_{23} - \sigma_{12}$$ **Equation 6**

where "3" represents the third medium. In this equation, the surface energies of liquids and free energies of liquid/liquid interfaces can be measured which yields to the estimate of adhesion energy (Figure 15).

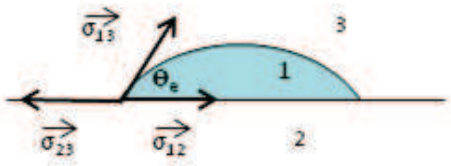

Figure 15: Representation of surface forces equilibrium between a solid surface and liquid/liquid interfaces.

Using the Young-Dupré equation describing an elementary three medium system (S: solid, L: liquid, V: vapor) (Equation 2), adhesion energy can be obtained:

$$W_{LS} = \sigma_{LV}\left(1 + cos\theta_e\right)$$ **Equation 7**

In which σ_{LV} and θ_e can be measured experimentally. However, application of these principles to biological systems is questionable because the multiplicity of specific interactions is not taken into account by the above equations.

A simple approximation, initially proposed by Raleigh and al. and later developed by Good et al. (Good, 1977) can be used, yet for a limited series of liquid media (either polar or non-polar fluids). Accordingly, the free interfacial energy σ_{12} can be written as a function of surface energies σ_1 and σ_2:

$$\sigma_{12} = \left(\sqrt{\sigma_1} - \sqrt{\sigma_2}\right)^2$$ **Equation 8**

Combining Equation 6 and Equation 8 leads to the work of adhesion between two mediums "1" and "2" embedded in a medium "3".

$$W_{12}^3 = 2\left(\sqrt{\sigma_3} - \sqrt{\sigma_1}\right)\left(\sqrt{\sigma_3} - \sqrt{\sigma_2}\right)$$ **Equation 9**

Equation 9 predicts that the work of adhesion is positive, i.e., medium "1" and "2" embedded in medium "3" will remain together, under one of the 2 conditions: $\sigma_3 > \sigma_1$ and $\sigma_3 > \sigma_2$, or $\sigma_3 < \sigma_1$ and $\sigma_3 < \sigma_2$. Interestingly, based on surface tension properties of liquid medium tested in this study, it will latter appear that DMEM and PFC might satisfy both conditions respectively. Otherwise, the conditions: $\sigma_1 < \sigma_3 < \sigma_2$ or $\sigma_2 < \sigma_3 < \sigma_1$ would lead to negative work of adhesion, (i.e., decrease in adhesion or repulsion).

Experiments were performed on blood neutrophils and platelets (Neumann et al., 1979), adherent to a series of polymer surface immersed in a saline solution supplemented with various amounts of dimethyl sulfoxide (σ_3=63-73 mN/m). Results obtained were in agreement with the above theory, since they show that adhesion was increased, i.e., $W_{12}^3 > 0$, when substrate surface energy (e.g., σ_2) was increased, i.e., $\left(\sqrt{\sigma_3} - \sqrt{\sigma_2}\right) < 0$, if the medium surface energy σ_3 was lower than the estimated free energy of the cell surface, e.g., σ_1, leading to negativity for the second factor of W_{12}^3, namely $\left(\sqrt{\sigma_3} - \sqrt{\sigma_1}\right) < 0$. Note that for values of medium surface energy σ_3 greater than the estimated free energy of the cell surface, e.g., σ_1, we have: $\left(\sqrt{\sigma_3} - \sqrt{\sigma_1}\right) > 0$ leading to $W_{12}^3 < 0$ which means a decrease in adhesion. This type of estimation, although rudimental, has been confirmed for treated erythrocytes (Schakenraad et al., 1988) as well as for different cell lines (Absolom et al., 1985). Interestingly, if the surface energy σ_3 of the bulk medium is equal to the surface energy of

one of the two media ($\sigma_3 = \sigma_1$ or σ_2), Equation 9 predicts that the work of adhesion becomes zero. Because cell adhesion was observed even though the estimation of the work of adhesion was zero (Absolom et al., 1985), these findings reveal a result of prior importance for the direction of future studies on cell adhesion, because it suggests that other types of interactions play a role in cell-substrate binding. A more recent cell adhesion model based on a receptor-ligand bond controlled by force and inserted in its mechanical environment is presented next.

II.4.4.2 Receptor-ligand binding approach

This approach is based on a concept initially proposed by Bell (Bell, 1978) to estimate the effect of a force on the lifetime of a molecular bond. Using experimental data on the effect of various loads on bond lifetime (Zurkhov, 1965), Bell proposed an empirical expression describing the effect of a disruptive force on the rate of bond dissociation k_{off} in s^{-1}:

$$k_{off} = k_{off}^0 exp\left(xF/k_B T N_b\right) \qquad \textbf{Equation 10}$$

In Equation 10, x is an arbitrary distance of 0.5 nm (=5Å), N_b is the bond number, and k_{off}^0 is the (natural) dissociation rate at zero force. It was latter demonstrated that the validity of this formula can be extended to the probabilistic approach in which the bond number fluctuates randomly (Cozens-Roberts et al., 1990). After William (Williams, 2003), Isabey et al. (Isabey et al., 2013) have shown that a Bell type model can still be used to describe the kinetics of multiple non cooperative bonds with opposed (parallel and zipper) configurations, breaking randomly under the effect of a mechanical force. Important parameters issued from the Bell model applied to 1 bond are the pre-factor $k_{off}^0 = \left(\frac{1}{t_D} \Big/ exp\left(\frac{\Delta U}{k_B T}\right)\right)$ (or natural dissociation rate) which depends exponentially of the potential energy of the molecular bond ΔU. The reference force $f_\beta = k_B T / x_\beta$ obtained from the ratio of thermal energy $k_B T$ to the distance x_β at which energy barrier ΔU is detected. Whether one or several bonds are considered in the

bond-based adhesion model, the deterministic approach taken into account by the Bell model, remains consistent with the probabilistic approach usually described by a first order Markov process. According to this theory, the probability of bond survival $P(t)$ can be described by two equivalent equations which relate $P(t)$ to $k_{off}(f)$ (Equation 11), for a single bond:

$$\frac{dP(t)}{P(t)} = k_{off}\left(f(t)\right)dt \text{ leading to : } P(t) = exp\left[-\int_0^t k_{off}\left(f(t')\right)dt'\right] \quad \textbf{Equation 11}$$

Imposing a force ramp to a bond system, (e.g., by Atomic Force Microscope) such that $r_f = cste = df/dt$, enables to replace the force variable for the time variable and leads to the definition of the most probable rupture force:

$$f^* = f_\beta \ ln\left[\frac{r_f}{k_{off}^0 f_\beta}\right] \quad \textbf{Equation 12}$$

Equation 12 demonstrates a fundamental property of bond rupture force, which is the dependence of the adhesion strength by the logarithm of the loading rate. This theoretical result has numerous practical consequences in bond stretching experiments, such as the reinforcement of bonds with the increase of the loading rate. For consistency with the lifetime approach, it is easy to demonstrate that f^* is proportional to a most likely lifetime $t_{off}^* = 1/k_{off}^*$ through $f^* = r_f \cdot t_{off}^*$.

A number of experiments on biological systems essentially conducted on a variety of isolated bond systems by Atomic Force Microscope (AFM) (Lee et al., 2007; Noy and Friddle, 2013), optical trap force probe (Abbondanzieri et al., 2005; Evans and Kinoshita, 2007; Kuo and Sheetz, 1993), biomembrane force probe (Bayas et al., 2006; Evans et al., 2005), Optical tweezers (Simmons et al., 1996) have brought, on a broad range of biological

systems, a confirmation of the experimental pertinence of the bond rupture theoretical approach.

A fundamental question was raised by Discher (Discher et al., 2005) concerning how contractile traction forces exerted by a cell tend to increase with the stiffness of the cell's substrate and how to model this cell sensitivity. A comprehensive model has been developed by Féréol et al. (Fereol et al., 2009). This theoretical model is inspired from the Bruinsma approach (Bruinsma, 2005) but the predictions are confronted to cell sensitivity experiments performed on substrate of various stiffness (from glass to soft gels). The proposed model integrates the potential energy of the receptor-ligand binding, a constant acto-myosin force generated intracellular, a viscoelastic extracellular matrix and the thermal noise. The results of this dynamic adhesion site model are compared to a standard stationary adhesion model. This stationary model could not predict cell sensitivity to environment stiffness, because the stress field is insensitive to stiffness. By contrast, the dynamic adhesion site model demonstrates the physical origin of the cell sensitivity in not fully mature adhesion sites (Figure 16).

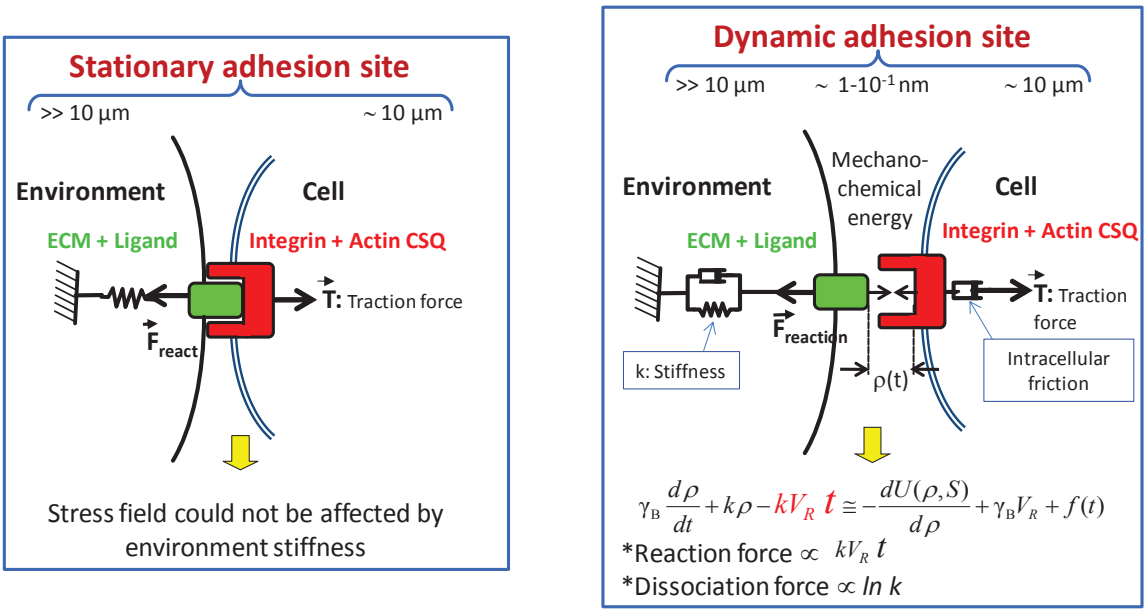

Figure 16: Modified from (Fereol et al., 2009). Schema of the stationary adhesion site (left) and the dynamic adhesion site model (right). The dynamic adhesion site model takes into account the chemico-physical link: cytoskeleton, adhesion site and extracellular matrix (ECM), and the associated forces and mechanical properties. The adhesion site and the actin bundle can move along the axis direction x under the action of constant traction T, exerted on actin bundle and the viscoelastic recoil exerted by the substrate on the adhesion site. The relative distance between the adhesion site and the actin bundle is called r(t). The link between adhesion site and actin filament bundle is described by a ''two state'' potential energy of mean force whose state varies between passive (S= -1) and active (S= +1).

This physical origin resides in the intimate coupling between the chemical energy of the bond, and the mechanical energy of the spring, here represented by the matrix stiffness on which a constant traction force is exerted. This traction generates a time-proportional reaction force which depends on both the elasticity of the matrix (stiffness k) and the retrograde velocity of actin (V_R) which can be related to molecular motor activity and therefore reflect intracellular tension. Noteworthy, the higher the matrix stiffness, the higher the reaction force, whereas, the higher the retrograde velocity of actin the higher will be the reaction force. Indeed, the product $k \cdot V_R$ acts as the specific loading rate of the stretched bond. The

expression of the most likely rupture force for this bond stretched in its local extracellular and intracellular environment is given by:

$$\frac{f^*}{f_\beta} \approx ln\left\{\frac{\mathrm{k}V_R}{k_{off}^0 f_\beta}\right\} + \frac{\langle \Delta \mathrm{U} \rangle}{k_B T}$$ **Equation 13**

Equation 12 and Equation 13 are consistent, and show that independently of the origin of the loading rate, the bond behavior remains dependent of the loading rate. In Equation 12 and Equation 13 the loading rate dependence of f^* is logarithmic, and thereby large changes in loading rates lead to only moderate increases in bond strength. Nevertheless, this model which combined stochastic and deterministic effects contains the essence of a mechanism of substrate-dependent sensitivity for adhesion sites which are not fully mature. This is the case for initial adhesion (IA), focal complex (FC), or podosomes. An important assumption of this non-mature adhesion site model is that force regulation occurs while the size of the adhesion site is maintained constant, suggesting that adhesion site reinforcement is not equivalent to adhesion size increase. Optical trap assays using micron-sized, ligand-covered beads of fixed surface area exhibit the same reinforcement phenomena as actual adhesion sites (Choquet et al., 1997). By contrast, there is a reversible size regulation in mature focal adhesion sites on which an external force is exerted. It has been shown that the size of mature focal adhesion reversibly increases and decreases as a function of the applied force (Geiger and Bershadsky, 2001). In a parallel study, the same group has shown the existence of a close correlation between force and focal adhesion intensity, as well as between direction of the force and adhesion site elongation. Moreover, focal adhesion area is linked on a time scale that is faster than a few seconds which corresponds to experimental resolution (Balaban et al., 2001).

III. MATERIALS AND METHODS

III.1 Materials

III.1.1 Cell culture of A549

A549 cell lines are human Alveolar Epithelial Cells (AEC) from ATCC issued from a human lung carcinoma but having the phenotype of alveolar type II epithelial cells (Lieber et al., 1976). Cells are grown at confluence in DMEM containing 10% FCS (Fetal Calf Serum), 1%PS (Penicillin Streptomycin), 2 mM L-glutamine, 50 IU/ml penicillin, 50 µg/ml streptomycin, and incubated in a 5% CO_2-95% air atmosphere. Routine subcultures (passages 89 to 92) are done at one twentieth split ratios by incubation with 0.025 g% trypsin–0.02 g% EDTA in calcium-and-magnesium free PBS for 10 min at 37℃ (Planus et al., 2005). When forming a monolayer, A549 cells adopt a polygonal shape and are closely packed, exhibiting a clear and uniform distribution of lamellar bodies (Stroetz et al., 2001) they express a variety of cytokines, growth factors and transmembrane integrin receptors onto their apical face, that enables attachment of ligand-coated microbeads (Wang et al., 1993). They possess functional pro-inflammatory signaling pathways and synthesize lecithin and phosphatidylcholine (Vlahakis and Hubmayr, 2000). Moreover, A549 cell lines have been shown to exhibit metabolic and transport properties consistent with type II AECs *in vivo* and, importantly do not functionally differentiate in culture into Type I AECs (Foster et al., 1998). A study showed that A549 cells still have the ability to form adherent and tight junctions when grown to confluence (Kawkitinarong et al., 2004). Therefore, despite the limitations inherent to the use of transformed cell lines, A549 cell lines offer many advantages for *in vitro* studying of the mechanical response of alveolar epithelium.

III.1.2 Cell viability of A549 cells

PFC (perfluoro-N-octan) is from F_2 Chemicals and contains no nutriments and is not soluble into aqueous liquids such as DMEM (Varani et al., 1996) and the Magnetic Twisting Cytometry (described in III.2.3.1) machine is confined to the use of a 6 mm-diameter well that cannot be replaced by a transwell chamber. Preliminary viability tests using both trypan blue test, MTT test, were performed to know the limit in terms of cellular viability of A549 exposed exclusively to PFC. We verified that cellular viability until 3h (hours) of sole PFC exposure is comparable to an exposure to DMEM, as expected from previous reports underlying the absence of toxic effects of PFC (Krafft, 2001). Beyond 3h of exposure to the sole PFC, viability test reveal that cells are suffering due to the lack of nutritive elements in PFC while these elements are constitutively present of DMEM. For durations of PFC exposure above 3h, we use double chamber with a permeable membrane separation with the nutritive DMEM on the bottom chamber and PFC on the top chamber.

III.1.3 Exposure of A549 cell to hypoxic conditions

Cells seeded for different assays described in Methods (section III.2) were placed all along the exposure duration in an hypoxic incubator at 1% O_2-5% CO_2 (kindly lent by team 03 of IMRB). The mediums to which cells are exposed namely PFC and DMEM+0.5BSA were placed inside this hypoxic chamber during 2 full days before the experiments, in order to guarantee the presence of a low percentage of oxygen dissolved in the medium at the beginning of each exposure procedure.

III.1.4 Cell culture of alveolar macrophages (AM)

Alveolar macrophages are issued from mouse RAW 264.7 (ATCC). Cells are seeded at a density of $7x10^4$ per chamber, in a 6 mm-diameter well coated with fibronectin at 1.6 ug/cm^2.

Cells adhered after 2h of incubation in DMEM, 10% FCS and 1% PS. FCS medium is then replaced by DMEM+0.5%BSA 0.5h before experiments. In the PFC-exposed cell group, cells are exposed to PFC for two different durations: 0.5h and 1.5h.

III.1.5 Cell culture of bronchial epithelial cells (HBE)

Bronchial epithelial cells HBE14o- are human bronchial cells (gift from Dr. C. Grunaert, University of California). Cells are seeded at a density of 7×10^4 per chamber, in a 6 mm-diameter well coated with type I Collagen at 20 ug/cm^2. Confluence is reached after 24h of incubation in DMEM, 10% FCS and 1% PS. FCS medium is replaced by DMEM+0.5%BSA 0.5h before the experiments. In the PFC-exposed group, cells are exposed to PFC for two different durations: 0.5h and 1.5h.

III.2 Cell Experimental Methods

III.2.1 Cell migration and repair

A549 cells are seeded in a 12-well transwell chambers (Figure 17) (Corning) with a diameter of 12 mm, at a density of 10^5 per chamber. A confluent monolayer is reached after 72h of incubation in DMEM, 10% FCS and 1% PS (Sigma Aldrich).

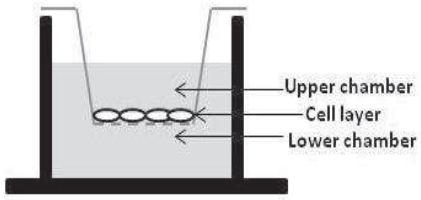

Figure 17: Transwell chamber

The cell monolayer is scratched with a pipette tip of 5 μm-diameter to create a wound and rinsed 3 times with medium in order to remove the entire detached cell population., With this type of double chamber system, the cell monolayer is exposed to the two liquids of interest from the top chamber: i.e., DMEM+0.5%BSA (control group) or liquid PFC (PFC group), while in both conditions, cells are constantly exposed to DMEM+10%FCS beneath the transwell filter. Transmission images of the cell monolayer are taken 3 times per day with a CDD camera (Zeiss) and a fluorescent-transmission microscope AxioVert 200 (Zeiss). The quantification of the repair of the monolayer is made by measuring the wound area at different times using ImageJ (W.S. Rasband; NIH, Bethesda, MD; http//rsbweb.nih.gov/ij/). The evolution of the repaired area is quantified using the following equation.

$$\text{Repaired area}(\%) = \frac{\text{Initial area - Current area}}{\text{Initial area}} \times 100\% \qquad \textbf{Equation 14}$$

The wound repair was followed until complete closure (Repaired area=100%).

III.2.2 Cell structure: staining of F-actin, focal adhesion and glycocalyx

A549 epithelial cells are seeded in DMEM, 10% FCS and 1% PS at a density of $8x10^4$ over 16 mm glass coverslides coated with fibronectin at 1.6 ug/cm^2. DMEM+10%FCS medium is replaced by DMEM+0.5%BSA the night before experiments. Cells are exposed either 2h to PFC, or to DMEM+0.5%BSA (control group). The effects on F-actin network and on focal adhesion are evaluated and measured by quantifying the fluorescence of alexa 543-phalloidin, and of antibody against phosphotyrosin PY99 (sc-7020, Santa Cruz Biotechnology) coupled with a secondary antibody Alexa Fluor 488 of paraformaldehyde fixed cells. For the focal adhesion and F-actin network analysis, images are acquired with an Axio Imager confocal microscope from Zeiss at 63x magnification. We analyze the phosphotyrosin PY99 staining using the threshold method, and the particle analyzer of ImageJ. Coverslides are mounted on a slide with the cell side down in prolong Thermo Fisher. Glycocalyx distribution is evaluated in live cells by staining glycocalyx using fluorescein isothiocyanate-labelled wheat germ agglutinin (WGA-FITC) at a concentration of 5 µg/ml incubated during 10 min 37°C in a 5% CO_2 – 95% as in (Rai et al., 2015).

III.2.3 Cell mechanical evaluation

We present in the following sections the principle of MTC and cellular preparation III.2.3.1, the measured parameters III.2.3.2, the models behind the parameters III.2.3.3, the adhesion model III.2.3.3.1, and the microrheological models III.2.3.3.2.

III.2.3.1 Measure in adherent cells by Magnetic Twisting Cytometry (MTC)

Cells are seeded at a density of $7x10^4$ per 6 mm-diameter plastic well coated with fibronectin at 1.6 ug/cm^2. Confluence is reached after 24h of incubation in DMEM, 10% FCS and 1%PS

(Penicillin Streptomycin). DMEM+10%FCS medium is replaced by DMEM+0.5%BSA the night before the experiments. Cells are exposed to PFC at different times, from 5 min to 2h. For the surfactant studies, a layer of surfactant is added at the cell monolayer surface before adding DMEM or PFC for 0.5h or 1h30. A minimal quantity of surfactant, poractant alfa (Curosurf®), adhered to the cell layer. The excess of surfactant is removed by aspiration and 3 successive washings. To verify that a thin layer of surfactant remains adherent despite the washing procedure and PFC exposure, the surfactant was made fluorescent using fluorescein (SERB), and its presence was verified under fluorescent microscope. Ferromagnetic beads of 4.5 µm-diameter (Spherotech) are coated with fibronectin at a concentration of 0.4 mg/ml. Fibronectin being a protein recognized by the integrins, notably expressed by the apical layer of A549 cells. After the exposure of the cells to different mediums, beads are left to adhere for 30 min at 37°C in a 5%CO_2-95% air incubator. Unbound beads are washed away with serum-free medium: DMEM+0.5%BSA. Ferromagnetic beads are then magnetized using a short pulse (150 ms) of a 0.15 T-uniform magnetic field (i.e., above a residual magnetic field of 0.13 T corresponding to the upper limit of hysteresis). This magnetization field is horizontal, i.e., parallel to the monolayer of adherent cells (Figure 18). A magnetic torque, C ($C = \mu_0 mH \sin\Phi(t)$), (μ_0 :permeability constant ; m : magnitude of the bead magnetic moment; H : amplitude of the magnetic field; Φ : rotation angle, see Figure 19), is then generated by a predetermined current intensity in Helmholtz coils, which generates a vertical uniform twisting magnetic field H ($H \leq 6.3$ mT), whose intensity is at least two orders of magnitude lower than the magnetization field in order to prevent re-magnetization. This magnetic torque induces cytoskeleton (cellular) displacement reflected by a "mean" but instantaneous bead rotation angle which is measured as a time-dependent signal from the decay in remnant magnetic field (Figure 19). Because the remnant magnetic field is continuously measured by a magnetometer, the ratio between instantaneous bead magnetic

moment projected in the culture plane B(t) and initial bead magnetic moment, B_0 enables to obtain - through arccos(B(t)/B_0) - an homogenized quantity corresponding to the "mean" cell/CSK deformation (Ohayon et al., 2004). B(t) is measured with a magnetometer equipped with low noise probes, i.e., ≈0.14 nT, for a B_0 of the order of 1 nT.

Figure 18: A) Cell culture with adherent magnetic beads. B) Magnetization of the beads in the same direction using a strong magnetic field. C) Twisting magnetic torque that causes the bead rotation which reflects an homogenized cellular response and, after appropriate analysis, the mechanical and adhesion parameters of these living adherent cells (see section III.2.3).

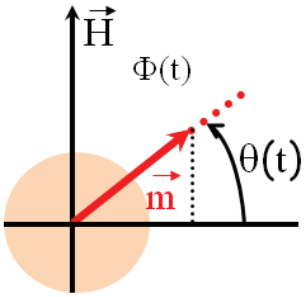

Figure 19: Evaluation of instantaneous "mean" bead rotation from measure of the projected magnetic bead moment. m : magnitude of the bead magnetic moment; H : amplitude of the magnetic field; Φ : rotation angle.

The beads that adhere to the cell are sensed by the cell as small matrixes. The integrin-ligand bonds are stretched during the minute of application of the magnetic torque. Most of the bonds survive and transmit the torque to the cytoskeleton whose viscoelastic properties are

reflected by the bead rotation Figure 20. The rheological models used are (i) a viscoelastic solid with 1 Voigt element, in agreement with the rather limited small frequency content of the MTC signal (see Fourier analysis of MTC signal Figure 21) or an infinite series of "n" viscoelastic elements with relaxation times continuously distributed according to a power law (Balland et al, 2006).

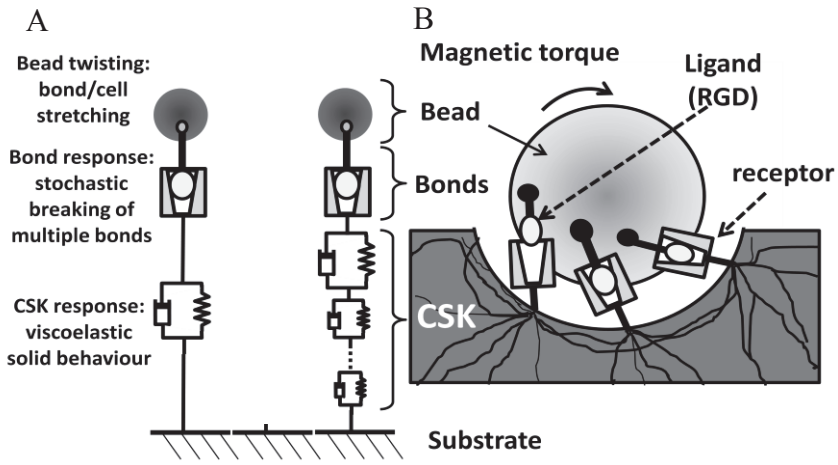

Figure 20: A) Equivalent molecular and cellular models used to analyze the cellular response to the loading by ferromagnetic bead. In the right is represented the viscoelastic model, and left the power law model, with an infinite series of Voigt elements. B) Sketch of the bead-cell system. The pertinent parameters for the mechanical and adhesion analysis are defined in section III.2.3. They are obtained from the MTC signal by the best curve fitting.

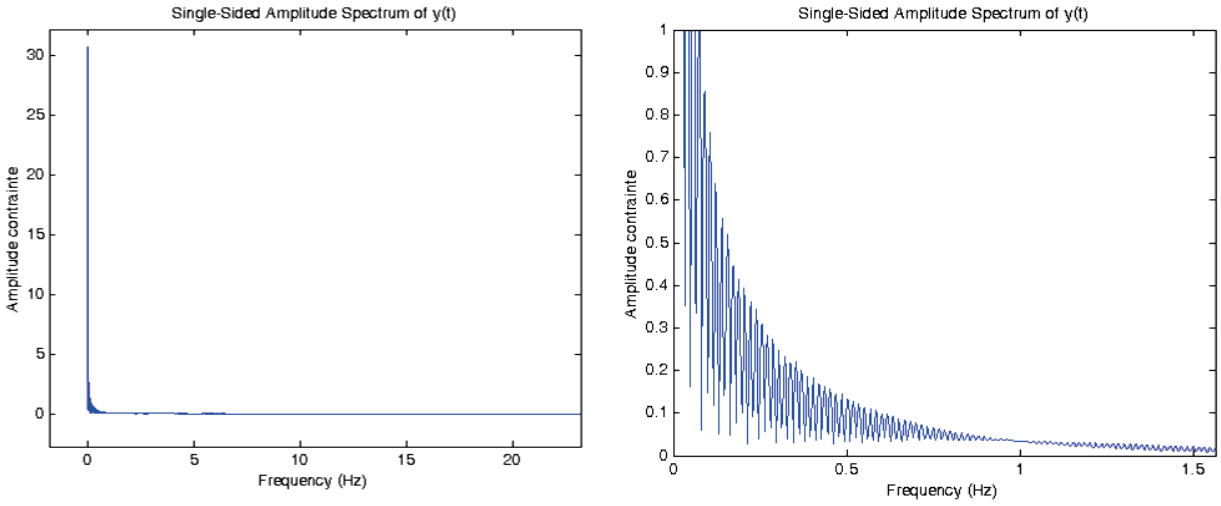

Figure 21: Left: Fourrier analysis of the MTC applied stress. Right: amplification of the image at the left for the low frequencies area. This analysis shows the reduce content of harmonics frequency above 0.5Hz, suggesting the frequency content of the signal is in a small range of frequencies of low values. At representative frequency of the 1 min of applied stress (1/60 s=0.02 Hz), the signal has no high frequency content.

III.2.3.2 Parameters measured by Magnetic Twisting Cytometry (MTC)

MTC generates a 1min stress step of physiological magnitude followed by relaxation (Figure 22 A, blue), and provides a creep response (Figure 22 A, red) from which simultaneous assessment of cell adhesion parameters and cell mechanical properties are deduced. The applied stress is the apparent stress (magnetic torque / bead volume): $\sigma(t) = \frac{\mu_0 m H(t) \sin\Phi(t)}{\frac{4}{3}\pi R^3 \xi}$ corrected for geometrical effects by a factor (ξ) which depends on the degree of bead immersion and the cell type, as previously described in (Laurent et al., 2003; Laurent et al., 2002; Ohayon et al., 2004). For the bead-cell adhesion system (e.g., integrin-fibronectin binding), this step loading is basically a clamp. This clamp generates some bond detachment shown by the non complete recovery of bead position after loading (Figure 22 B) interpreted as a partial bead sliding from which a probability of detachment and beyond adhesion parameters are determined. The model used to quantify this de-adhesion is a probabilistic model rewritten for multiple uncooperative bonds breaking stochastically and for which Bell-type model provides a satisfactorily description, see (Isabey et al., 2016). The mechanical and adhesion parameters associated to each model are adjusted by best curve fitting on the experimental MTC signal considering that at each instant, the estimated bead rotation angle is the sum of a recoverable component and a non-recoverable component (Figure 22 C and D).

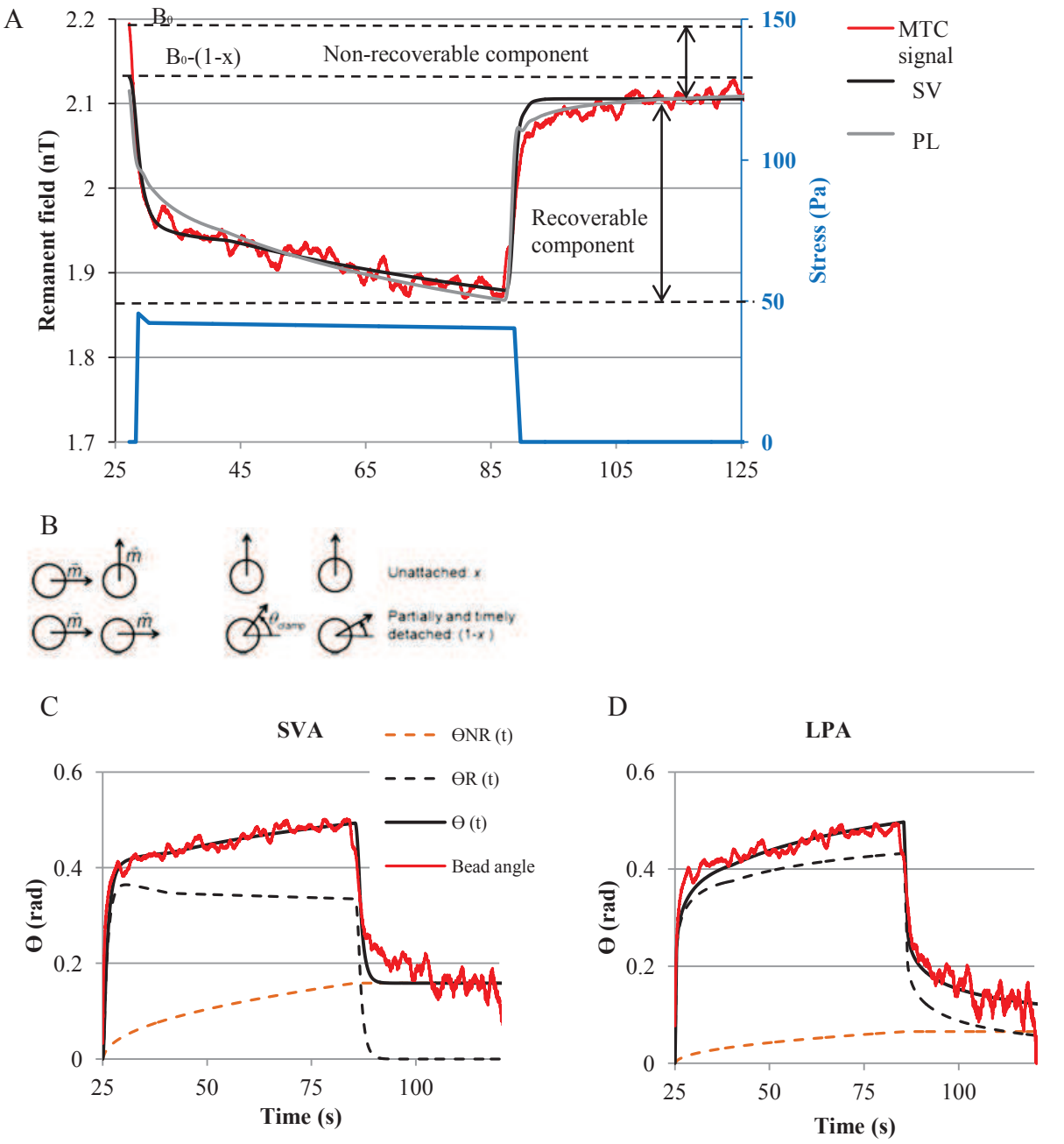

Figure 22: Diagram of the signal obtained during MTC assays (in red). A step stress loading acting as a clamp for the bonds is applied during 1 min (in blue) causing decay in the remnant magnetic field representing bead rotation and thus cell deformation. After loading, i.e. in the relaxation period, there is a partial recovery of the signal. The recoverable component of the signal gives the mechanical parameters while the non-recoverable component of the signal leads to adhesion parameters. Some bonds are supposed to break randomly during the minute of torque application.

B) Sketch of the changes in the direction of bead magnetic moment $\vec{m}$ throughout the entire MTC experiment. *x* is the percent of free (unattached) beads rotating by 90° as soon as the magnetic torque is applied (*t* = 0). The remaining beads *(1 − x)* contribute to the time-dependent cell response signal through a reversible component $\theta_R(t)$ which describe the mechanical response, and a non-reversible component $\theta_{NR}(t)$ which is related to the probability of bond detachment. θclamp is the bead position reached near equilibrium after 1 min of torque application. The bead position during relaxation differs from the initial bead position because partial bead detachment occurs during the clamping period.

C and D) The rotation angles recalculated after best curve fitting by the 2 microrheological models used (C: visco-elastic Voigt model, SV ; D: power law model, PL). The cellular deformation shown in A for magnetic field (in red) is in C and D expressed in terms of bead deviation angle (in radians) and shown versus time in seconds. The experimental signal is obtained after transformation of the relative change in remnant magnetic field into bead rotation angle. These two quantities are related through the arcosine function. The thick continuous black curve corresponds to the bead rotation angle: θ(t), obtained with the two microrheological models : on left (SV) and on right hand side (PL). The two components of the bead rotation angle are recalculated using the mechanical and adhesion parameters obtained by the curve fitting: a reversible component $\theta_R(t)$, a non reversible component $\theta_{NR}(t)$.

The parameters provided by the de-adhesion model are: (i) the natural dissociation rate K_{off}^0 (s^{-1}) which essentially reflects the chemical energy of the adhesion state between integrin and the matrix ligand, partially modulated by bond number and bond configuration, and (ii) the reference stress σ_c (Pa) which also depends on bond number and bond configuration (e.g., zipper or parallel), and is proportional to the bond number for the parallel configuration (Isabey et al., 2013).

The unbroken bead-cell adhesion system (Fibronectin-integrin-F-actin binding) transmits the cytoskeleton deformation in response to the loading. Two different micro-rheological models are used to describe this system. The mechanical parameters depend on

the micro-rheological model used. The first micro-rheological model used is a viscoelastic solid-like model (Single Voigt element, SV, see Figure 20A, left) which has been widely used in early MTC experiments (Wang et al., 1993). The solid-like behavior is defendable because the MTC loading through integrins specifically addresses structural properties of the cytoskeleton (Canadas et al., 2006). The choice of a unique relation time is in agreement with the low frequency content of the 1 min-stress step signal. Two independent parameters are extracted from this viscoelastic solid-like model: the cytoskeleton elastic modulus or cytoskeleton stiffness (E in Pa), which has been shown to be proportional to intracellular tension or prestress (Wang et al., 2002), and the viscoelastic relaxation time (T in s). The second micro-rheological model used is an infinite series of viscoelastic solids (see Figure 20A, right) with relaxation times distributed according to a power law model (PL): $T = T_m i^{\left(\frac{-1}{1-\alpha}\right)}$ where T_m represents the largest relaxation time in the cell, most likely close to the SV relaxation time (Balland et al., 2006; Fabry et al., 2001). Two mechanical parameters are provided by the power law model (Fabry et al., 2001): the exponent α of the power law that is related to the nature of the cell α [=0 for solid], α [= −1 for liquid], and the prefactor A_0 which is inversely related to the elasticity modulus at 1 Hz (G_0). Alternatively, the frequency-dependent complex storage modulus $G_e(\omega)$ leads to the modulus $|G_e|$ which is calculated at an arbitrary frequency of 1 Hz.

III.2.3.3 Description of the models behind the MTC parameters

III.2.3.3.1 The de-adhesion model

The de-adhesion model aims at accounting for the imperfect recovery of the bead deviation signal, a phenomena which is observed almost systematically in cells during MTC assays. The global dissociation rate describing de-adhesion is assumed to obey a Bell-type model, rewritten for the applied stress (instead of a force as in Equation 10) calculated from the

attachment area at the bead–cell interface. A major assumption of the de-adhesion model is that multiple bonds behave as unique one:

$$K_{off}(\sigma) = K_{off}^{0}\ exp\left(\frac{\sigma}{\sigma_c}\right)$$ **Equation 15**

The stress-dependent dissociation rate $K_{off}(\sigma)$ is exponentially increased by the normalized stress σ/σ_c. The kinetics of bond rupture can thereby be characterized by the prefactor K_{off}^{0}, or natural dissociation rate, and a reference stress σ_c. The relationship between the dissociation rate and the probability of bond detachment is described by a first-order Markov process which relates the presumably unique time-dependent dissociation rate to the probability of bond survival $P(t)$:

$$\frac{dP(t)}{P(t)} = K_{off}\left(\sigma(t)\right)dt \text{ or equivalently } P(t) = \exp\left[-\int_0^t K_{off}\left(\sigma(t')\right)dt'\right]$$ **Equation 16**

This approach assumes that a multiple bond behaves as a unique equivalent bond, whose dissociation rate - derived from the Kramer Smoluchowski theory - is modified to take into account the multiplicity of bonds. We recently applied this approach to two typical cases of bond configurations, namely the parallel and the zipper configurations which correspond to a fully homogeneous and fully heterogeneous distribution of force amongst the bonds, respectively. In the case of a force/stress clamp such as the one exerted during MTC, solving Equation 16 allows us to deduce $K_{off}(\sigma)$ from the slope of the linear $\ln P(t)$ - t relationship.

$$P(t) = \exp\left[K_{off}\left(\sigma\right)\times t\right] \text{ with } P(t) = cos\left(\theta_{NR}(t)\right)$$ **Equation 17**

where $\theta_{NR}(t)$ is the time-dependent non reversible component of the bead rotation angle corrected for the contribution of free-rotating beads.

III.2.3.3.2 The two microrheological models

The two microrheological models used in the present study aim at describing the viscoelastic solid-like or power law behaviors of the cells in response to the applied stress step. The solid-like model takes into account the recoverable component of the bead rotation $\theta_{R(t)}$, and let the entire non-recovery component to the de-adhesion phenomena. The power law acts as if a part of the non recovery phenomena still belongs to the microrheological behavior of the cell, letting only a few (possibly insufficient) information to de-adhesion phenomena. The relationship between the strain $\theta_{R(t)}$ and the stress σ depends on the total history of the loading up to time *t* (creep function) (see Figure 22 C and D):

$$\theta_{R(t)} = c(t)\sigma_0 + \int_0^t c(t-t')\frac{d\sigma}{dt'}dt' \qquad \textbf{Equation 18}$$

Where *c*(t) is a creep function which depends on the type of microrheological model used: the viscoelastic solid-like model with a unique relaxation time T (Single Voigt element noted SV model) or the power law equivalent to an infinite series of "n" Voigt elements with relaxation times distributed according to a power law model (Balland et al., 2006) (Power Law model noted PL model).

III.2.3.3.2.1 The Single Voigt model (SV model)

For a single compartment with a viscoelastic solid-like behavior, the creep function is given by:

$$c(t) = \frac{1}{E} + \frac{t}{\eta}, \text{ i.e., } \theta_R(t) \approx \frac{\sigma_0}{E}\left(1 - exp\left(-\frac{t}{\mathrm{T}}\right)\right) \qquad \textbf{Equation 19}$$

E is the elastic modulus of the CSK structure and η is the dissipation (loss) modulus due to friction in between CSK elements and cytoplasm in a confined volume with steric properties. $T \approx \frac{\eta}{E}$ is the unique relaxation time.

III.2.3.3.2.2 The Power Law model (PL model)

For the power law the creep function is given by:

$$c(t) = A_0\left(\frac{t}{t_0}\right)^{\alpha}, \text{ i.e., } \theta_R(t) \approx \sigma_0 A_0\left(\frac{t}{t_0}\right)^{\alpha} \quad \textbf{Equation 20}$$

The exponent α reveals the nature of the cell material as it is allowed to cover from solid-like (α=0) to fluid-like (α=1). The prefactor A_0 is inversely proportional to an elasticity modulus, and t_0 is an arbitrary response time conventionally fixed at 1s. The viscoelastic complex modulus $Ge(\omega)$ is given by:

$$Ge(\omega) = \frac{\sigma(\omega)}{\theta_R(\omega)} \quad \textbf{Equation 21}$$

The norm of $Ge(\omega)$ is given by:

$$|Ge| = \frac{\omega^{\alpha} t_0^{\alpha}}{A_0 \Gamma(1+\alpha)} \quad \textbf{Equation 22}$$

here $\Gamma(1+\alpha)$ is the Euler-Gamma function given by: $\Gamma(1+\alpha) = \int_0^{+\infty} e^{-x} x^{\alpha} dx$. $\omega = 2\pi f$ is the pulsation, where f is the frequency in Hz. $|Ge|$ in Pa is calculated at f=1Hz using the values of α and A_0 obtained by best curve fitting. The parameter $|Ge|$ will be used with α to characterize the power law behavior of the cells.

III.2.4 Magnetic Twisting Stimulation (MTS)

Magnetic Twisting Stimulation (MTS) was initially proposed by Chen et al. (Chen et al., 2001) to mechanically stimulate gene expression in endothelial cells. Note that this MTS does not permit to measure cell mechanics because it is not equipped with magnetic probes which enable to measure cell deformation. The laboratory-made MTS device has been used to study

the influence of a sustained mechanical stress on the permeability of microvascular endothelial cells (Wang et al., 2012). Indeed, this method which derives from MTC, enables to exert cyclic stress through ferromagnetic beads for hours moreover in a CSK-specific manner, and uniformly over the whole cell culture (Figure 23). A sinusoidal stress of 1h of amplitude around 10 Pa and at a frequency of 3 Hz, is used in pulmonary cells as an equivalent of 1 day of mechanical ventilation in a patient. The amplitude of the associated oscillating stress is approximately given by the magnetic torque divided by the bead volume (Laurent et al., 2002): $\sigma = \frac{\mu_0 mH}{\frac{4}{3}\pi R^3 \xi}$. ξ is a correcting geometric factor for bead immersion in the cytoplasm, R is bead radius, H amplitude of the magnetic field, m the bead magnetic moment. The MTS device is composed of a Petri dish holder, a microbead magnetization system, a system for creating an oscillating magnetic field perpendicular to the cell culture plan, a temperature control device (cooling), and an incubator.

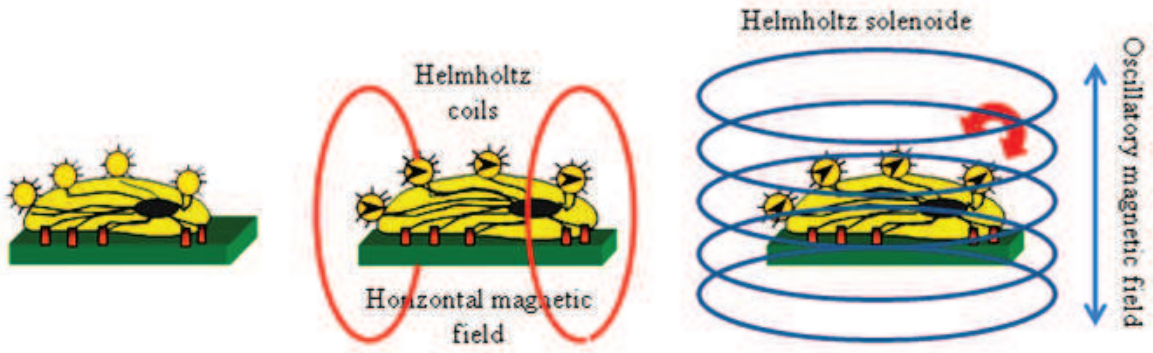

Figure 23: MTC and MTS share a common principle except that cell deformation cannot be measured during MTS, but only after, by using MTC on the same culture: A) Cell culture with adherent ferromagnetic beads. B) Magnetization of the ferromagnetic beads in the direction of the culture plane using a strong magnetic field. C) Applied mechanical and homogeneous stretch induced by a cyclic stress.

III.2.5 Procedure for the MTC measurements

Cytochalasin D (cytoD) from Sigma Aldrich was used to depolymerize the F-actin network for 20 min at a concentration of 10 µg/ml, the response was measured using MTC. Heparan sulfate of glycocalyx was degraded using Heparinase III from Sigma Aldrich as in (Yao et al., 2007) at a concentration of 5 mU/ml for 30 min, the response was measured by MTC.

III.2.6 Procedure for the MTS measurements

For the PFC-exposed group, cells are exposed to either 0.5h or 1.5h of PFC, for the control group, cells remained on DMEM+0.5%BSA medium. Beads were left to adhere as previously described. After the standard 3 successive washings, the cell mechanical and adhesion parameters are evaluated using the MTC device, as described in III.2.3.1. After this first evaluation, every cell sample was left in incubator at 37°C, 95% Air -5%CO_2, for the MTS stimulation. After a short initial magnetization procedure of the ferromagnetic beads, a cyclic magnetic torque is applied for 1 h throughout the coated beads (Figure 23). The cyclic stress is of fixed amplitude and frequency: presently around 10 Pa and 3 Hz, respectively, over the whole culture. Then, a second measurement using the MTC device is made to obtain the mechanical properties after sustained mechanical stimulation on the CSK.

III.2.7 Statistics

Data are presented as mean ± standard deviation. Assessment of cellular and molecular parameters are obtained by using the best fit between the model and MTC signal using a least squares method based on the Levenberg-Marquardt algorithm. All correlations between the data and the model smaller than 95% are rejected. Statistical differences between different MTC groups (control and PFC exposure) are assessed using ANOVA tests. For the analysis of the same group after the action of drug such as cytoD or heparinase III we used Wilcoxon tests. For fluorescent images, the differences between groups are analyzed using Mann-Whitney U tests.

III.3 Physical methods

III.3.1 Experimental measurement of surface tension of fluids

III.3.1.1 The capillary rise method

Amongst a number of methods proposed to measure, relatively to air, the surface tension of liquids, (e.g., Noüy ring method, Wilhelmy plate method, Pendant drop method, Bubble pressure method (Jaeger's method), Stalagmometric method, Sessile drop method, Capillary rise method…), we used the capillary rise method because we found it more adapted to the microscopic imaging methods of a cell laboratory. Moreover, the capillary rise method enables to measure surface tension between 2 liquids, by creating a double drop system inside the capillary (Bico and Quéré, 2000). Since a precise knowledge of the contact angle between liquid and air (de Gennes, 1985) or at the interface between the 2 liquids is critical for the accuracy of the measure (Bico, 2000), our idea has been to measure the contact angle inside the capillary by microscopy using transmission and/or fluorescence (whenever possible), after appropriate optical correction for the double spherical diopter that the two capillary walls form. The condition to satisfy for measuring surface tension in a capillary tube is that surface tension effects dominate over gravity effects. This assumption is verified if the radius of the capillary (R_{cap}) is smaller than the capillary length (δ) of the liquid, i.e., $R_{cap} < \delta$ (see Equation 23 below). A straightforward definition of the capillary length can be obtained by considering a spherical drop of water of radius *R* and comparing the surface tension effects governed by Laplace law, i.e., $\Delta P = 2\sigma / R_{cap}$ to the gravity effects described by the hydrostatic pressure between the bottom and the top the drop, i.e., $2\rho g R_{cap.}$. Surface tension in the drop will dominate gravity effects if:

$$2\rho gR << \frac{2\sigma}{R} \rightarrow R^2 << \frac{\sigma}{\rho g} \rightarrow R << \delta = \sqrt{\frac{\sigma}{\rho g}}$$ **Equation 23**

with σ: surface tension, ρ : liquid density and g : gravitational acceleration. Typical values of capillary length obtained for different liquids are presented in Table 4:

Table 4: Capillary length for current liquids. PFC yields to the smallest capillary length, i.e., less than 1 µm.

Liquid	*σ (mN/m)*	*ρ (kg/m^3)*	*δ (mm)*
Water (DMEM)	73	898	2.81
Oil	32	900	1.9
Surfactant	33	968	1.86
PFC	14	1755	0.89

Capillary tubes used for testing PFC surface tension with the capillary rise method must have $R_{cap.} < 1$ µm. We use glass capillaries tubes of two diameters: 0.6 mm and 0.9 mm.

A more accurate expression is required to relate capillary rise to surface tension. At pressure equilibrium of the drop inside the capillary, one must consider that the meniscus is not necessarily a sphere but a portion of sphere with a radius $R_{meniscus} > R_{cap}$:

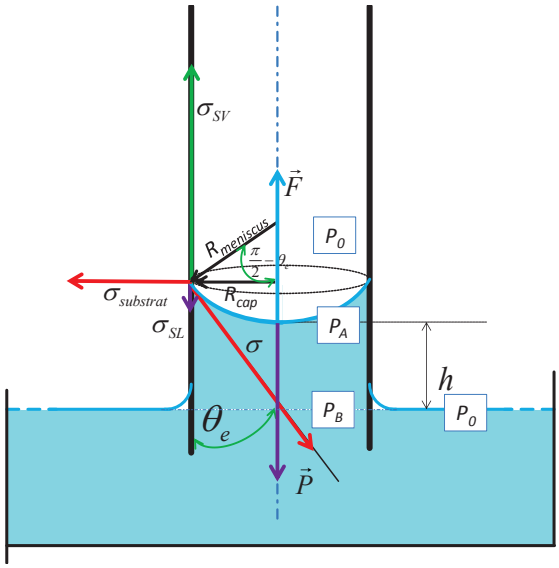

Figure 24: Equilibrium forces for the capillary rise of a liquid in a tube

In Figure 24 the pressure difference across the meniscus is given by the Young-Laplace equation:

$$P_0 - P_A = \frac{2\sigma}{R_{meniscus}}$$

The hydrostatic pressures in the capillary is given by:

$$P_B - P_A = \rho g h \qquad \text{with} \quad P_B = P_0$$

At equilibrium, one can obtain an expression of the capillary rise:

$$h = \frac{2\sigma}{\rho g R_{meniscus}}$$

If the capillary meniscus is a portion of a sphere, it can be shown that :

$$\cos\theta_e = \frac{R_{cap.}}{R_{menicus}}$$

Hence the well-known Jurin's law expression :

$$h = \frac{2\sigma cos\theta_e}{\rho g R_{cap.}} \quad \text{or equivalently} \quad \sigma = \frac{h\rho g R_{cap.}}{2cos\theta_e}$$

It is easy to verify that a µm-size drop of liquid on a solid surface (Figure 25) is equivalent in shape to the meniscus of a drop of liquid trapped in a capillary tube (Figure 26). In both cases, capillary forces predominate on gravity effects.

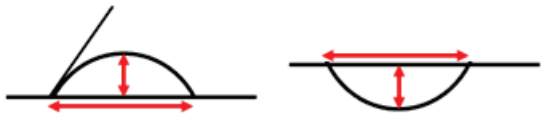

Figure 25: Equivalence between a µm-size drop of a liquid put on a solid surface and the meniscus of a drop of liquid trapped in a capillary tube.

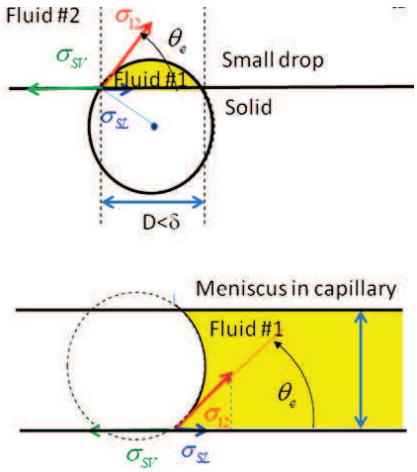

Figure 26: Equivalence between a drop laying on a solid surface and a meniscus in a capillary tube. The shape of the drop on the surface and the meniscus shape are both spherical, because the same surface force system applies to them.

Predominance of surface tension forces in the capillary tube enables to assume that (i) the meniscus is spherical, and (ii) the difference in hydrostatic pressure between the center of the meniscus and its edge is negligible in front of the capillary rise, a condition already satisfied by Equation 23 and Figure 26 and note that when capillary condition is satisfied, the drop is locked inside the capillary once removed from the medium. This property is used to measure the capillary rise not vertically but horizontally as indicated in Figure 27.

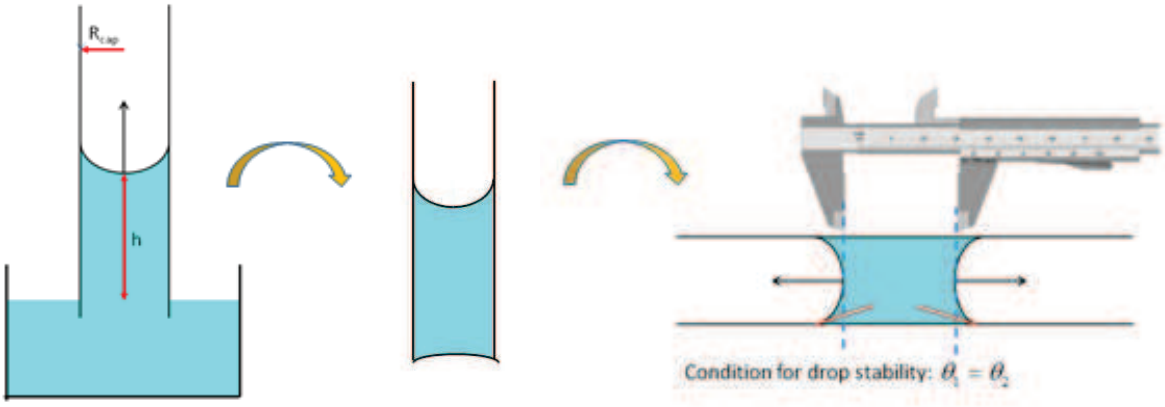

Figure 27: Representation of the method used to measure the height of a liquid inside the capillary tube. A capillary tube is plunged into the tested liquid, the height reached by that liquid is proportional to the surface tension of the liquid (Jurin's law). This height is unchanged if the capillary moves from vertical to horizontal, if capillary forces predominate over gravity forces, enabling to measure the capillary pressure in the horizontal position of the tube. The stability of the drop supposes equivalent meniscus on each side of the drop, which is easy to verify for a single drop of a given fluid.

The same property is also used in the case of a double drop system created inside the capillary. Based on this assumption, stability of the double drop can be assumed. The liquid with the lower surface tension (subscript 1) first enters the tube by capillarity over a certain height h_1 followed by the liquid with the higher surface tension (subscript 2) which enters the tube over a height h_2 (Figure 28). The surface tension forces of liquid 1 plus surface tension at the interface between the 2, liquids equilibrating the gravity effects applied on the two liquid drops of respective heights h_1 and h_2.

$$\sigma_{12} = \left(-\sigma_1 \cos\theta_1 + \left(gR_{cap}/2\right)\left(\rho_1 h_1 + \rho_2 h_2\right)\right) \Big/ \cos\theta_{12} \qquad \textbf{Equation 24}$$

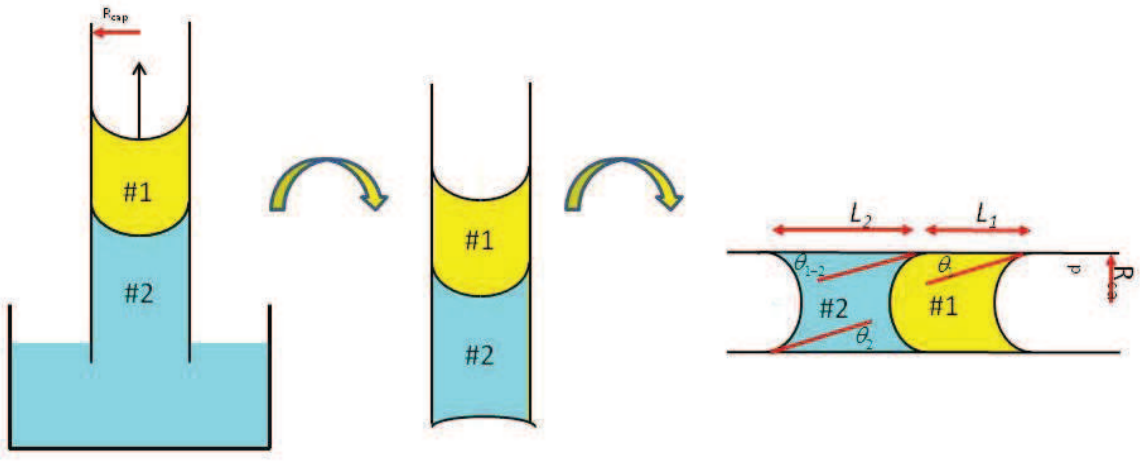

Figure 28: Representation of the method used measure the height of two liquid inside the capillary tube. The liquid with the lowest surface tension must enter at first place, followed by the liquid with the highest surface tension.

Equation 24 for the double drop, as well as the Jurin's law used for the single drop, both consider that contribution of surface tension is null as if the tube was vertical and plunge in a reservoir, i.e., contact angle θ_2 is assumed to tend toward 90°. In Equation 24 which actually corresponds to the case of a vertical tube opened to atmosphere. It has been shown by (Joanny, 1985) that the drop length limit in the case of a tube opened to atmosphere is fixed by the capillary length.

III.3.1.2 Measure of the contact angle of the liquid with the capillary tube

Knowledge of contact angle is required for measurement of surface tension. The equation $\cos\theta_e = R_{cap}/R_{meniscus}$ is not only valid in the condition of perfect wetting ($\theta_e = 0°$) of the liquid with the capillary wall (case of thermodynamic equilibrium according to de Gennes (de Gennes, 1985) but also in the case of partial wetting. In that case, contact angle can be calculated by Equation 25, classically proposed to calculate the contact angle of a drop placed on a solid surface.

$$2\theta_e = \arctan\left(H/R_{cap}\right)$$ **Equation 25**

Demonstration of this relation is summarized in the following Figure 29:

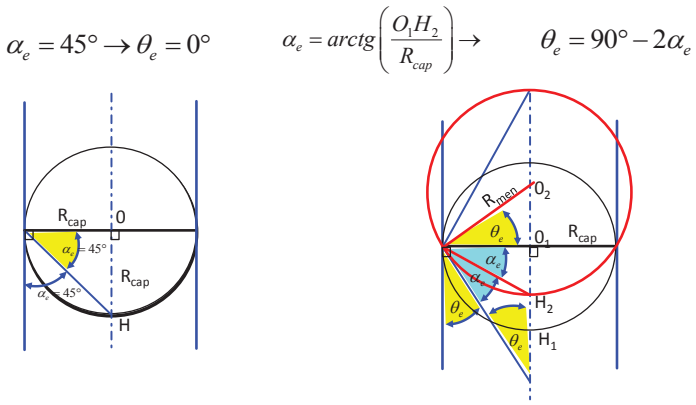

Figure 29: Demonstration of the geometrical relation used to calculate the contact angle (i) in the case of perfect wetting, and (ii) in the case of partial wetting.

III.3.1.3 Microscopic method to measure surface tension from capillary pressure

When the light of the microscope passes through the glass tube, a distortion of the transversal image occurs, because each capillary wall constitutes an interface between two mediums of different refraction indices (air and glass for the outer capillary wall, glass and liquid medium studied (e.g., PFC) for the inner capillary wall) Figure 30. Moreover the surfaces are not plane but spherical, meaning that the capillary wall acts as a double spherical dioptre.

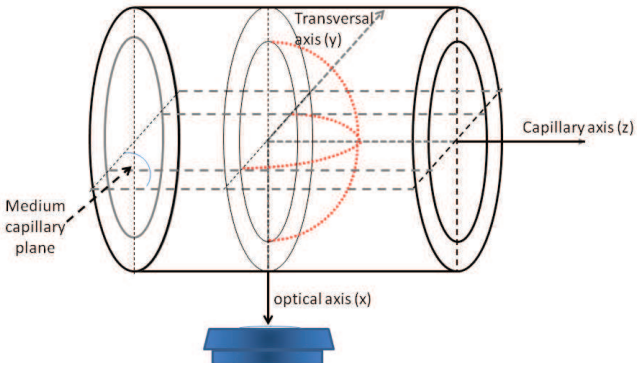

Figure 30: Schematic representation of the capillary used to measure the liquids surface tension under the microscope. The light passes through the two glass walls which act as a double spherical dioptre, causing a

distortion of the obtained image in the transversal axis which depends in the refraction index of each medium.

We used the Gullstrand formula - initially given by Allvar Gullstrand - whose main interest is to reduced two centered optical systems into a unique one, and calculate its equivalent characteristics in terms of magnification. This magnification theoretically depends on the medium in which the light propagates, and on the geometry (inner and outer capillary radius). For the two capillary tubes tested, we find that the modified image has to be decreased in the transversal axis (i.e. the plane where the meniscus is studied) proportionally to the refraction index (n) of the liquid.

$$n = \frac{increased\ diameter}{real\ diameter}$$ **Equation 26**

In the capillary image obtained by the microscope, two diameters are available. We verified both, using the Gullstand formula, and experimentally that the diameter of both capillary tested with air inside do not suffer a magnification, because de refraction index is equal to 1, so the microscopic image corresponds to the true diameter of the tube (in Equation 26 "real diameter"). The capillary diameter with water or PFC inside (they both have the same refraction index), or PFC corresponds to the increased diameter (in Figure 31 "Increased diameter"). To correct the image, the dimensions according to the horizontal axis must be decreased proportionally to "n" (Figure 31).

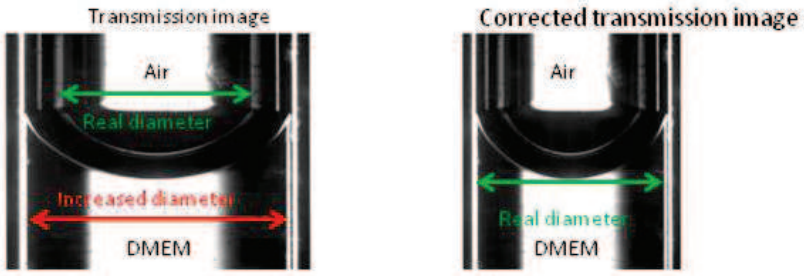

Figure 31: Left: Image of the capillary with DMEM at the inside, the meniscus is with air. In green is represented the real diameter of the tube, not distorted, and in red is represented the diameter dilated by the liquid medium. Right: image of the capillary tube with the liquid medium after correction.

After the correction of the microscopic image of the meniscus, the angle of contact between the liquid and air can be obtained and used for the calculation of the surface tension of the different liquids with air as well as for the liquid-liquid interface such as water and PFC or surfactant and PFC.

III.3.2 Theoretical estimation of interfacial energy on cell culture for the different fluids

Measuring directly the surface energy at the interface between cells and the different liquids used remains a challenge. We thus follow a theoretical approach in which the change in interfacial energy is estimated from the free energy of each phase and a theoretical expression of the work of adhesion which takes into account the different components of surface tension, i.e., an expression which is more general than Equation 8. It is noteworthy that the cell surface is a complex system constituted by hydrophilic elements (*e.g.,* glycocalyx) and hydrophobic elements (*e.g.,* the lipids of the membrane), as many other complex molecules, so the cell surface tension has most likely a polar and a non-polar components and not only a non polar component as in Equation 8.

This work of adhesion, W, is classically obtained on the one hand experimentally using the Young-Dupré (Young, 1805) adapted from Equation 5, to a solid-liquid surface.

$$W_{SL} = \sigma_S + \sigma_L - \sigma_{SL}$$ **Equation 27**

This work of adhesion, W, is classically obtained experimentally using the Young-Dupré equation in which σ_L and $cos\theta_e$ are supposed to be measurable while $\pi_e \approx 0$ is still assumed, (i.e., case of a high energy liquid on a low energy solid), adapted from Equation 7:

$$W_{SL} = \sigma_L \left(1 + cos\theta_e\right)$$ **Equation 28**

It is clear that the context of a confluent cellular monolayer, as in the case of epithelial cells, renders difficult the use of this expression. Alternatively, W can be obtained by different theories of adhesion issued from thermodynamic or chemical considerations. We mentioned below the most commonly accepted expressions issued from thermodynamic considerations which indeed implicates the expected effects of the polar and non-polar components for each phase:

-Owens and Wendt model, (Owens and Wendt, 1969) given for solid surfaces with relatively high surface energy:

$$W = 2\Psi\sqrt{\sigma_A\sigma_B} \text{ with } \Psi = \sqrt{\frac{\sigma_A^d\sigma_B^d}{\sigma_A\sigma_B}} + \sqrt{\frac{\sigma_A^p\sigma_B^p}{\sigma_A\sigma_B}}$$ **Equation 29**

-or the Wu's model, which uses the harmonic means of the interfacial interactions instead of the geometric ones. This model is more appropriate for solid surfaces with low surface energy, (i.e., partially wetted) (Wu, 1973):

$$W = 4\frac{\sigma_A^d\sigma_B^d}{\sigma_A^d + \sigma_B^d} + 4\frac{\sigma_A^p\sigma_B^p}{\sigma_A^p + \sigma_B^p}$$ **Equation 30**

-The Zisman approach (Zisman, 1964) applied for non polar liquids and is based on the relationship:

$$\cos\theta_e = 1 + b\left(\sigma - \sigma_c\right)$$ **Equation 31**

σ_c is the critical surface energy of the solid phase obtained by extrapolation at $\theta_e = 0$ while b is an empirical constant.

Placing phase A, e.g., a solid, and phase B, e.g., a liquid, into contact, generates association and a gain in energy called work of adhesion W, as previously defined. The interfacial energy σ_{AB}, or energy at the interface between the two phases in contact, is given by Dupré equation and assuming $\pi_e \approx 0$. It represents the surface energy that is sensed by the cell.

$$\sigma_{AB} = \sigma_A + \sigma_B - W_{AB}$$ **Equation 32**

σ_A and σ_B are the free energy at the surface of each phase, alternatively called surface energy for solids or surface tension for liquids.

III.4 Physiological Methods: evaluation of respiratory mechanics of pigs ventilated in liquid PFC (Total Liquid Ventilation)

III.4.1 Extraction of respiratory mechanical parameters by a RIC-EEP model

In quasi-static conditions, compliance is strongly dependent on interfacial energy between the fluid used to ventilate and lung tissue. Indeed, the evolution of lung compliance reflects the evolution of the equilibrium existing between surface forces and tissue forces in the course of liquid ventilation. Compliance (C) is defined by the ratio between the component of airway pressure in phase with the lung volume. We extracted the compliance parameter of 20kg-pigs ventilated with PFC with Liquid Ventilator specifically designed for the project ANR ABYSS. The ventilator as set at a controlled volume of 15 ml/kg and at a frequency of 5 cycles per minute (T_{inspi}=5s T_{expi}=7s) typical of TLV ventilation (Hutin et al., 2015), from the pressure and flow signals recorded during the pig ventilation. There were two distinct groups of animal in this study: one has received Hypothermic TLV (34°C), while the second group has received a Hypothermic TLV after a provoked cardiac arrest treated by cardiac massage. The second group corresponds to animals in severe cardiopulmonary conditions. The pressure signal was acquired using a PFC-compatible transducer EMKA® (Bourré), and the flow signal was acquired using an ultrasound flowmeter Transonic™ (Ithaca) calibrated for PFC. These two signals have been acquired respectively through a low-pass filter with a 40 Hz cutoff frequency.

III.4.2 The RIC-EEP model

The determination of compliance was obtained by fitting the RIC-EEP model on recorded signals using a least square method. This method is similar to the one previously used to determine the mechanical parameters of patients ventilated with air (Fauroux et al., 2008).

The modification concerns the addition of an EEP (End Expiratory Pressure) component and the inertance (I), which are presently considered as an unknown parameters. Sudden interruption of inspiratory flow, followed by a short zero flow plateau near the end of inspiration, is a method integrated in most of conventional gas ventilators. However, this cannot be done with PFC because PFC inertia (twice higher than water) is too elevated to have a rapid equilibrium and pressure stability within a duration compatible with a transient interruption of TLV. Hence alveolar pressure could not be measured and thus monitor in the course of liquid ventilation due to PFC physical properties. For similar reasons, EEP measurement usually performed during a pause created at the end of the expiration phase was not possible. Thus EEP contribution to the signals was integrated has an unknown parameter in the mechanical model of respiratory response. This contribution as well as the contribution of other respiratory parameter is described by the following second order differential equation reflecting, for each cycle, the averaged values of resistance, inertance and compliance as well as the level of positive end expiratory pressure in alveoli.

Equation 33

$$P_{aw} - EEP = \underbrace{R\dot{V}}_{P_{resistive}} + \underbrace{I\frac{d\dot{V}}{dt}}_{P_{inertial}} + \underbrace{\frac{1}{C}\int \dot{V}dt}_{P_{elastic\ recoil}}$$

Equation 33 is the equation of motion of the respiratory system (Guerin and Richard, 2007) modified to include inertance, which relates the pressure P_{aw} measured at airway or endotracheal tube (ETT) entrance, to the successive derivative components of volume displacement V: $\dot{V}$; $\ddot{V}$. The first derivative $\dot{V}$ is the measured instantaneous flow rate. The volume-acceleration $\ddot{V}$ signal is obtained as classically done by deriving versus time the flow signal issued from the flowmeter while the volume signal, V is obtained by integrating versus time the same flow signal. EEP is the End Expiratory pressure which is induced by discrepancies between the inspiratory and expiratory administered volumes of PFC. PFC is a

fluid of particularly elevated density and dynamic viscosity (Wolfson and Shaffer, 2004) so the resistive and inertial parameters are found much more elevated during TLV than during air ventilation.

Values of parameters are selected in order to provide the best curve fitting on the experimental pressure signal of the respiratory mechanic model given by Equation 33. Noteworthy, the specific values of PFC surface tension only act on compliance, so we will focus only on this parameter, while the others mechanical parameters will only be used for model validation. The validation of the curve fitting method was performed by 2 ways: (i) by analyzing a simulated pressure signal created with imposed values of R, I, C, EPP, and (ii) by comparing the values of mechanical parameters obtained. First comparison by the curve fitting method, and second by the flow interruption method in a patient ventilated with a standard gas ventilator.

III.4.2.1 Validation of the RIC-EEP model by pressure signal simulation

To generate a pressure signal, we used Simulink (Figure 32) to calculate from Equation 33 the pressure signal P_{aw} from a realistic TLV flow rate (during an actual TLV experiment in a pig (Figure 33) and for a given set of realistic respiratory parameter values.

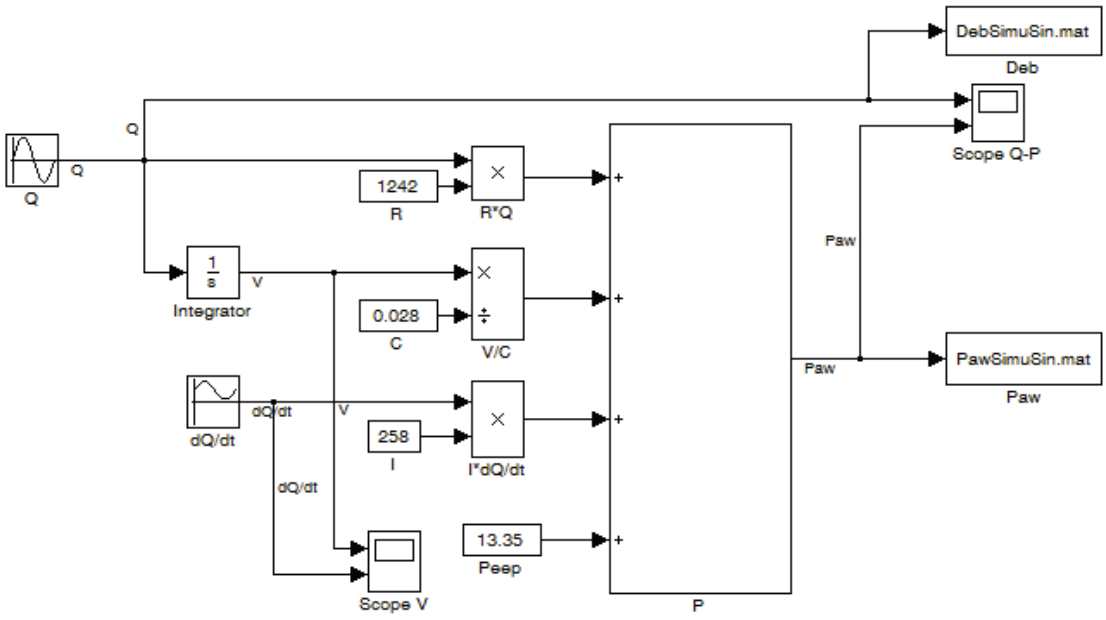

Figure 32: Schematic of the Simulink procedure

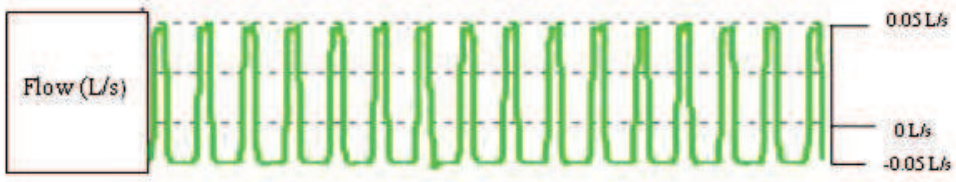

Figure 33: TLV-flow rate of a pig is used to simulate pressure signals for typical values of R, I, C, EPP parameters. Horizontal scale time in (A.U).

For the simulation, the set of R, I, C, EEP parameters is as follow: $R_{imposed}$ =1242 $cmH_2OL^{-1}s$; $I_{imposed}$ = 250 $cmH_20L^{-2}s$; $C_{imposed}$ = 28 ml/cmH_2O; $EEP_{imposed}$ =13.35 cmH_2O. After reconstruction of the simulated P_{aw} and flow rate signals, the RIC-EEP model was used to feed up the curve fitting method and the values obtained were very close from the imposed values, i.e., $R_{measured}$ = 1265.8±2 $cmH_2OL^{-1}s$; $I_{measured}$ =228±2.7 $cmH_2OL^{-2}s$; $C_{measured}$ = 32± 2 ml/ cmH_2O; $EEP_{measured}$ =14.5 ± 0.7 cmH_2O). This constitutes a first validation of the RIC-EEP method proposed to extract mechanical parameters during TLV.

III.4.2.2 Validation of the RIC-EEP model by comparison between proposed and standard methods applied in ICU patient

Typical pressure and flow signals obtained in an ICU patient with Acute Respiratory Distress Syndrome (ARDS) ventilated in air with a standard gas ventilator (Figure 34) are analyzed by the proposed RIC-EEP method and by the flow interruption method, standardly used in ICU. The criterion is based on the similarities of the values of R, C and EPP obtained with each method.

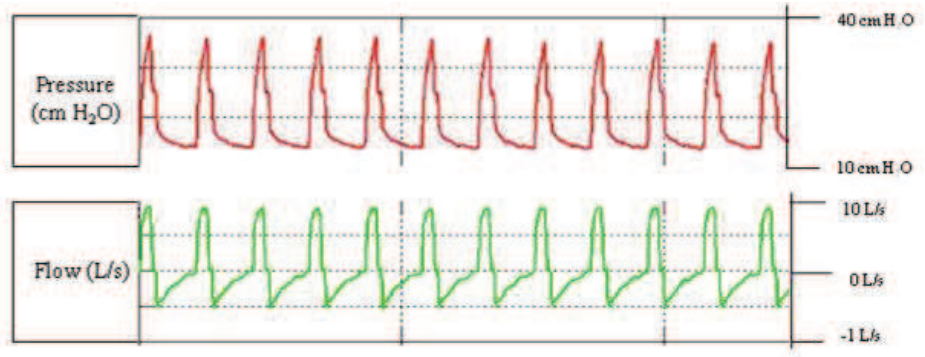

Figure 34: Pressure (cm H2O) and flow (L/s) signals for an ICU (ARDS) patient ventilated in air. Horizontal scale time in (A.U).

In an intensive care unit (ICU), by using air mechanical ventilation with controlled volume or flow in a curarized patient, it is possible to calculate the respiratory parameters by imposing a zero-flow at selected instants of the respiratory cycle. Imposing a pause at the end of inspiratory flow phase results in a pressure plateau (Figure 35) allowing to measure separately the resistive component from the elastic recoil component of pressure. Imposing a second flow pause at the end of the expiratory flow phase results in a pressure plateau (Figure 36) representing the end expiratory pressure or alveolar pressure level at the end of expiration. Static compliance can be calculated by:

$$Quasi\ static\ compliance(C) = \frac{Insuflated\ volume}{(Plateau\ pressure\ - EEP)}$$ **Equation 34**

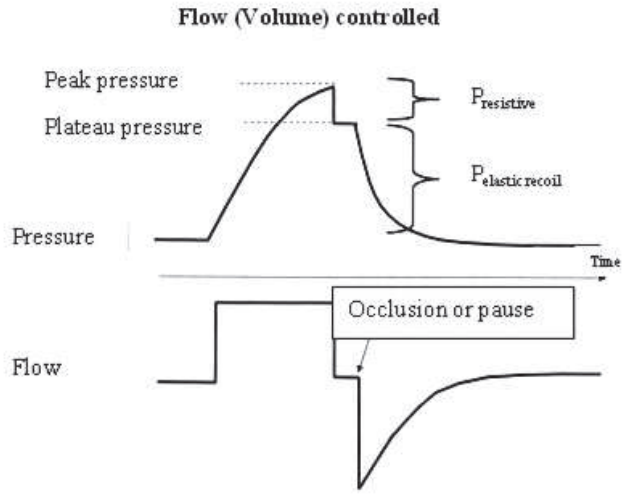

Figure 35: Modified from Brochard and Mancebo, 1994. Flow interruption technique applied at the end of an inspiratory phase to measure resistive and elastic component of pressure in the course of a flow-controlled air ventilation.

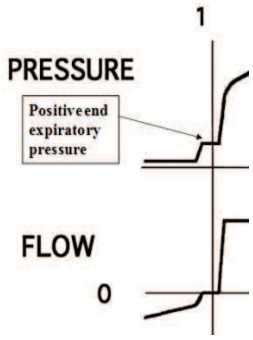

Figure 36: Modified from Brochard and Mancebo, 1994. Flow interruption technique applied at the end of an expiratory phase to measure Positive End Expiratory Pressure in the course of a flow-controlled gas ventilation.

To validate the curve fitting method used in the present study, we compared in Table 5 the R-I-C parameters and EEP Pressure in a given ARDS patient mechanically ventilated with air using (i) the standard ICU flow interruption method, and (ii) the presently proposed curve fitting method.

Table 5: Values of R, I, C, EEP, obtained by the curve fitting method (left columns) and by the standard flow interruption method (right columns).

	Values predicted by the curve fitting model				Values predicted by the ICU method		
Cycle	R ($cmH_2O.L^{-1}.s$)	C (ml/cm H_2O)	I ($cmH_2O.L^{-1}.s^2$)	EEP (cmH_2O)	R ($cmH_2O.L^{-1}.s$)	C (ml/cm H_2O)	EEP (cmH_2O)
1	14.3	29.4	0.07	13.5	12.1	30.2	14.2
2	14.5	29.5	0.07	13.9	12.7	26.5	13.9
3	14.4	29.4	0.06	13.7	11.4	25.7	13.9
4	14.4	29.6	0.09	13.7	11.8	26.9	13.8
5	14.4	29.1	0.06	13.3	11.4	27.3	14.0
6	14.5	30.1	0.08	13.7	12.0	23.6	13.7
7	13.7	29.8	0.07	13.3	10.5	24.7	13.7
8	13.8	31.2	0.05	13.7	10.9	24.2	14.0
9	14.2	28.8	0.06	13.0	10.3	23.2	13.9
10	13.8	30.6	0.07	13.4	11.4	27.4	13.7
11	13.8	31.1	0.05	13.6	11.2	26.7	13.8
12	13.6	31.1	0.07	13.6	10.8	27.5	13.9
13	13.8	30.1	0.07	13.2	11.0	27.4	13.8
14	13.7	30.8	0.07	13.4	11.0	26.6	13.9
15	13.8	30.1	0.07	13.3	10.8	25.2	13.7
16	13.8	31.5	0.03	13.8	10.5	29	13.8
17	13.6	30.3	0.07	13.2	12.1	28.1	14.0
18	13.6	30.7	0.06	13.5	10.8	29	13.8
19	13.6	30.7	0.06	13.7	10.7	28.5	14.7
20	13.7	30.2	0.07	13.5	10.2	29.5	14.9
21	13.6	31.1	0.07	13.6	10.9	28.1	14.0
22	13.7	30.2	0.08	13.2	10.9	31	14.3
23	13.5	31.5	0.06	13.5	9.5	33.9	15.5
24	13.6	30.2	0.06	13.3	10.5	26	13.9
25	13.6	30.5	0.06	13.6	12.0	27.3	13.7
26	13.7	30.2	0.07	13.3	11.7	28	13.9
Average	13.9	30.3	0.1	13.5	11.1	27.4	14.0
SDE	0.3	0.7	0.0	0.2	0.7	2.3	0.4

The values found by the 2 methods are very close. The differences calculated between the values obtained by the 2 methods reach 22 ± 5 % on average for the resistance values, 12 ± 6 % for the compliance values and 4 ± 3 % for the EEP values. Inertance could not be calculated with the flow interruption method because the use of air leads to negligible inertance values. In the RIC-EEP method, the inertance parameters is taken into account and

the consistency of the method is shown by values of inertance close to zero as expected with air. The differences between the values obtained with the RIC-EEP method and the flow interruption method comes from the difficulty of detecting the pressure values for the plateau (the plateau is not perfectly flat) and for the peak

IV. RESULTS

IV.1 Cellular response to PFC exposure in A549

IV.1.1 Cell migration and repair up to four days of PFC exposure

To estimate the alveolar epithelial cells response with time, over a long term exposure to PFC, (up to 4 days, in double chamber Figure 37A) we evaluate the repair of a wound done in an epithelial alveolar cell monolayer, in both control condition (DMEM) and during PFC exposure. We find that complete wound closure was reached in both groups, but cells in presence of PFC are more willing to migrate and repair the wound faster with PFC than in control conditions (Figure 37B). So for cells exposed to PFC, the area covered by migrating cells is systematically higher, and complete closure is reached earlier in the PFC group compared to the control group, suggesting that PFC improves the kinetics of wound repair, i.e., is able to modulate cell function without having deleterious consequence on fundamental biological processes (Figure 37B). It is important to note that the difference in wound repair observed between the two groups is evident from the very beginning of wound repair assessment, i.e., 4 and 7 hours, hence a precise characterization of cell modifications in response to PFC can be done from the early phase of exposure, i.e., a few hours only.

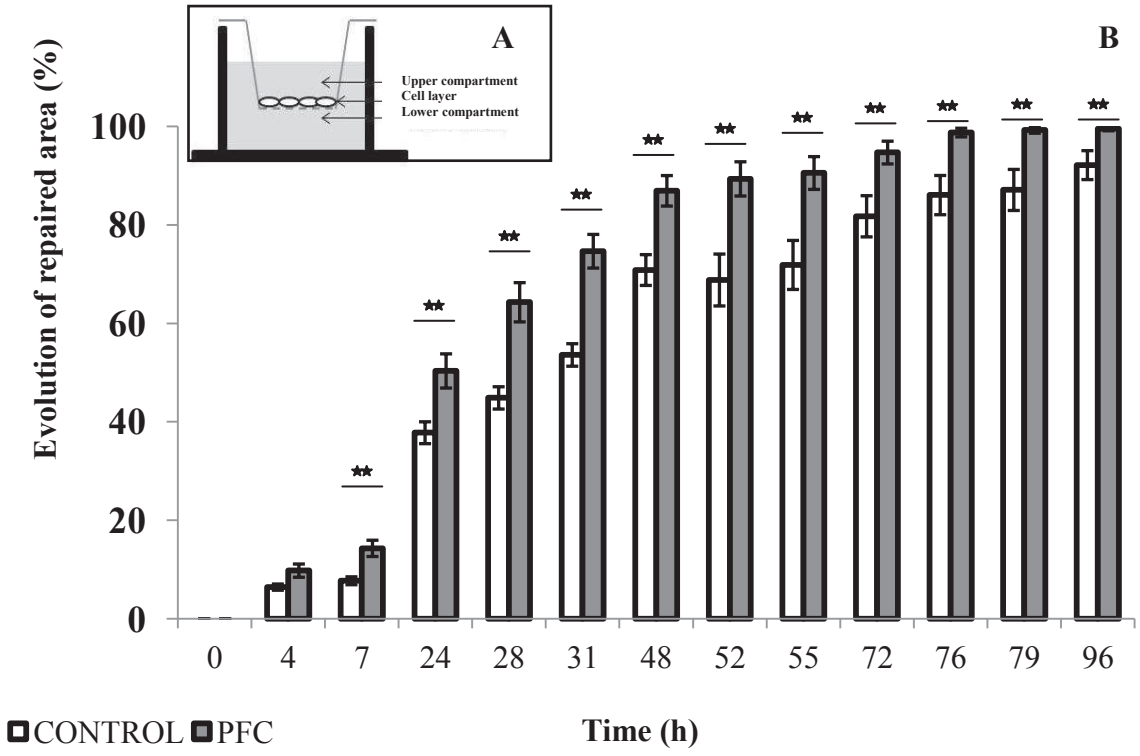

Figure 37: Evolution of repaired area in a wound layer of alveolar epithelial cells (A549) exposed to control medium or to PFC. (A) Transwell chamber, lower compartment: DMEM+10%FCS; upper compartment: DMEM+0.5%BSA (Control) or PFC. (B) The quantified repaired area (in % of the initial area of wound) followed over 4 days. The variation observed between control group and PFC group were analyzed using Mann-Whitney tests. Areas evolutions are statistically different ($p < 0.01$) between the control group and the PFC group starting from a few hours (7h) after the beginning of the experiment, this tendency is maintained until complete closure. Number of experiments (n): $n_{control}= 45$; $n_{PFC}=44$.

IV.1.2 Evolution of key cellular and molecular structures after 2 hours of PFC exposure

IV.1.2.1 F-actin remodeling

Fluorescence of F-actin network was imaged and quantified in control cells and after 2h of PFC exposure (Figure 38, A-D). In control conditions, A549 cells show a highly organized and interconnected actin network with a large number of stress fibers, a characteristic pattern in tensed adherent epithelial cells. By contrast, after PFC exposure, cells exhibit a decreased

in F-actin and a loss in stress fibers organization. Cell shape appears more rounded suggesting a loss in intracellular tension. A significant decay in actin is confirmed by quantification of fluorescence after PFC exposure (Figure 38, G). These results suggest that PFC exposure induces a significant remodeling of F-actin network.

IV.1.2.2 1.2) Focal adhesion alteration

It is well known that the increase in size of focal adhesion is associated to a highly tensed F-actin network (see section II.4.3). Thus, the reported changes in cell morphology and F-actin organization induced by PFC exposure are indicative of alterations in the interaction between the cell and the extracellular substrate. To explore this possibility, we examine whether PFC exposure induces changes in the size of focal adhesion sites. We find a reduction in the fluorescent phosphotyrosine staining at focal adhesions in cells under PFC exposure. Focal adhesions are imaged and quantified by fluorescent confocal microscopy. The analysis of the number of focal adhesions per cell and their distribution per size in the control group and after 2h of PFC exposure (Figure 38, B and E) show a wider number of focal adhesion with a large area in the control group compared to the PFC-exposed group. PFC exposure induces a loss of focal adhesion in number and size, as observed by the loss of fluorescence of tyrosine phosphorylation (PY99) at the focal adhesions. The average number of focal adhesion per cell decreases by 31% in the PFC-exposed group compared to the control group (Figure 38, H). Whereas the number of focal adhesions with areas superior or equal to 2 μm^2 decreases by 35% (Figure 38, I). These observations correlate with a decrease in highly polymerized F-actin network and some loss of stress fibers after PFC exposure.

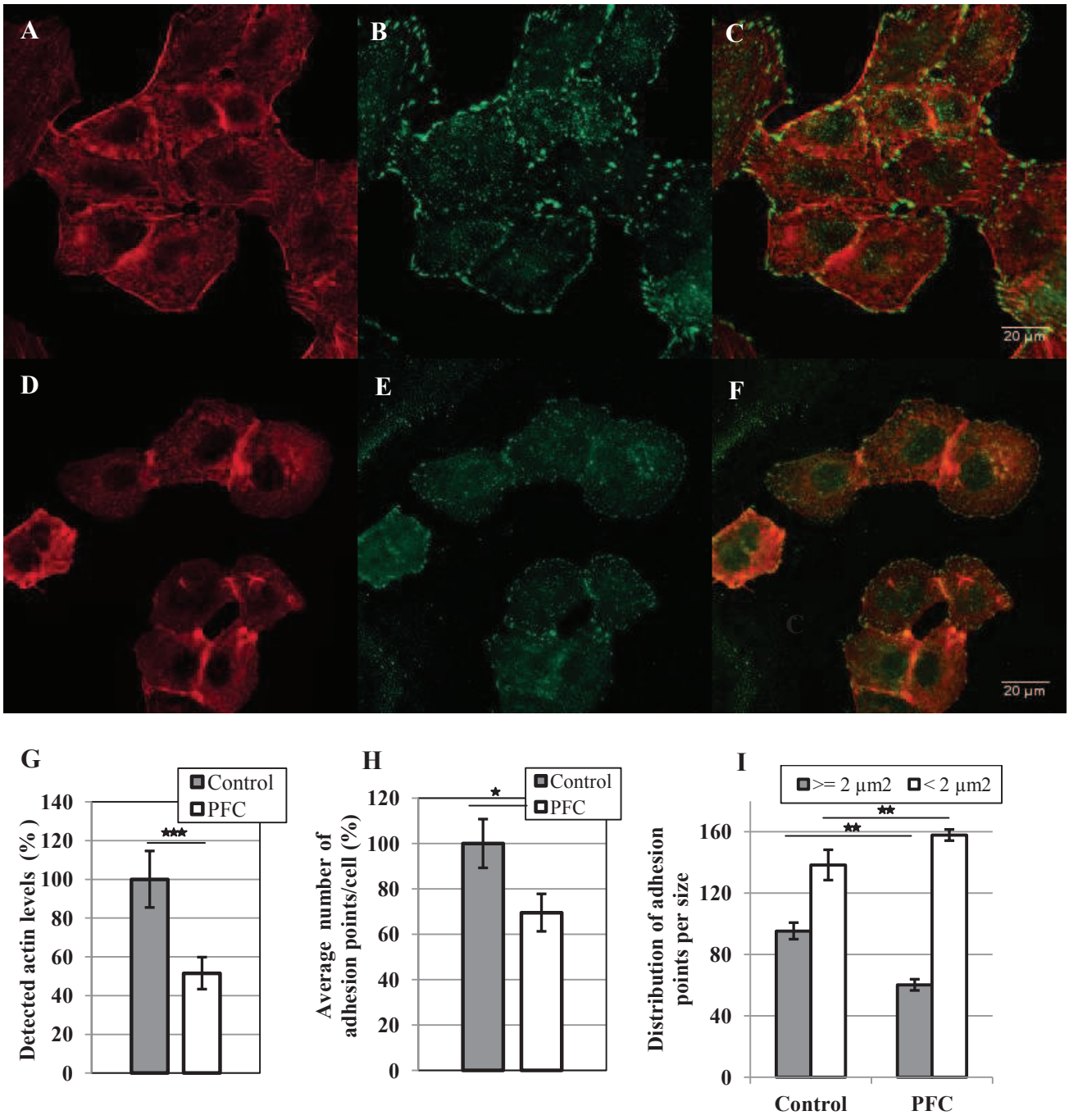

Figure 38 : Co-staining of F-actin (phalloidin, red) and of focal adhesion sites (phosphotyrosin, green) in fixed A549 cells. (A, D) F-actin staining, (B, E) focal adhesion staining, (C, F) merge. (A-C) Control group, (D-F) cells after two hours of PFC exposure. (G) Quantification of F-actin fluorescence for control group and after PFC exposure. (H) Average number of adhesion points per cell for control and PFC. (I) Distribution of adhesion points per size for control and PFC. F-actin in control group is highly reticulated and exhibits many stress fibers, as typically observed in adherent epithelial cells. After PFC exposure, F-actin structure is weakened which is confirmed by the significant decay in fluorescent intensity between control and PFC-exposed cells. After PFC-exposure, cells acquire a more rounded shape that indicates a

decrease in internal tension with less stress fibers expressed. The quantification of fluorescence is significantly different between the two groups ($p<0.001$). Control cells also have several large focal adhesion points linked to actin stress fibers near the cell periphery, and a smaller number in the center. After PFC exposure, focal adhesion points at the cell periphery are thinner in size and less intense than in control. There is a significant decrease in the number of focal adhesion points per cell after PFC exposure ($p<0.05$). Scale bar: 20 µm. ($n_{control}=6$; $n_{PFC}= 6$).

IV.1.2.3 Glycocalyx expression

We imaged and quantified the fluorescence of glycocalyx stained with WGA-FITC after 2h of PFC exposure (Figure 39 A-C). Cells of the control group express a rather uniform distribution layer of glycocalyx at the cell surface (Figure 39A). After PFC exposure, there is a marked alteration in glycocalyx expression, and a loss in the uniformity of the glycocalyx distribution (Figure 39B), with significant decay in glycocalyx expression confirmed by the measure of the fluorescence levels (Figure 39C).

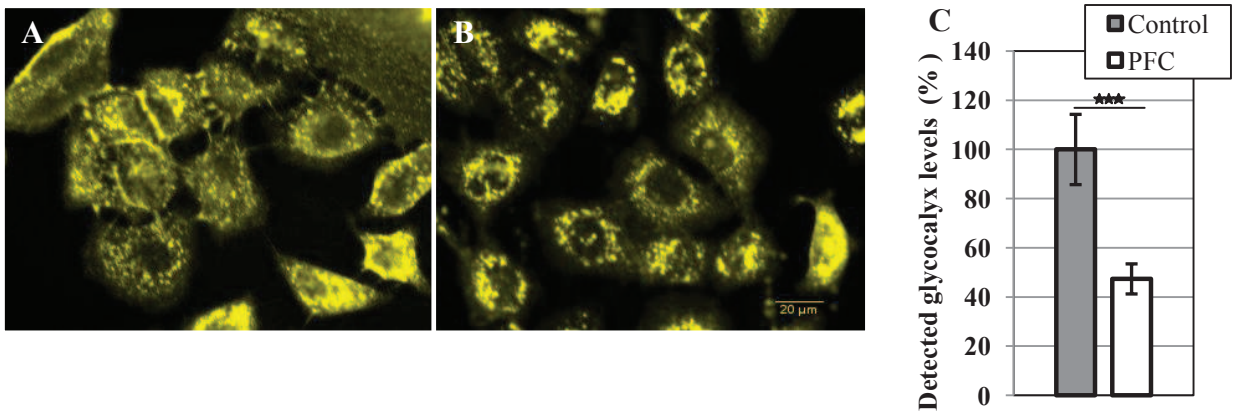

Figure 39: Glycocalyx staining (WGA-FITC, yellow) of live A549 cells (A) control and (B) after 2h of PFC exposure. (C) Quantification of glycocalyx by measure of fluorescence for the control and after 2h of PFC exposure. Glycocalyx in control cells is more uniformly distributed and largely expressed. Cells after PFC exposure exhibit a decrease in glycocalyx expression and less uniform layer of glycocalyx, suggesting a redistribution a redistribution of glycocalyx toward the cell periphery. The quantification of fluorescence is significantly different between the two groups ($p<0.001$). Scale bar 20 µm. ($n_{control}= 7$; $n_{PFC}= 7$).

IV.1.3 Cell mechanics and cell adhesion after PFC exposure assessed by MTC

IV.1.3.1 Cell mechanical properties and adhesion parameters after different durations of PFC exposure (≤ 2 hours)

Testing different durations of PFC exposure, from 5 min to 2 hours, reveals significant changes in cell mechanical properties from 0.5 h of PFC exposure (Figure 40). With the SV model (Figure 40 A-D), we observe a time-dependent decrease in cell stiffness, E (Figure 40A), whereas the viscoelastic relaxation time (T, Figure 40B), is unaffected. Moreover, we observe a slight but clear increase of the natural dissociation rate, K_{off}^{0} (Figure 40C), is observed from 1.5 h of exposure and a significant decrease in reference stress, σ_c (Figure 40D) is found from 0.5h. The evolution of the parameter σ_c suggests a reduction in the number of adherent connections between cell and extracellular matrix from 0.5 h of PFC-exposure. These results depict a change in mechanical cell behavior in response to PFC exposure characterized by a significant cell softening (decay in CSK stiffness E) as well as adhesion weakening both in terms of chemical energy of adhesion (K_{off}^{0}) and number of adhesion bonds through the decay in σ_c.

With the PL model (Figure 40 E-H), the same cellular trend is observed from the mechanical properties: the norm of the complex elastic modulus |Ge| (Figure 40E) (at 1 Hz) decreases significantly with the duration of PFC exposure, in a way consistent with the evolutions of CSK stiffness E found with the SV model. The real part of the complex modulus (PL model) recalculated at the fundamental frequency of MTC signal, i.e., 1/60 s ≈ 0.02 Hz, is quantitatively the same than E (SV model). The evolution of the parameter α (Figure 40F) with duration of PFC exposure is characterized by a significant increase suggesting some fluidification process . However the values of the exponent of the power law

α never exceed 0.13, (by comparison to α = 0.11 in control conditions) suggesting that the solid-like behavior remains a satisfactorily assumption as already shown by the SV model. By contrast to the SV model, the adhesion parameters K_{off}^{0} and σ_c (Figure 40 G-H) obtained with the PL model remain unaffected by PFC exposure, and are one order of magnitude smaller than those obtained with the SV model. It appears that the PL model fails to describe the PFC-induced evolutions of the focal adhesion site shown previously Figure 38.

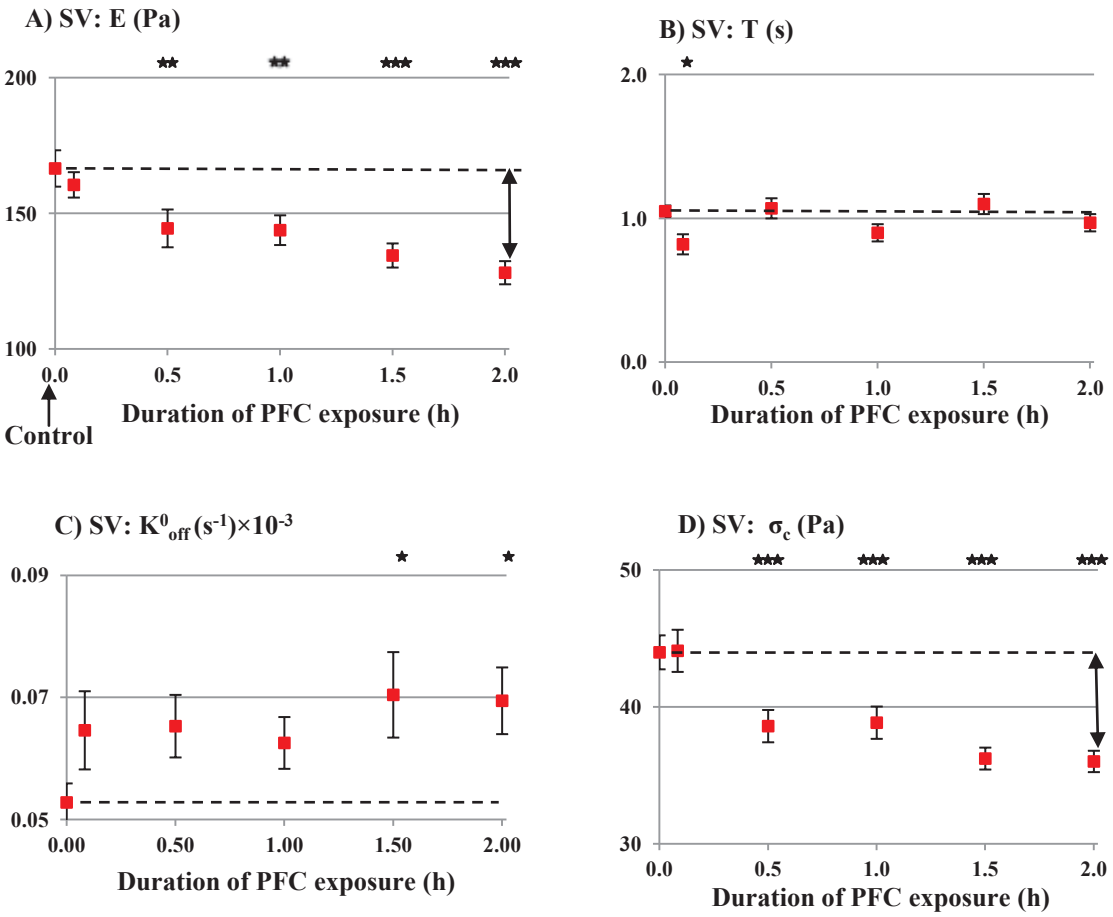

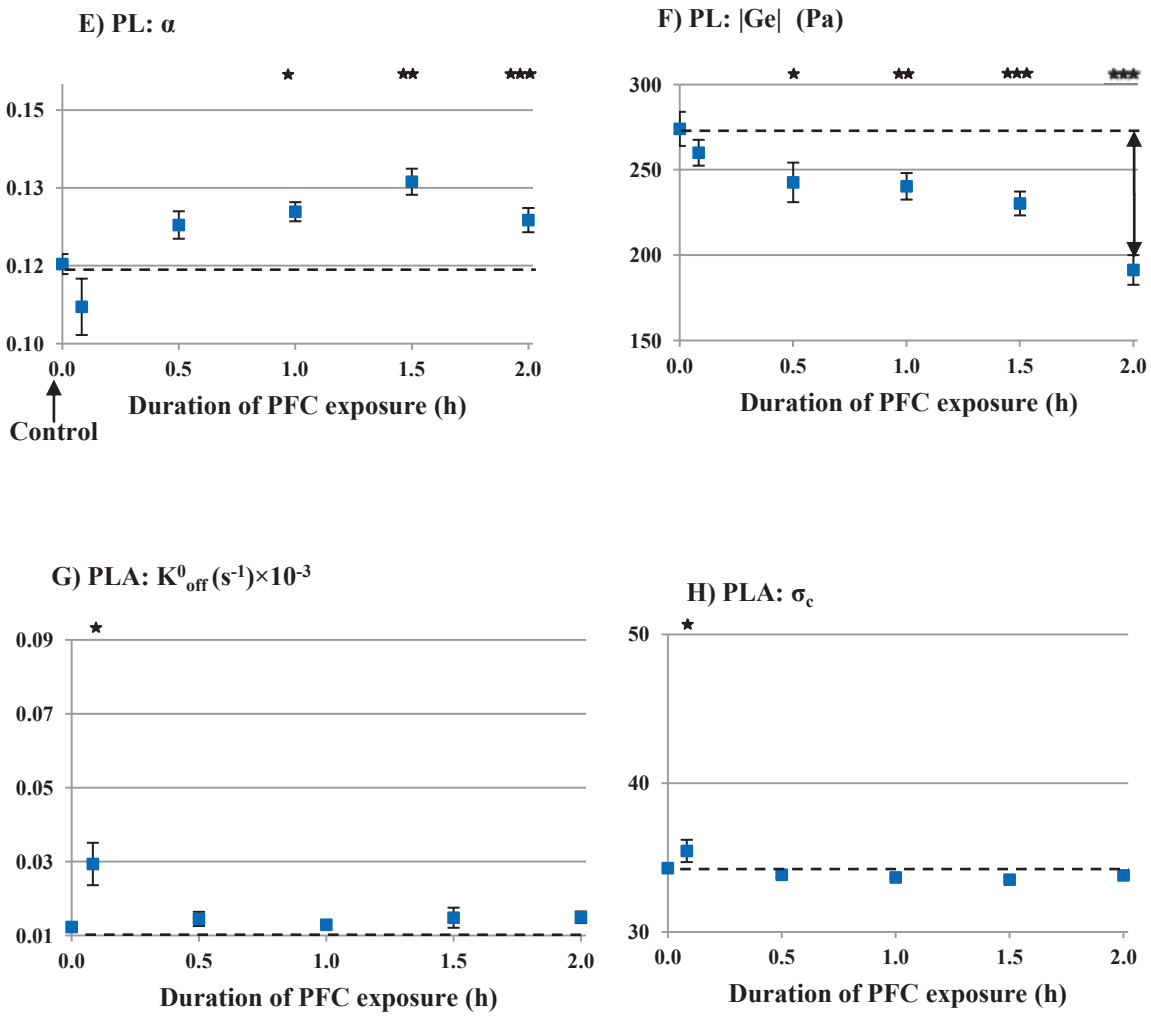

Figure 40: Mean values and SEM of mechanical properties and adhesion parameters, for control conditions (t=0h) and after PFC exposure at different durations (from 5 min to 2 h). The parameters of the viscoelastic solid-like model with adhesion parameters (SV model, in red): (A) cytoskeleton elastic modulus *E* in Pa, (B) viscoelastic relaxation time T in s, (C) natural dissociation rate K_{off}^{0} in s^{-1}, (D) reference stress σ_c in Pa. The parameters of the power law with adhesion model (PLA model, in blue): (E) exponent of the power law: α, (F) modulus of the complex storage modulus: |Ge| at f=1 Hz in Pa, (G) natural dissociation rate K_{off}^{0} in s^{-1}, (H) reference stress σ_c in Pa. The differences between the control group and PFC exposure were analyzed using ANOVA tests (number of stars quantifies the significance by reference to the measured value in control conditions, i.e., the dotted horizontal line, (*: $p < 0.001$; **: $p < 0.01$; * : $p < 0.05$). $n_{Control}$=59, $n_{PFC\ 0.1h}$=33, $n_{PFC\ 0.5h}$=36, $n_{PFC\ 1.0h}$=40, $n_{PFC\ 1.5h}$=29, $n_{PFC\ 2.0h}$=68.**

IV.1.3.2 Effect of cyto D on cell response to PFC exposure

Cells from both control and PFC-exposed groups are treated by cytoD after each MTC measurement. The aim is (i) to confirm the actin cytoskeleton specificity of the cell response expected from the specific integrin recognition of the bead coating, and (ii) to assess the role of the tensed cytoskeleton in the cell response to PFC exposure. Two key parameters of the cell response are presented in Figure 41, , namely the elastic modulus *E* and the norm of the complex elastic modulus |Ge|. The parameter differences measured with and without cytoD treatment are all highly significant. Depolymerizing F-actin filaments with cytoD results in a largely documented CSK weakening process with loss of internal tension (cell prestress is decreased and cell stiffness is lowered) (Wang et al., 1993; Wendling et al., 2000; Zhang and Moy, 2003). Parameters measured in treated cells before and after PFC exposure, demonstrate a cell stiffness level identical to the control level for all exposure durations. In other words, once the contribution of actin stress fibers is removed by cytoD treatment, cell stiffness in all groups become insensitive to PFC exposure suggesting that intracellular tension plays a key role in cellular adaptation to PFC exposure.

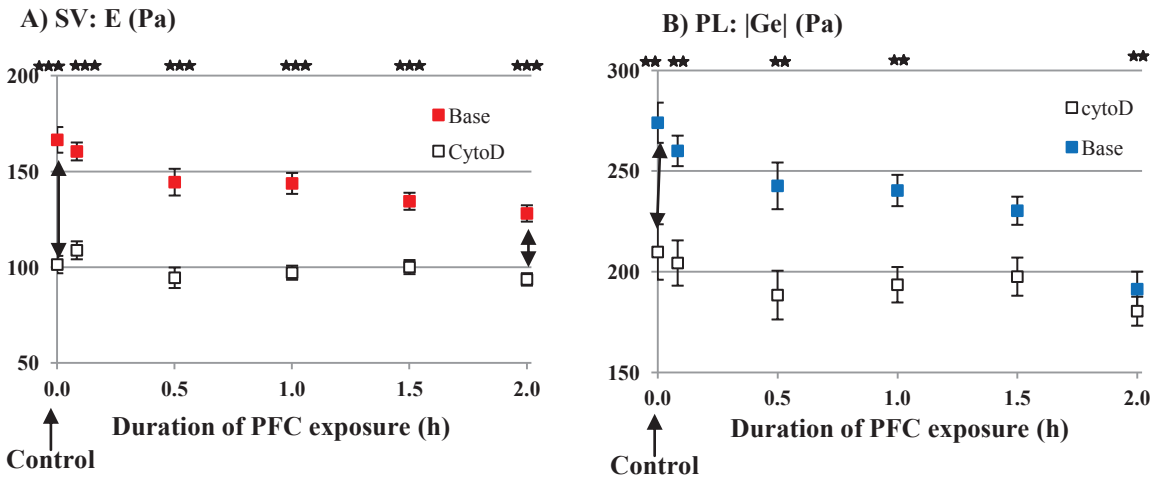

Figure 41 : Effect of cyto D treatment on CSK stiffness *E* (from SV model) and norm of complex modulus |Ge| (from PL model) for control (t=0h) and after various durations of PFC exposure (from 5 min to 2 hours). The differences observed with and without cytoD treatment were analyzed using Wilcoxon tests and are all highly significant (* : $p < 0.001$). Once the F-actin contribution to the CSK stiffness is removed by cytoD treatment, the decay in cell stiffness caused by PFC exposure is removed and all groups drop to the same level of cell stiffness, suggesting that internal tension contributes to the control of the cell response after PFC exposure. $n_{base}=59$, $n_{PFC\ 0.1h}=33$, $n_{PFC\ 0.5h}=36$, $n_{PFC\ 1.0h}=40$, $n_{PFC\ 1.5h}=29$, $n_{PFC\ 2.0h}=68$.**

IV.1.3.3 Effect of glycocalyx degradation on cell response to PFC exposure

Heparinase III is used to degrade HS, the most abundant component of glycocalyx while the mechanical and adhesion parameters are measured (Figure 42). Both cells in control conditions and cells exposed to PFC for 0.5 h and 1.5 h are treated with heparinase III. The two models (SV and PL) show that cells of both groups treated with this degrading enzyme experience a significant increase in CSK stiffness (Figure 42 A and F). The adhesion parameters obtained by the SV model in heparinase-treated cells, reveal an adhesion stabilization of adhesion after PFC-exposure (Figure 42 C and D). It appears that by degrading the glycocalyx layer, the cell loses its capacity of adaptation to PFC, resulting in a raise in intracellular tension, mimicking the onset of an apoptotic process (Wickman et al., 2013) (see Figure 43). This increase in intracellular tension occurs both in control conditions as well as cells after PFC exposure. Noteworthy, the reported PFC-induced decay in internal tension is lost when glycocalyx is degraded. Moreover, the PFC-induced decay in adhesion stability revealed by the SV model (and actually not by the PL model) is also removed after glycocalyx degradation. Indeed, only SV model is able to reveal that cell adhesion is more stable (K_{off}^{0} is decreased in Figure 42C) whereas cell-matrix interconnections are increased (σ_c is increased in Figure 42D). These results demonstrate that glycocalyx layer acts as an interfacial regulatory, and mechanosensitive structure and thereby plays a key role in the cellular response to PFC exposure.

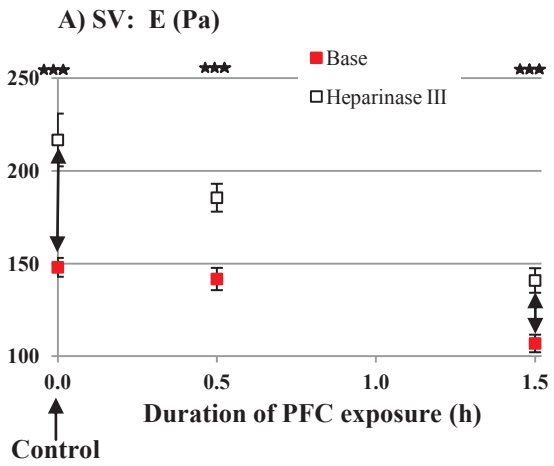
A) SV: E (Pa)
Base
Heparinase III
250
200
150
100
***
***
***
0.0
0.5
1.0
1.5
Duration of PFC exposure (h)
Control

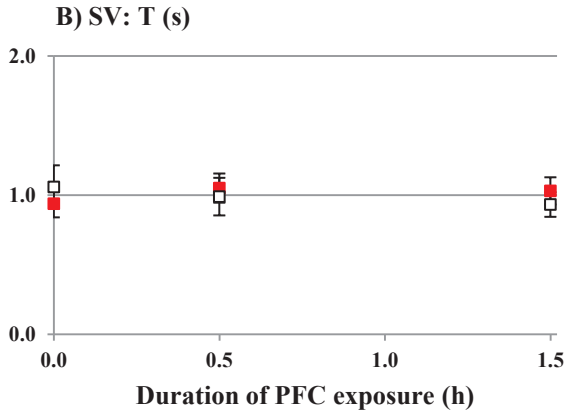
B) SV: T (s)
2.0
1.0
0.0
0.0
0.5
1.0
1.5
Duration of PFC exposure (h)

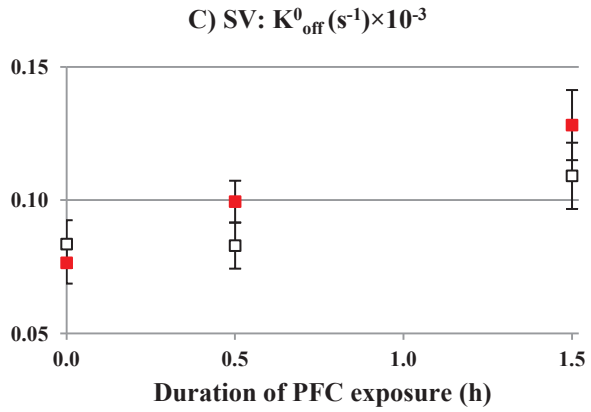
C) SV: K0off (s-1)×10-3
0.15
0.10
0.05
0.0
0.5
1.0
1.5
Duration of PFC exposure (h)

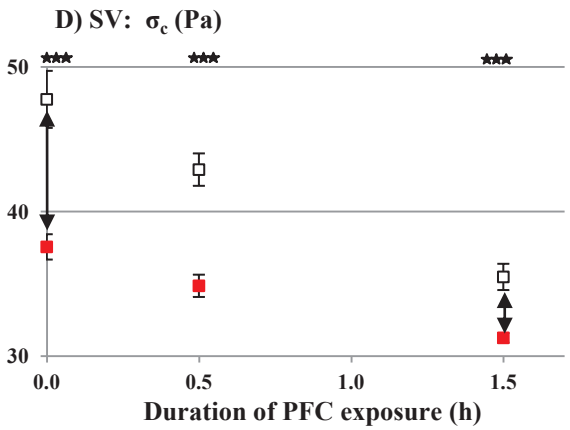
D) SV: σc (Pa)
50
40
30
***
***
***
0.0
0.5
1.0
1.5
Duration of PFC exposure (h)

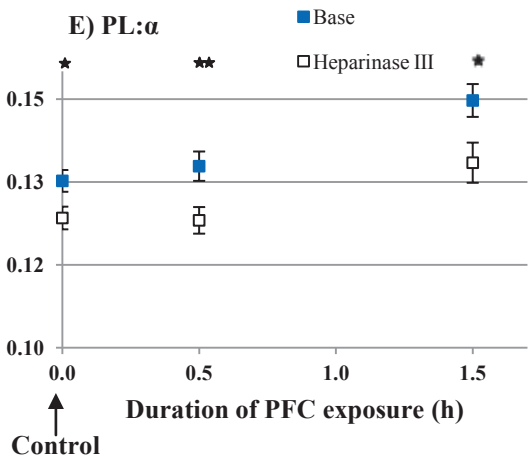
E) PL:α
Base
Heparinase III
0.15
0.13
0.12
0.10
*
**
*
0.0
0.5
1.0
1.5
Duration of PFC exposure (h)
Control

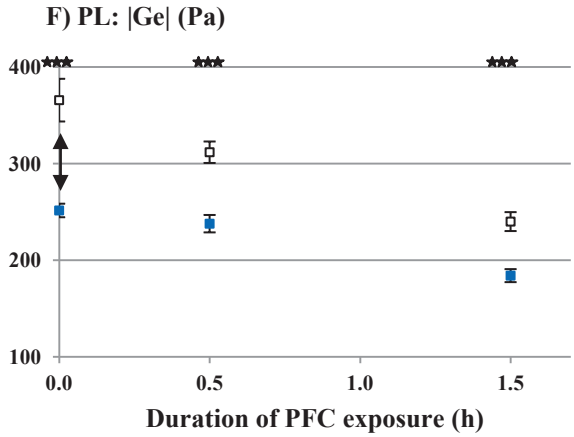
F) PL: |Ge| (Pa)
400
300
200
100
***
***
***
0.0
0.5
1.0
1.5
Duration of PFC exposure (h)

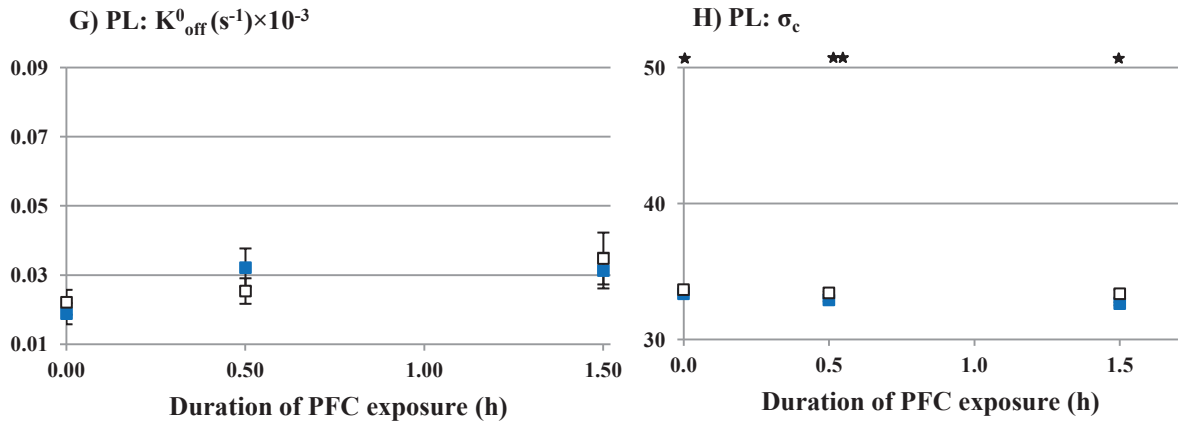

Figure 42: Effect of glycocalyx degradation by Heparinase III. Mean values and SEM of mechanical properties and adhesion parameters are given for control condition (t=0h) and after two durations of PFC exposure (0.5h and 1.5h). The parameters of the viscoelastic solid-like model (SV, in red) are plotted: (A) cytoskeleton elastic modulus *E* in Pa, (B) viscoelastic relaxation time T in s, (C) natural dissociation rate K_{off}^{0} in s^{-1}, (D) reference stress σ_c in Pa. The parameters of the power law with adhesion model (PLA, in blue): (E) exponent of the power law: α, (F) norm of the complex storage modulus: |Ge| at f=1 Hz in Pa, (G) natural dissociation rate K_{off}^{0} in s^{-1}, (H) reference stress σ_c in Pa. The differences between the heparinase treated cells and the untreated cells for control condition and for PFC-exposed group are analyzed using Wilcoxon tests (number of stars quantifies the significance by reference to the measured value in control conditions, i.e., the dotted horizontal line, namely ***: $p < 0.001$; **: $p < 0.01$; * : $p < 0.05$). $n_{Control}=25$, $n_{PFC\ 0.5h}=31$; $n_{PFC\ 1.5h}=31$.

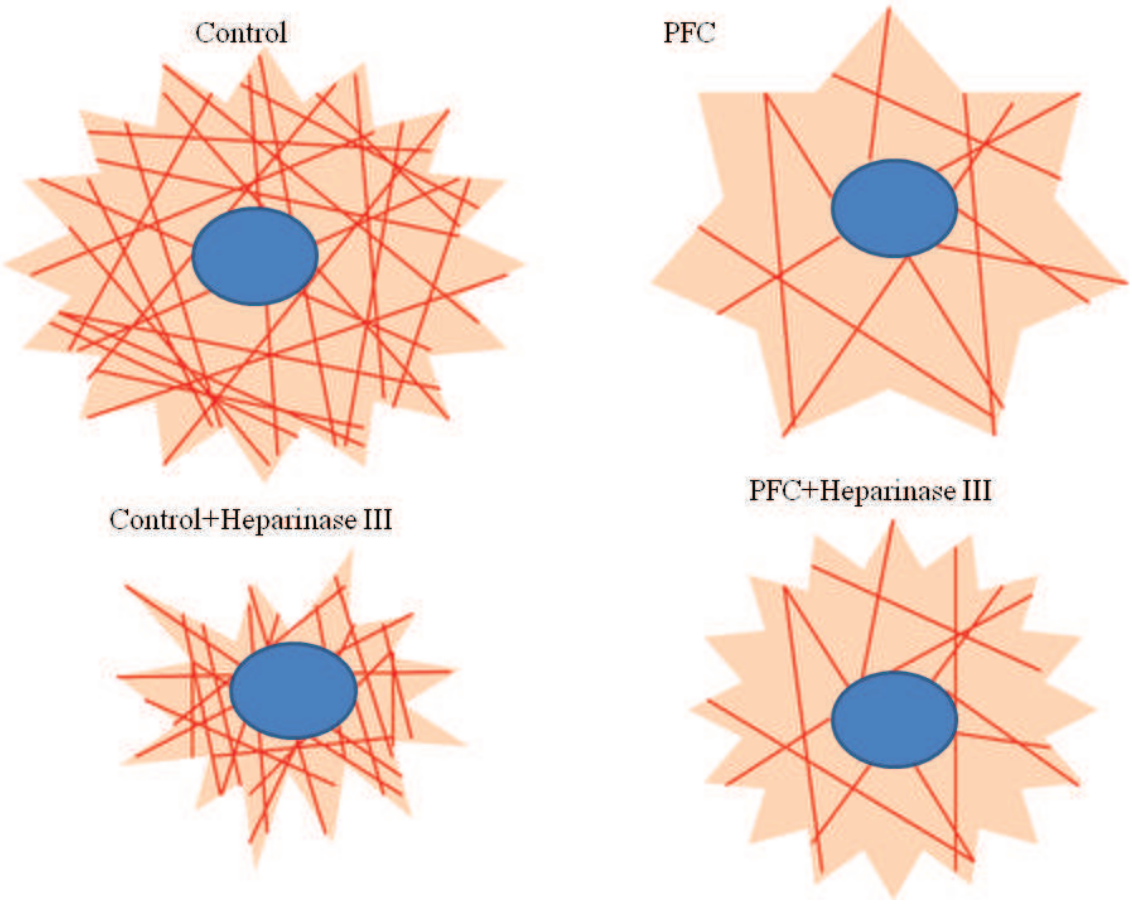

Figure 43: Schematic representation of a A549 cell with actin and the nucleus. A) A549 control cell. The cell has a normal internal tension and actin network. C) A549 control cell after Heparinase III exposure. There is a increase of internal tension, actin network is maintained. B) A549 cell after PFC exposure. There is a loss of internal tension and of actin. D) A549 cell after PFC and heparinase exposure. There is an increase of internal tension, the actin network is maintained.

IV.2 PFC properties susceptible to induce an alveolar epithelial cell response

Two main PFC properties related to the chemical structure of PFC (see section II.1) could be responsible for the reported alveolar epithelial cell response: one is the elevated amount of dissolved oxygen in the PFC, the other is the low surface tension of PFC.

IV.2.1 Evaluation of the role of oxygen

IV.2.1.1 Effect of severe hypoxia on wound healing

In normal atmospheric and temperature conditions, PFC contains a higher percentage of dissolved oxygen (28%) than air (21% of O_2) due to the great affinity of PFC for this molecule (Wesseler et al., 1977). Moreover, it has been shown by Sen (Sen, 2009) that a higher amount of oxygen is profitable for helping wound healing. Thus, due to the elevated fraction of oxygen dissolved in PFC, oxygen might be responsible for the reported increase in efficiency of wound repair. In order to verify the role of oxygen on cell migration and repair while maintaining cells exposed to PFC, we tested migration of cells exposed to PFC in an hypoxic chamber adjusted at 1% of O_2. We thus performed wound healing assays in severe hypoxic conditions and then tested cell mechanics and adhesion by MTC assays. Results clearly show that during hypoxia, cells migrate and repair at the same speed than cells without hypoxia, i.e., in normoxic atmospheric conditions (Figure 44). Moreover, the enhanced migration and repair induced by PFC exposure was maintained, whatever the fraction of oxygen dissolved in PFC (Figure 44). Incidentally, it should underlined at this point that physiological concentration of oxygen met *in vivo* in tissues is definitely much lower than the standard oxygen concentration encountered in cell cultures exposed to 21% of atmospheric oxygen (Carreau et al., 2011; Herzenberg and Herzenberg, 2013). It means that cells are used

to function in hypoxic physiological conditions but this is by reference to artificial laboratory conditions not to actual physiological conditions.

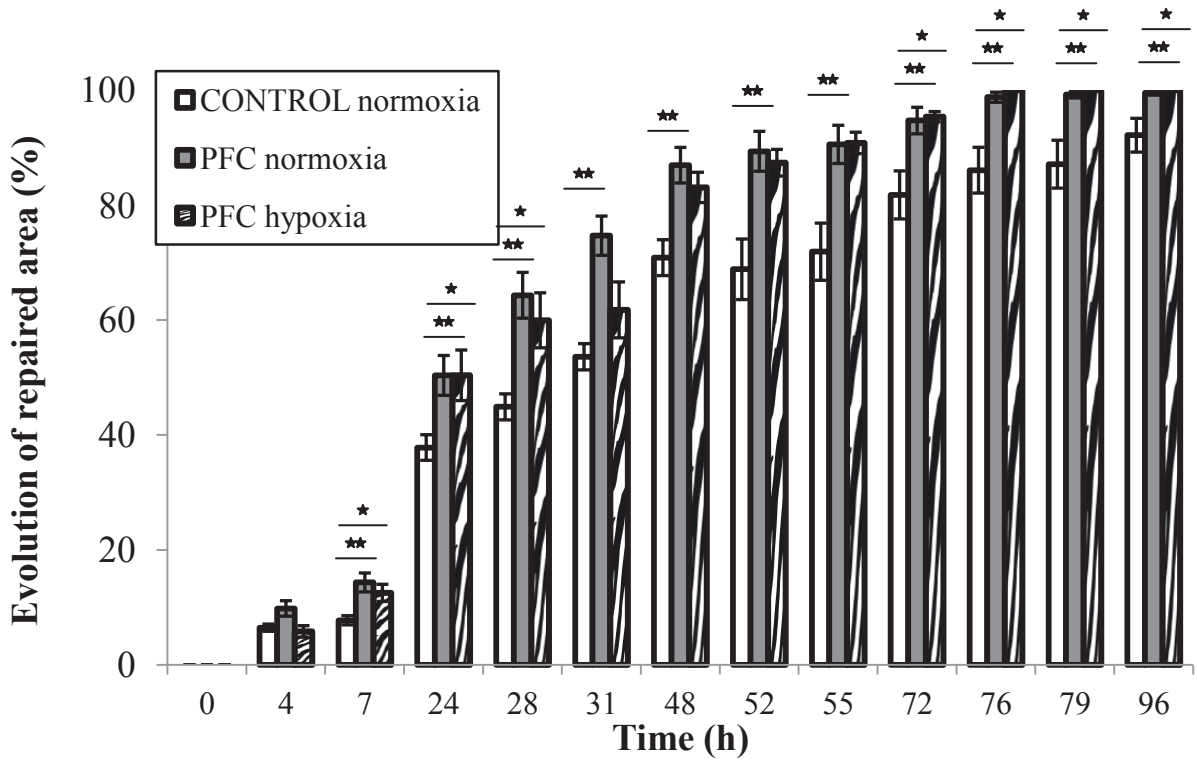

Figure 44: Evolution of the repaired area in a wound made in alveolar epithelial cell (A549) monolayer exposed to control medium and to PFC in normoxic conditions, and to PFC in hypoxic conditions. The quantified repaired area (in % of the initial area of the wound) followed over 4 days. The variations observed between the groups were analyzed using Mann-Whitney tests. Areas evolutions are statistically different ($p < 0.01$) between the cell groups exposed to 2 normoxic conditions : control and PFC exposure, starting from seven hours after the beginning of the experiment. This tendency is maintained until complete closure. Areas evolutions are statistically different ($p < 0.05$) between the control group and PFC exposure during hypoxic conditions: at t= 7, 24, 28, 72, 76, 79, 96h. $n_{control}$= 45; n_{PFC}=44, $n_{Hypoxic\ PFC}$=24.

IV.2.1.2 Effect of severe hypoxia on mechanical properties

MTC assays provided the evolution of mechanical properties and adhesion parameters in alveolar epithelial cells after exposure to normoxic and hypoxic PFC. We find that the CSK stiffness, E, and the norm of the complex elastic modulus $|Ge|$, are both decreased after PFC

exposure in severe hypoxic conditions (Figure 45). In a similar tendency, treatment by cytoD reduces CSK stiffness and abolishes the cellular response to PFC exposure. Altogether, migration and mechanical results enable to eliminate the possible role of oxygen in the functional and mechanical response to PFC exposure.

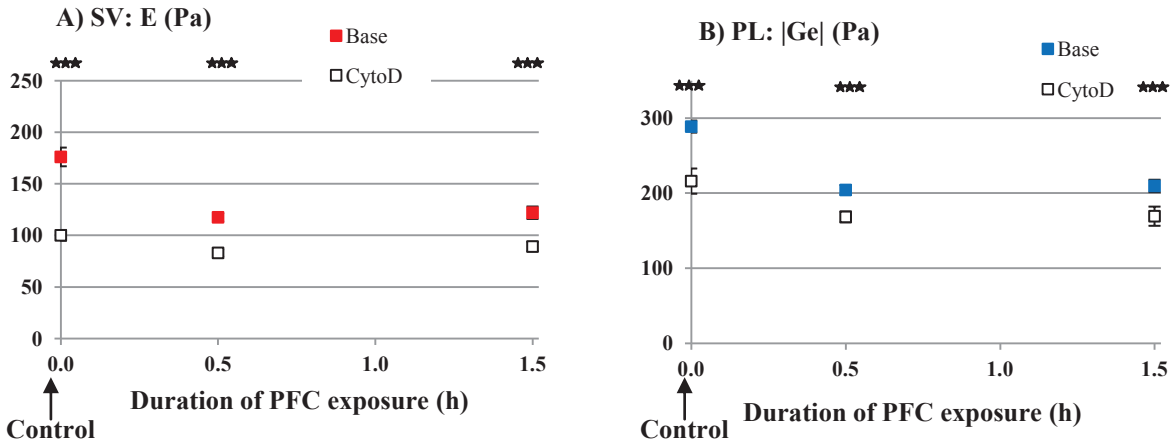

Figure 45: A549, mean values and SEM of cytoskeleton mechanical properties and adhesion parameters during severe hypoxic condition (1% of O_2) for control (t=0h) and for two durations of PFC exposure (0.5 and 1.5 hours) before and after cytoD treatment. A) cytoskeleton elastic modulus *E* in Pa. (B) norm of complex elastic modulus $|Ge|$. The difference between the control group in hypoxic conditions and the PFC group also in hypoxic conditions were analyzed using ANOVA tests. For *E* and $|Ge|$ significant differences ($p < 0.001$) were observed between the groups. The variation observed after and before cytoD treatment were analyzed using Wilcoxon tests and were always significantly different ($p < 0.001$).$n_{control}$= 6; $n_{0.5h\ PFC}$=14; $n_{1.5h\ PFC}$=12.

IV.2.2 Evaluation of the role of surface tension by intercalating a surfactant layer

A549 alveolar epithelial cells do not produce their own surfactant under cell culture condition (Swain et al., 2010), so to study the effect of surfactant and better mimic the physiology of the alveolar cell monolayer surface, surfactant was added as a layer (see section III.2.3.1). The

effect of intercalating a surfactant layer between the cell and the apical fluid (DMEM or PFC) on cell response, was studied for two exposure durations namely 0.5 h and 1.5 h. Evolutions of mechanical and adhesion parameters with a layer of surfactant deposited are analysed by comparison to the control condition, i.e., without a surfactant layer intercalated (dotted line) (Figure 46). Adding a surfactant layer results in a significant decrease - compared to control (E=167 Pa) - in cytoskeleton stiffness in cells exposed to PFC (E=119 Pa), and also in cells exposed in DMEM (E=148 Pa), although this decrease is not statistically significant (Figure 46 A and F). The values for 1.5h (DMEM) are outside the error range of the control. The decrease in cell stiffness reflected by the PFC-induced decrease in cytoskeleton stiffness appears even more marked when a surfactant layer is intercalated between PFC and cells. Concerning the adhesion parameters, a marked increase in K_{off}^{0} at 1.5 h of exposure duration with a significant decay in σ_c is obtained with SV model (Figure 46 C and D), but not with the PL model. These results show that intercalating a surfactant layer during PFC exposure does not suppress the cell response to PFC, but on the contrary, the cell response to PFC exposure tends to be increased which can be seen through values of K_{off}^{0} higher with surfactant than without (K_{off}^{0} *1.5h PFC*=0.07x10^{-3} s^{-1} and K_{off}^{0} *1.5h PFC with surfactant*=0.11x10^{-3} s^{-1}).

It is also interesting to note that adding a surfactant layer in the control condition (DMEM) also tends to induce a decrease in cell stiffness (*E control*=167 Pa to *E 1.5h*=148 Pa) and reference stress (σ_c *control* =44 Pa to σ_c *1.5h* =39 Pa) as well as an increase in K_{off}^{0} (K_{off}^{0} *control* =0.053x10^{-3} s^{-1} to K_{off}^{0} *1.5h* =0.064 x10^{-3} s^{-1}), compared to control, which are altogether at the limit of significance at 1.5h (at least). This effect of surfactant visible on control conditions demonstrates the same direction of cellular evolution than the PFC exposure with however a less marked effect.

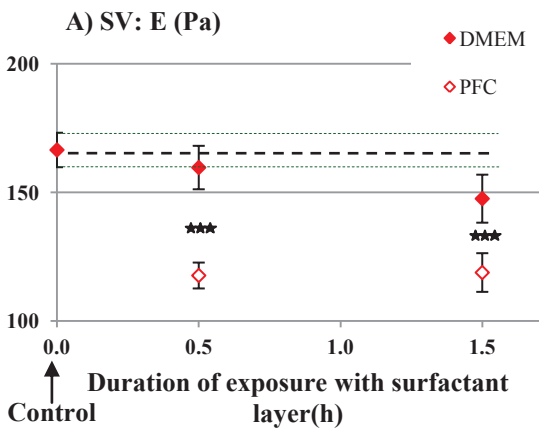
A) SV: E (Pa)
DMEM
PFC
200
150
100
0.0
0.5
1.0
1.5
***
***
Control
Duration of exposure with surfactant layer(h)

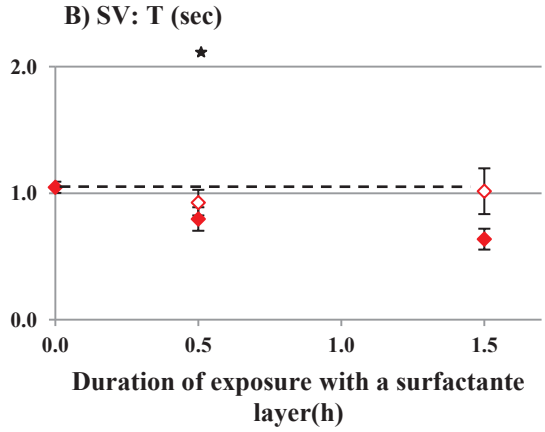
B) SV: T (sec)
2.0
1.0
0.0
0.0
0.5
1.0
1.5
Duration of exposure with a surfactante layer(h)

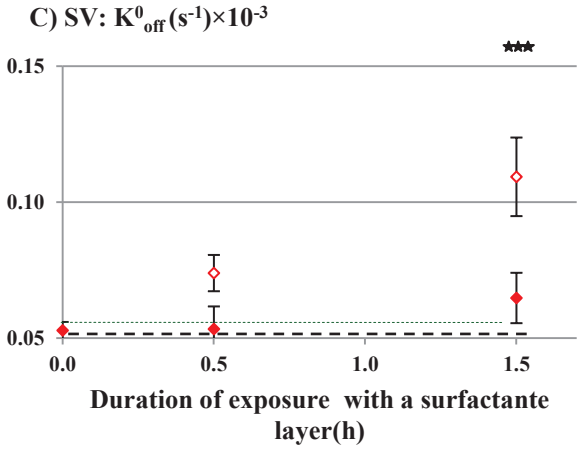
C) SV: K0off (s-1)×10-3
0.15
0.10
0.05
0.0
0.5
1.0
1.5
***
Duration of exposure with a surfactante layer(h)

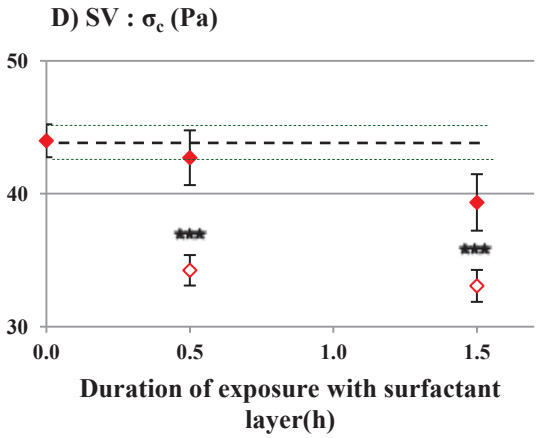
D) SV : σc (Pa)
50
40
30
0.0
0.5
1.0
1.5
***
***
Duration of exposure with surfactant layer(h)

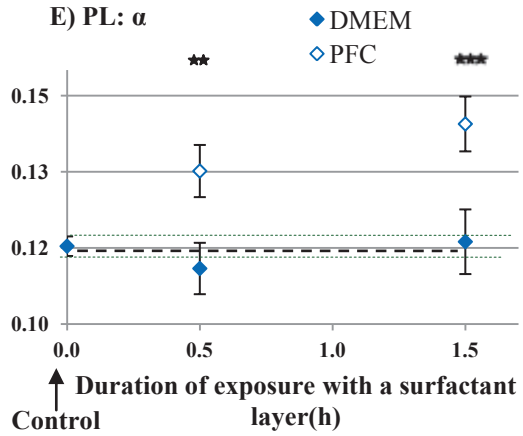
E) PL: α
DMEM
PFC
0.15
0.13
0.12
0.10
0.0
0.5
1.0
1.5
**
***
Control
Duration of exposure with a surfactant layer(h)

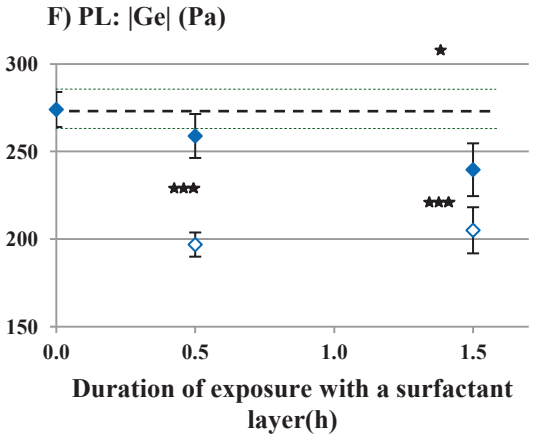
F) PL: |Ge| (Pa)
300
250
200
150
0.0
0.5
1.0
1.5
***
***
Duration of exposure with a surfactant layer(h)

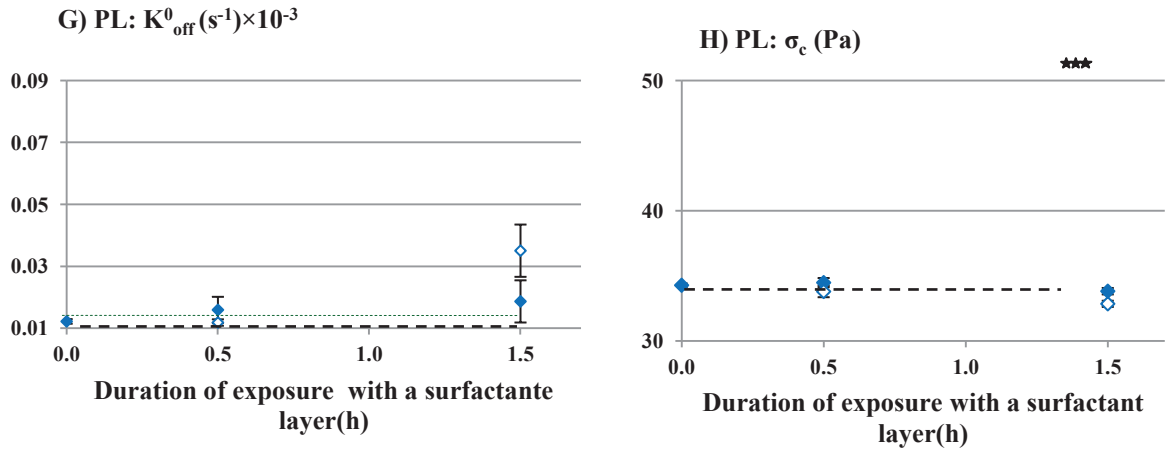

Figure 46: Effect of intercalating a surfactant layer on cellular response to DMEM or PFC. The mean values and SEM of cytoskeleton mechanical properties and adhesion parameters are given for control condition (t=0h) and after two durations of either DMEM or PFC exposures (0.5h and 1.5h) while a surfactant layer is intercalated. The parameters of the viscoelastic solid-like model with adhesion parameters of the SV model (in red) are plotted: (A) cytoskeleton elastic modulus *E* in Pa, (B) viscoelastic relaxation time T in s, (C) natural dissociation rate K_{off}^{0} in s^{-1}, (D) reference stress σ_c in Pa. The parameters of PL model (in blue): (E) exponent of the power law: α, (F) norm of the complex storage modulus: |Ge| at f=1 Hz in Pa, (G) natural dissociation rate K_{off}^{0} in s^{-1}, (H) reference stress σ_c in Pa. The differences between the control group and the cells with a surfactant layer were analyzed using ANOVA tests (number of stars quantifies the significance by reference to the measured value in control conditions, i.e., the dotted horizontal line, namely ***: $p < 0.001$; **: $p < 0.01$; * : $p < 0.05$). The effect of surfactant layer on cell for control conditions (DMEM) is visible at 1.5h of exposure where the mean values of *E* and K_{off}^{0} for SV model are beyond the variance values obtained for control conditions. This also true for the |Ge| of the PL model.n_{base}=59, $n_{base\ surfactant\ 0.5h}$=20, $n_{base\ surfactant\ 1.5h}$=15, $n_{PFC\ surfactant\ 0.5h}$=22, $n_{PFC\ surfactant\ 1.5h}$=17

IV.3 Cellular response to PFC exposure on other lung cell types

IV.3.1 Alveolar macrophages

Mechanical behavior and mechanosensitivity of alveolar macrophages have been intensely studied in the laboratory (Fereol et al., 2006; Fereol et al., 2009; Fereol et al., 2008). To understand the effect of PFC exposure on this cell type, we measured the mechanical and adhesion properties of adherent macrophages in a rigid substrate. The exposure of alveolar macrophages to PFC doesn't seem to induce cellular changes in the mechanical parameters, or alternatively, macrophages seem insensitive to PFC. This is surprising since alveolar macrophages were found highly sensitive to mechanical properties of environment in previous studies. To understand this result, it might be useful to focus on the deep differences found in the mechanical properties and adhesions parameters between alveolar macrophage and alveolar epithelial cells (Figure 47 and Figure 40). Macrophages (E=51 Pa) are much less stiff than A549 cells (E=167 Pa). Because they are immune cells contributing to lung defense, they easily and rapidly migrate and have mostly dynamic adhesion sites called podosomes. Measured values of the natural dissociation rate in macrophages reveals that K_{off}^{0} (de-adhesion) values are about 4 times higher for macrophages than for epithelial cells. This result confirms that macrophage adhesion sites have smaller lifetime and thus are more dynamic than focal adhesion sites. The reference stress σ_c is also drastically decreased compared to A549, suggesting that energy barrier is not only lowered, due to the increased K_{off}^{0}, but also displaced towards larger distances. Surprisingly, the relaxation time constant T is not modified between the two types of cells. CytoD at elevated concentrations has a significant effect in all mechanical and adhesion parameters. The cytoD effects for the mechanical parameter E (usually the most sensible to this drug) is greater in A549 than in macrophages

(in A549 *E* drops from 167 to 101 Pa after cytoD treatment, and in macrophages *E* drops from 51 to 38 Pa). This result suggests that macrophages have a lower level of internal tension. On the other hand cytoD has a stronger effect on K_{off}^{0} in macrophages that on A549. This result confirms that the interactions between the adhesion sites and CSK structure, are very different between cell types. Adhesion sites in macrophages have an organized actin structure integrated around the adhesion site. The adhesion site is easily accessible to cytoD due to its closeness to cell membrane, explaining the great effect of cytoD drug on macrophage de-adhesion, while the lack of stress fibers in macrophages explain the smaller effect of this drug on rigidity. In summary, macrophages are very distinct from A549, which could explain the difference in the mechanical and adhesion parameters after PFC exposure. Macrophages have lower internal tension, a different actin organization of adhesion systems, different glycocalyx expression, and many other factors that remain to be further tested. Another important difference between these two cellular types is that macrophages do not form a confluent monolayer. Thereby the interface with the medium implicates the cell (isolated) and the substrate and not only the cells as in A549 monolayer.

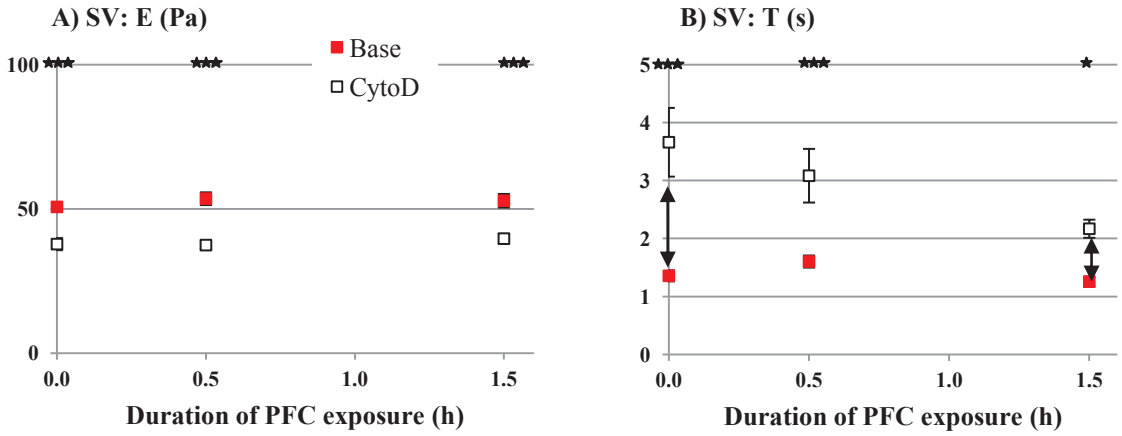

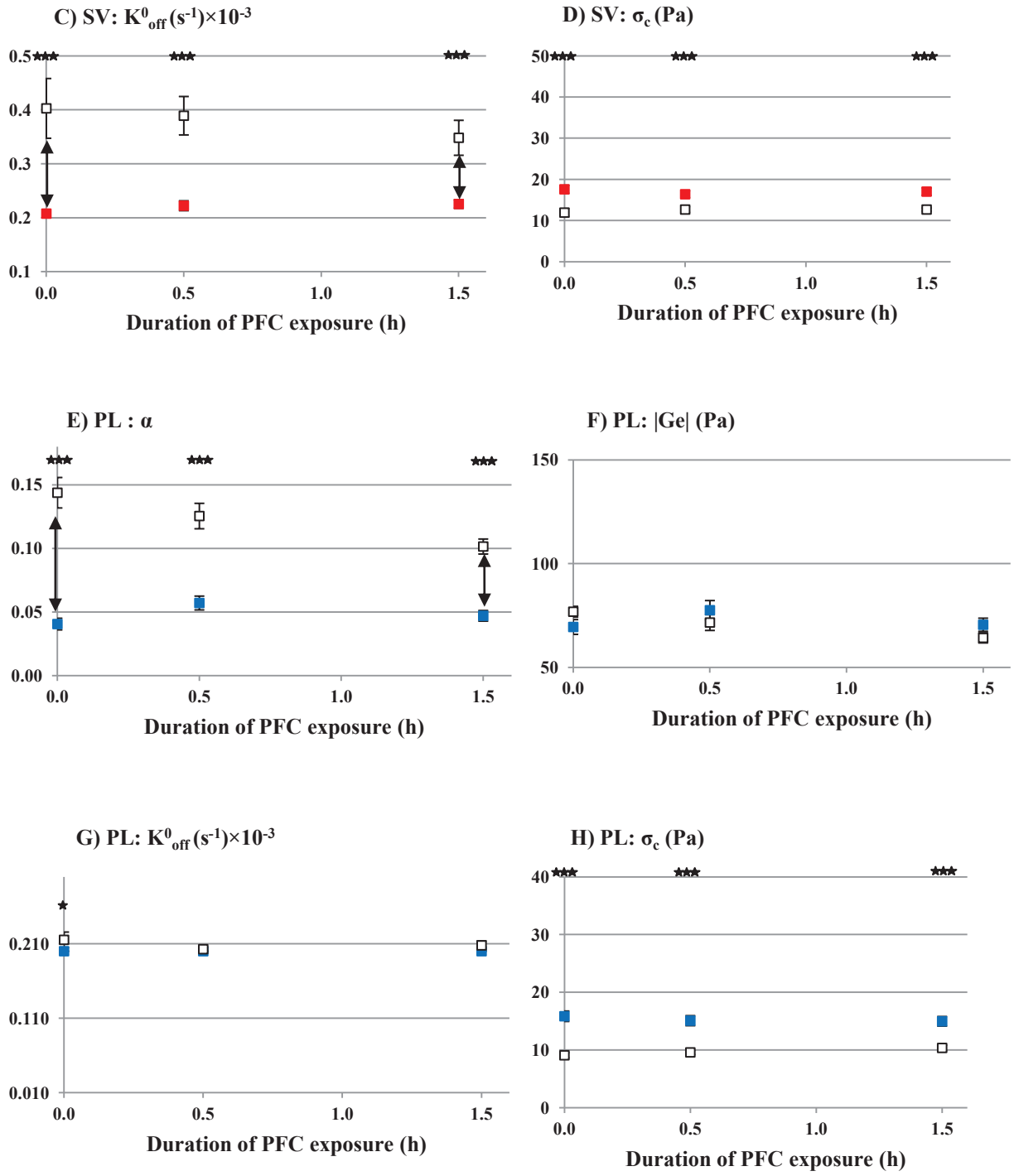

Figure 47: The response of alveolar macrophages to PFC exposure is analyzed - after exposure - in terms of mechanical properties and adhesion parameters with and without cytoD treatment. Mean values and SEM of cytoskeleton mechanical properties and adhesion parameters, for control (t=0h) and after two durations of PFC exposure (0.5 and 1.5 hours) before and after cytoD treatment. (A) cytoskeleton elastic modulus *E* in Pa. (B) viscoelastic relaxation time in s (C) natural dissociation rate K^0_{off} in s^{-1}. (D) reference stress σ_c in Pa. For the PL model, (E) exponent of the power law: α, (F) norm of the complex storage

modulus: |Ge| at f=1 Hz in Pa, (G) natural dissociation rate K_{off}^{0} in s^{-1}, (H) reference stress σ_c in Pa. The difference between control and PFC groups are analyzed using ANOVA tests. No significant differences were observed between these two groups. The differences observed with and without cytoD treatment are analyzed using Wilcoxon tests and they are all highly significant. $n_{control}$= 28; $n_{0.5h\ PFC}$=27; $n_{1.5h\ PFC}$=34.

IV.3.2 Bronchial epithelial cells (HBE)

IV.3.2.1 MTC assays

Present MTC results show that HBE express a moderate sensitivity to PFC exposure, mostly at the longer duration of 1.5h, where significant differences with control conditions are observed for most of mechanical and adhesion parameters (Figure 48). Note that the HBE response to PFC exposure goes in the same direction than the results obtained for A549: CSK stiffness is decreased while adhesion is weakened (Figure 40). It should be underlined that the maturation of 16HBE14o- is actually much slower than A549 cells. This lack of maturation has a clear impact on the mechanical properties and adhesion parameters measured by MTC. Indeed, these properties and parameters greatly differ from alveolar epithelial cells (compare Figure 48 to Figure 40). One day after seeding, the HBE stiffness is still as low as E=61 Pa while it reaches E=167 Pa in A549 after the same time of seeding. Indeed, HBE only reaches the values of stiffness of A549, after 4 days maturation (Doornaert et al., 2003). It has been shown by Doonaert et al. (Doornaert et al., 2003) that such a time of latency is necessary for HBE to develop a tensed actin structure. This is why, at only 1 day, the structure of CSK in HBE is still immature, or under maturation. So, the contribution of the tensed actin structure (or equivalently the CSK prestress) to CSK stiffness, which has been found to be the larger compared to microtubules and intermediate filament in the early study of Wang et al. (Wang et al., 1993), remains rather low, hence the low values of cell stiffness values measured at 1 day. At the same time, the natural dissociation rate K_{off}^{0} is 3 times higher in HBE compared to

A549, a result consistent with the link existing between adhesion site maturation and stability of adhesion. The lower values of σ_c might be attributed to a smaller number of bonds, in the non fully mature adhesion sites of HBE, compared to the fully mature focal adhesion sites which characterize A549. So present results obtained in HBE tend to confirm that these cells, in the immature phase, have a shortly polymerized actin network, are poorly adherent and most likely have a rounded shaped cell (Doornaert et al., 2003). Note that, HBE at day 1 of seeding, share with alveolar macrophages a low CSK stiffness, a low internal tension, a lack of stress fibers and an increase in de-adhesion. So, there is some reason to have a modified response to PFC exposure, e.g., this response appears indeed moderate for HBE and weak for macrophages. On the other hand, it is important to note that the lack of maturity of HBE tested does not totally suppress their sensitivity to PFC exposure while macrophage do not express such a sensitivity.

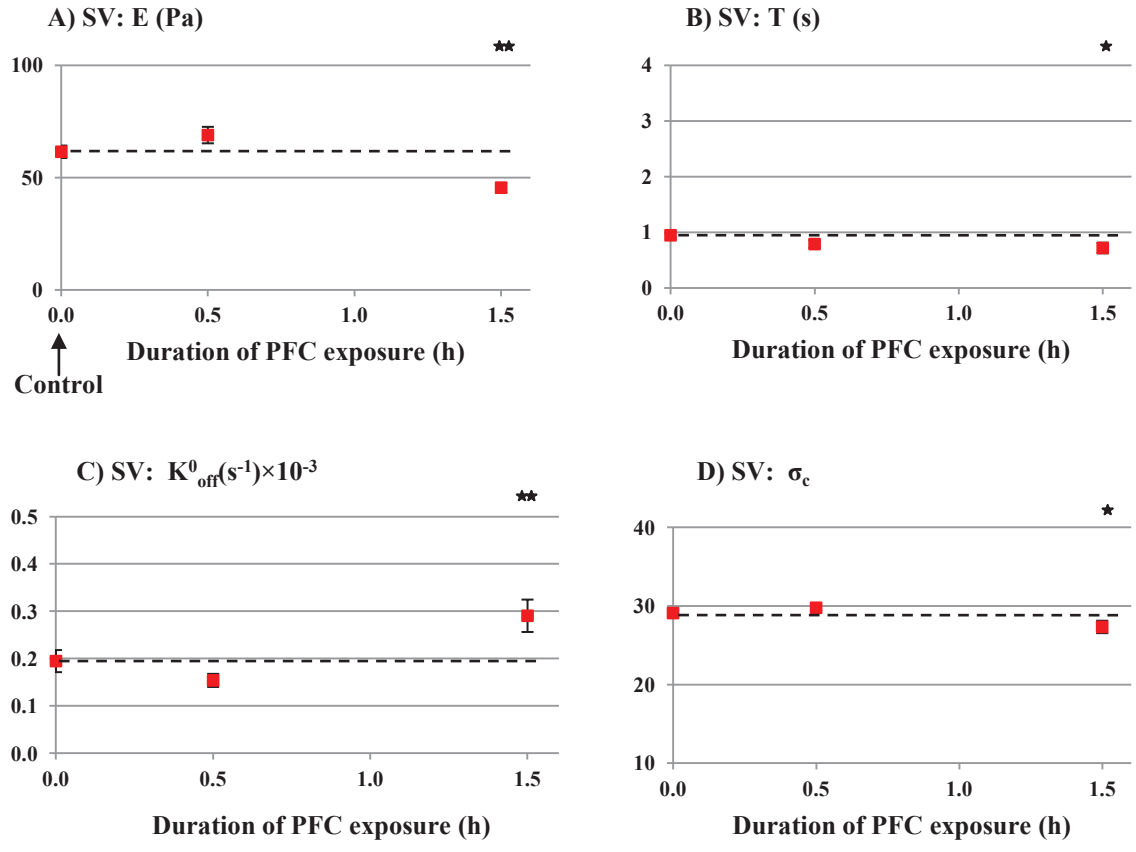

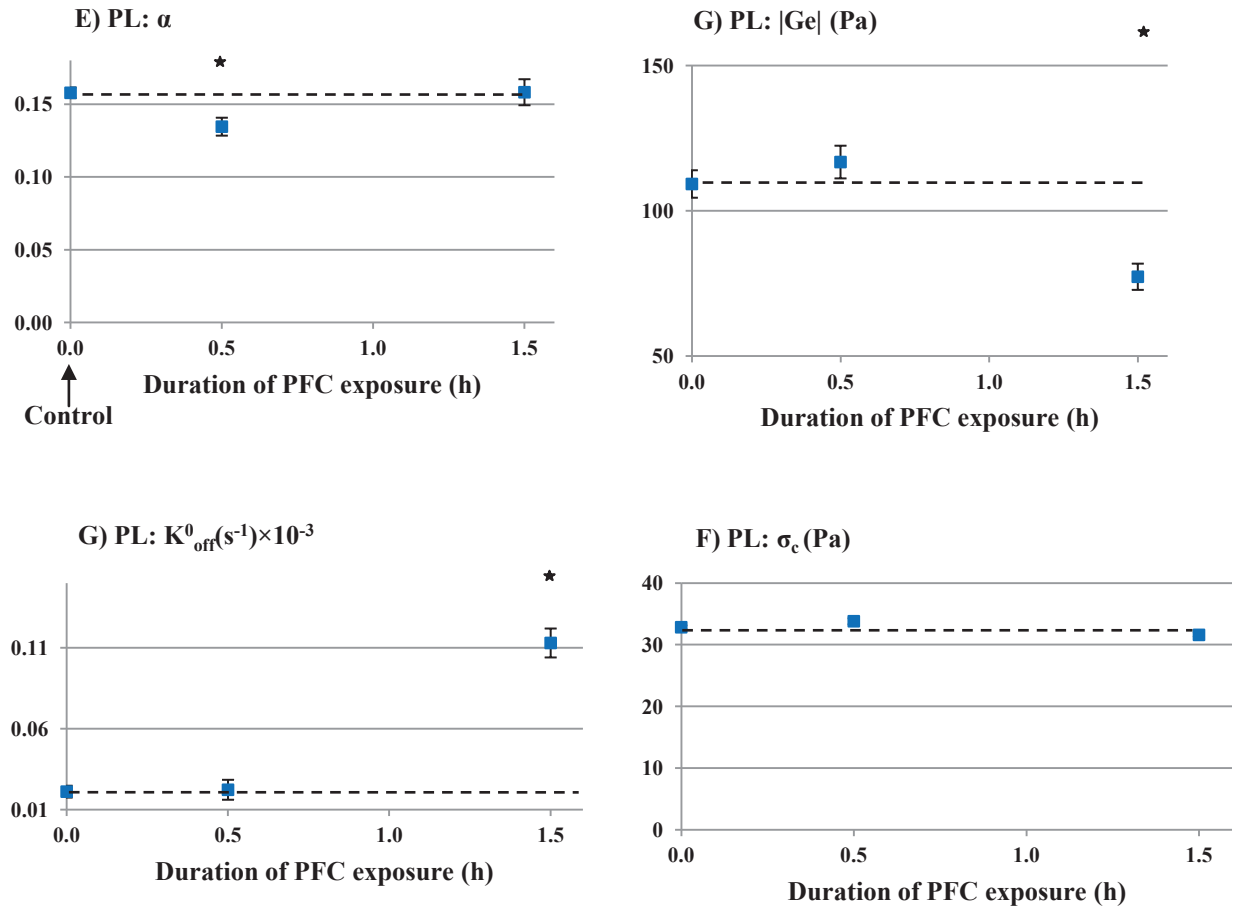

Figure 48: The response of Human Bronchial Epithelial (HBE) cells to PFC exposure is analyzed - after exposure - in terms of mechanical properties and adhesion parameters, assessed by MTC. HBE cells mean values and SEM of cytoskeleton mechanical properties and adhesion parameters, for control (t=0h) and after two durations of PFC exposure (0.5 and 1.5 hours). (A) cytoskeleton elastic modulus *E* in Pa. (B) viscoelastic relaxation time in s (C) natural dissociation rate K^0_{off} in s^{-1}. (D) reference stress σ_c in Pa. For the PL model, (E) exponent of the power law: α, (F) norm of the complex storage modulus: |Ge| at f=1 Hz in Pa, (G) natural dissociation rate K^0_{off} in s^{-1}, (H) reference stress σ_c in Pa. The difference between control group and PFC group were analyzed using ANOVA tests. (*: $p < 0.001$; **: $p < 0.01$; * : $p < 0.05$). $n_{control}$= 46; $n_{0.5h\ PFC}$=46; $n_{1.5h\ PFC}$=28.**

IV.3.2.2 MTS assays

During TLV, bronchial epithelial cells are susceptible to experience a considerable shear stress due to the increased density and viscosity of PFC liquid that replaces air. However, these cells are not necessarily used to support such a stress. The MTS technique enables to expose adherent cells to a cyclic 3D-stress generated by the beads (Ohayon et al., 2004). This stress aims at mimicking the effect of liquid ventilation, because this type of ventilation is cyclic and sustained during some minutes or hours. Thus, studying the bronchial epithelial cell response to a sustained periodic stress after cells have been exposed for 2 durations to PFC, might be of interest to investigate how PFC may affect the cell response to mechanical stress. This protocol mimics the reanimation conditions in which a patient resuscitated from cardiac arrest, is first treated during transport by Total Liquid Ventilation, and then admitted in intensive care to be conventionally or TLV ventilated. We remind that 1 hour stimulation at 3 Hz would correspond to 10800 breathes, i.e., around a day of TLV for a patient breathing at 0.1 Hz. Mechanical and adhesion results obtained for 2 durations of PFC exposure, are presented in Figure 49. It appears that preliminary PFC exposure does not significantly alter the HBE response to mechanical stress. Interestingly, mechanical stimulation and PFC exposure act in opposed directions in terms of CSK stiffness and cellular adhesion. On the one hand, PFC exposure tends to decrease CSK stiffness and to weaken adhesion, a tendency which is clearly observed in HBE right after PFC exposure, i.e., before mechanical stimulation (Figure 49 or Figure 48). On the other hand, mechanical stimulation is expected to increase intracellular tension and reinforce cell-matrix adhesion. This tendency is only weakly observed in HBE (see control condition in Figure 49) most likely because HBE at 1 day of culture remain in an immature state, and are only moderately tensed (E in HBE =61 Pa; E in A549 =167 Pa) and adhesion is still weak (K_{off}^0 in HBE=0.195x10^{-3} s^{-1} ; K_{off}^0 in A549= 0.053x10^{-3} s^{-1}). However, the interesting result is that PFC exposure does not suppress the

cellular adaptation to mechanical stimulation, since, after PFC exposure, stimulation still results in a discrete increase in E and σ_c and a significant decrease in K_{off}^0, as observed in Figure 49 A, C, D and to a certain extent, in E, G, H.

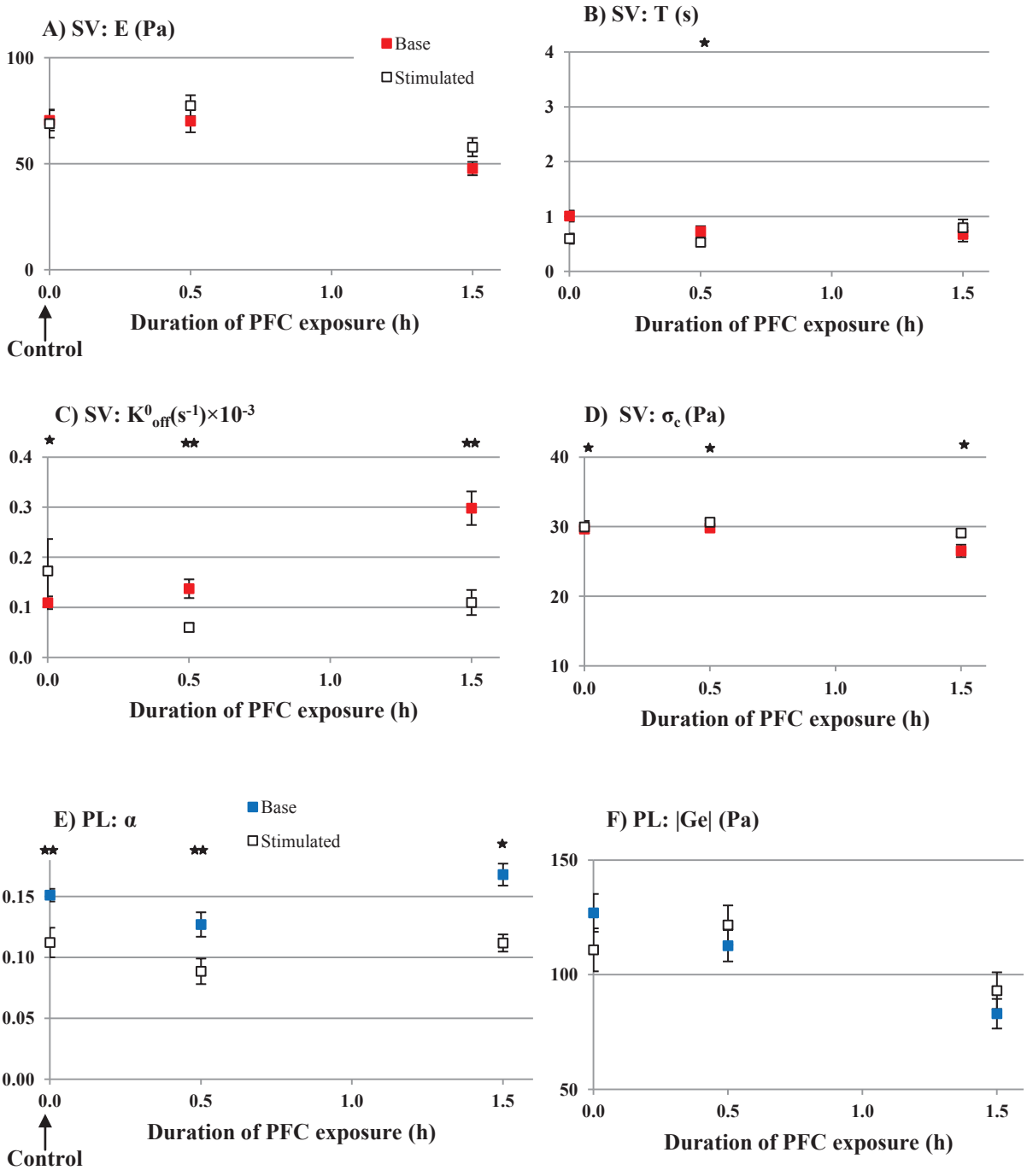

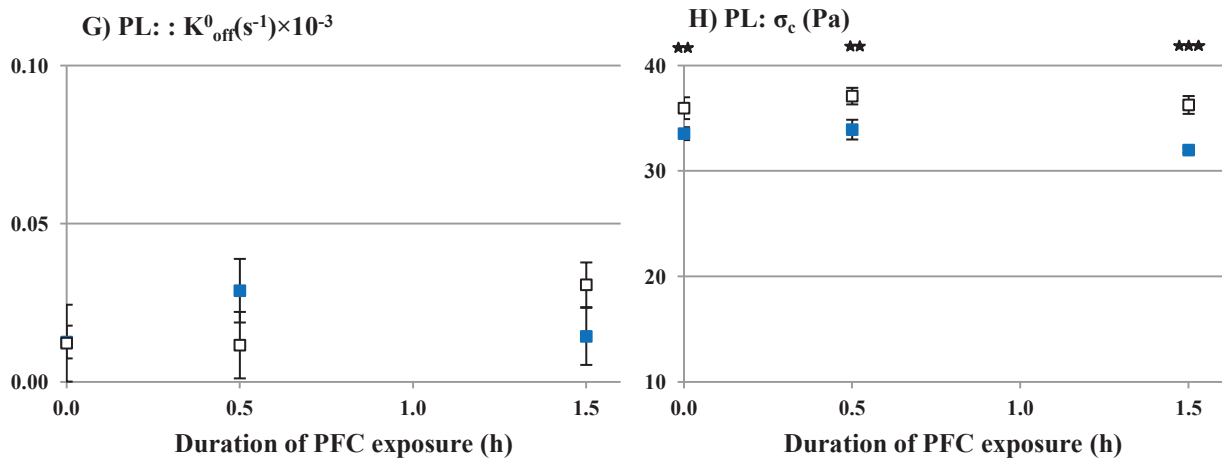

Figure 49: Effect of PFC exposure on mechanically stimulated and non stimulated bronchial epithelial cells. Mean values and SEM of cytoskeleton mechanical properties and adhesion parameters before and after 1h of stimulation (stimulated), for control (t=0h) and after two durations of PFC exposure (0.5 and 1.5 hours). (A) cytoskeleton elastic modulus *E* in Pa. (B) viscoelastic relaxation time in s (C) natural dissociation rate K^0_{off} in s^{-1}. (D) reference stress σ_c in Pa. The variation observed after and before 1h of stimulation were analyzed using Wilcoxon tests. For *E* there is no difference before and after stimulation. For *T* results are significantly different after stimulation for control and 0.5h of PFC ($p < 0.05$). For σ_c results are significantly different after stimulation for control ($p < 0.05$). For K^0_{off} results are significantly different after stimulation for control ($p < 0.05$), and for 0.5h and 1.5h of PFC exposure ($p < 0.01$). $n_{control}$= 22; $n_{0.5h\ PFC}$=19; $n_{1.5h\ PFC}$=26.

IV.4 Physical measurements of surface tension

IV.4.1 Measure of surface tension (with air) and surface energy (with PFC) of liquids used for the cellular study

Using the method described in III.3.1 we present in Table 6 a summary of the measured surface tension and surface energy obtained for the different liquids used in the present study. For the 3 liquids tested (DMEM, PFC, Surfactant) the measure of surface tension values, relatively to air, is in agreement with literature results (Bernhard et al., 2000; Bongrand, 1995; Wesseler et al., 1977) which validates the measurement technique described in III.3.1. The surface energy values of DMEM-PFC and surfactant-PFC on the other hand were basically unknown before this study. The surface energy of PFC and surfactant (liquid-liquid) has the smallest measured value. This outcome agrees with the cellular results where the most drastic cellular effects, especially on adhesion, were obtained for the PFC-surfactant interface. DMEM-PFC interface is relatively elevated but remains in the range expected from previous studies (Bico, 2000).

Table 6: Surface tension (with air) and surface energy (liquid-liquid) values for the 3 fluids used for cell exposure i.e., DMEM, PFC and surfactant, and the contact angle measured with capillary walls (wetted glass). The highest values of surface tension (or surface energy) were obtained with the DMEM interfaces, while the highest contact angles were obtained with the surfactant interfaces and to a lesser extent with PFC. n per condition=10.

	Capillary 0.9 mm		***Capillary 0.6 mm***	
	σ (mN/m)	***θ_e (°)***	***σ (mN/m)***	***θ_e (°)***
DMEM-Air	67.6 ± 1.9	2.2 ± 2.6	68.8 ± 3.0	8.4 ± 2.1
DMEM-PFC	49.4 ± 2.6	7.0 ± 2.9	44.5 ± 2.3	7.1 ± 0.5
Surfactant-Air	43.8 ± 3.7	30.3 ± 2.0	36.0 ± 2.3	29.4 ± 2.1

PFC-Air	18.2 ± 2.4	1.6 ± 2.6	20.12 ± 2.2	12.2 ± 2.7
Surfactant-PFC	17.6 ± 1.2	24.4 ± 1.0	20.6 ± 2.4	12.2 ± 1.6

IV.4.2 Measure of surface tension (with air) and surface energy (with PFC) of surfactant diluted at different concentrations in DMEM

During TLV or during PFC exposure, surfactant secretion is not interrupted (Modell et al., 1970; Rüdiger et al., 2003; Wemhöner et al., 2010). At the same time, infiltration of blood plasma inside alveoli, which is already a critical problem for air ventilation, may become an acute problem during TLV. This is due to ventilatory pressures, more elevated in PFC ventilation than with air ventilation, that increase the risk of baro/volotrauma. So, it is important to determine how surface energy evolves with PFC for various concentrations of diluted surfactant and compare the parallel evolution observed with air. From Table 6, we know that replacing surfactant (100%) by water (DMEM) at a PFC interface leads to an increase in surface energy (i.e., σ = 49.4 mN/m for the interface PFC/water; versus σ = 17.6 mN/m for the interface PFC/surfactant (100%) in the capillary of 0.9mm). Figure 50A gives the surface tension (with air) evolution for various dilutions of surfactant from 100% to 1%. Figure 50B gives the surface energy (with PFC) evolution for various dilutions of surfactant from 100% to 1%. An interesting aspect revealed by these curves is their non linear feature. Starting at surfactant concentration of 100% (no dilution), we observe specifically for air that surface tension increases rapidly with the decrease of the percentage of surfactant (i.e., surfactant dilution). By contrast, the surface energy with PFC, starts to increase for concentrations of surfactant of only 10%, i.e., for high levels of surfactant dilution. A straightforward message is that PFC is capable to maintain a low surface energy even in front of highly diluted surfactant.

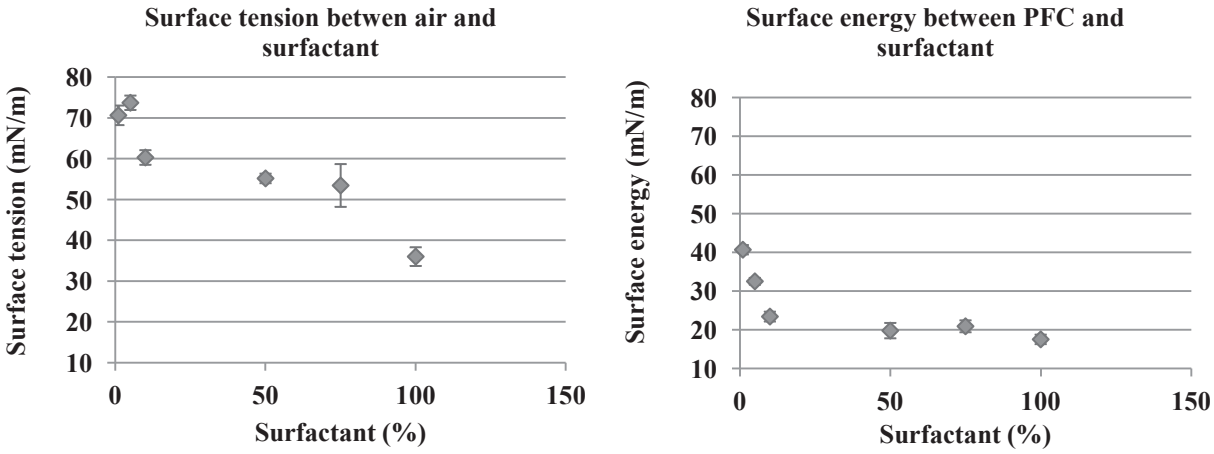

Figure 50: Evolution of surface tension (in mN/m) with air for different percentages of surfactant varying from 1% to 100% diluted in DMEM (n =3). With the decrease in percentage of surfactant from 100%, there is a rapid increase in surface tension. (B): Evolution of surface energy (in mN/m) with PFC for different percentages of surfactant from 1% to 100% diluted in DMEM (n =3). The surface energy with PFC of diluted surfactant starts to increase for concentrations of surfactant of only 10%.

IV.5 Measurements of lung compliance in the course of TLV

To estimate lung compliance in lungs ventilated with PFC, we used retrospective *in vivo* data obtained in 20kg-pigs ventilated by TLV. These data were obtained in the context of the ANR project (ABYSS) whose aim was to evaluate a new hypothermic treatment in the context of resuscitation of cardiac arrest (Hutin et al., 2015), we present two pigs by condition. Pressure and flow signals recorded during VLT were analyzed using the RIC-EEP model previously described in Material and Methods (see section III.4). We only consider here the results obtained for lung compliance (in ml/cm H_2O). These results correspond to pigs ventilated by hypothermic TLV either (i) without cardiac arrest or (ii) with cardiac arrest and resuscitation. The durations of TLV in each pig were highly variable (between 600 s and 2000 s), depending on their state. Results are presented in Table 7.

Table 7: Compliance results obtained for pigs ventilated with PFC without and with cardiac arrest (Horizontal scale: time in seconds).

Compliance (ml/cmH_2O)	
Hypothermic TLV in pigs for normal conditions (without cardiac arrest; (pig1 (left) pig2 (right))	
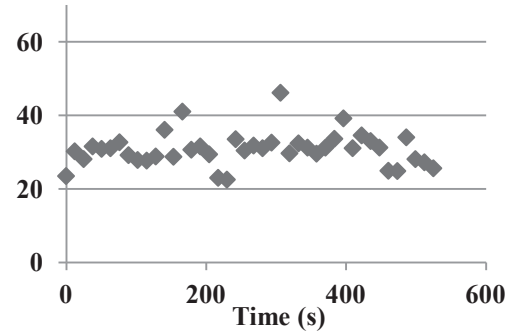	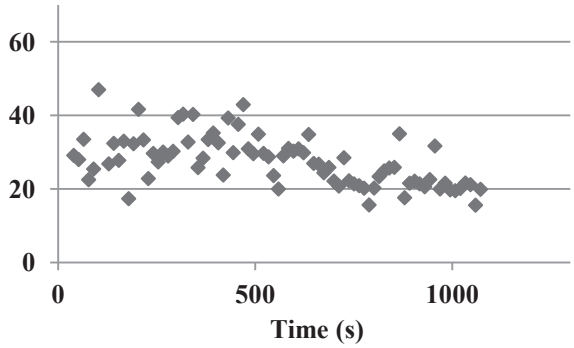
Hypothermic TLV with cardiac arrest and reanimation before ventilation (pig3; pig4)	
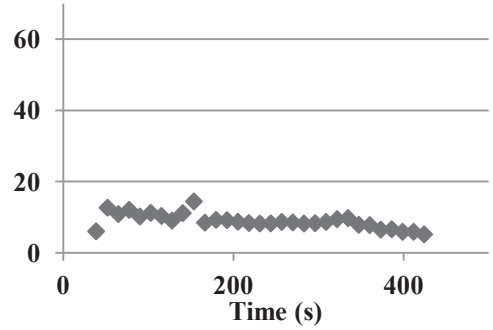	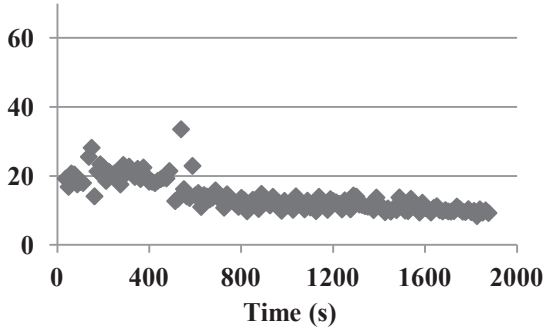

Lung compliance is a critical parameter for the outcome of artificial ventilation. In normal conditions, an increase in compliance compared to air ventilation is expected, due to the decrease in alveolar surface tension, permitted by the substitution of a liquid-tissue interface for the physiological air-tissue interface PFC (Beaulieu et al., 2012; Tooley et al., 1996; Wolfson and Shaffer, 2004). Note that compliance values presently obtained during TLV and normal lung conditions are ≈30 ml/cmH_2O (pig 1 and 2). Due to the lack of data of the same pigs ventilated in air, we compared the values of compliance above, with compliance values available in literature obtained in similar 20 kg-pigs ventilated in air, the

values of compliance for these pigs are ≈20 ml/cm H_2O (De Robertis et al., 2001; Kytta et al., 1995). So the values obtained during air ventilation on lung compliance, are smaller compared with liquid ventilation. On the other hand, pigs resuscitated from a cardiac arrest and treated by hypothermic TLV exhibit a marked decrease in lung compliance even when compared to lung compliance measured during air ventilation, ≈10 ml/cm H_2O (pig 3 and 4, Table 7). The reasons explaining why values of lung compliance during TLV and resuscitation of cardiac arrest are so low, might deal with cardiac massage. It has been shown that cardiac massage was found to induce a drastic decrease in lung compliance (Wenzel et al., 1998). It is reasonable to consider that cardiac massage might generate numerous baro/volotrauma i.e. due excess in alveolar pressure variations especially during TLV. We explain with more details in sections V.3 and V.4 how the changes in surface tension in the alveolar area caused by edema, are most likely the reason why lung compliance property is dramatically degraded after baro/volotrauma induced by cardiac massage.

V. DISCUSSION

V.1 Regulation of pulmonary cell response to PFC exposure

In the cellular part of the present study, we use fluorescent imaging of key structural elements (cytoskeleton, focal adhesion and glycocalyx), and an integrin-specific micromanipulation method (MTC) directed towards the same structural elements, to characterize the response of pulmonary cells (alveolar epithelial A549 cells, bronchial epithelial HBE cells, alveolar macrophages AM) exposed to PFC for a variety of durations . The first important message provided by this mechanobiological assessment is that epithelial cells exposed to PFC exhibit an adaptive response in terms of structure, mechanics, adhesion and function, thus significantly differing from cells in standard culture medium. The evolutions characterizing the cell response to this particular apical environment generated by PFC in epithelial cells are: remodeling of the F-actin structure, diminution of cytoskeleton stiffness and weakening of adhesion. Incidentally, we were not able to measure such a PFC-induced cellular response in AM. Such a PFC-induced epithelial cell response has never been reported in the literature and make us question about the mechanisms behind this cellular adaptation

To determine the cellular elements susceptible to play a role in this PFC-induced epithelial cell response, we used degrading molecular elements, respectively directed against F-actin structure integrity and glycocalyx layer. Thereby, two complementary signaling systems have been identified for their role played in this cellular adaptation. One is the intracellular tensed actin structure, which has already been proved to play a key role in mechanotransduction (Ingber, 2008; Maniotis et al., 1997; Wang et al., 1993; Zhu et al., 2000). The other is the surfacic glycocalyx layer, which is known to play a role on the shear stress adaptation of endothelial cells (Yao et al., 2007) (see also Figure 13) and is also present

in AEC (Martins and Abairos, 2002). These two cellular elements: F-actin and glycocalyx layer, are physically connected as they work together to the cellular regulation (Squire et al., 2001; Thi et al., 2004). These two cellular elements are of measurable significance in the cell response to PFC exposure: (i) the PFC-induced cell softening response is erased by cytoD treatment (Figure 41), confirming the contribution of F-actin-network to cell stiffness and the role of cell prestress (Stamenovic et al., 2002); (ii) similarly, when the glycocalyx layer is degraded by heparinase III, the measured mechanical and adhesion parameters converge toward values close to those of the control, confirming that glycocalyx contributes to cell adaptation to PFC exposure (Figure 42) most likely through glycocalyx redistribution (Figure 51).

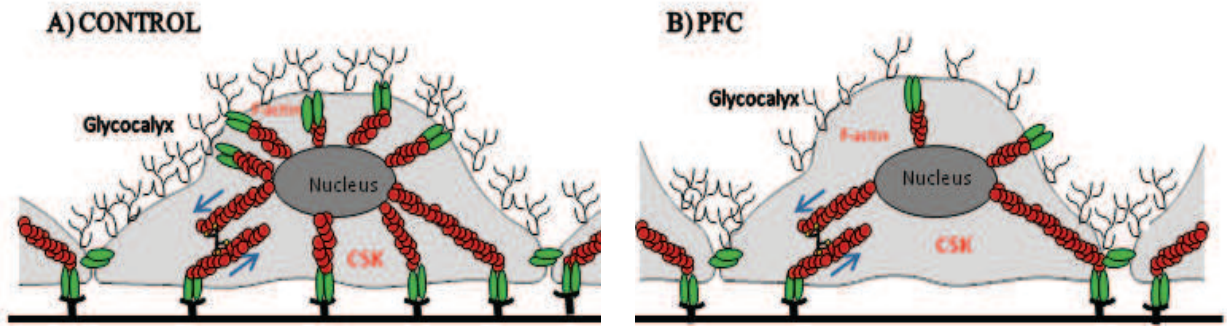

Figure 51: Schematic representation of configuration of F-actin, focal adhesion and glycocalyx in control and after PFC exposure.

These results strongly suggest that the tensed F-actin structure and the glycocalyx layer at the cell membrane, are key components of the cell signaling response involved during PFC exposure.

Imaging F-actin structure and focal adhesion reveals that PFC exposure results in changes in structural organization through F-actin remodeling, decay in number and size of focal adhesions, and redistribution of glycocalyx (Figure 38 and Figure 39). The decay in fluorescent F-actin and the vanishing of stress fibers is consistent with the decay in cell

stiffness measured by MTC and predicted by the two different micro-rheological models, namely the solid viscoelastic model (single Voight) and the power law model. We remind that the two models, with specific mechanical and adhesion parameters defined by the least square method both exhibit a correlation with experimental data above 95%. However, the loss in adhesion stability in exposed cells, visible in the reduction of number and size focal adhesions, is only predicted by the solid viscoelastic model (SV) where the natural dissociation rate K_{off}^{0} tends to increase, and the characteristic stress σ_c to decrease (Figure 40). By contrast, the power law model (PL), seen as an infinite series of Voigt elements with relaxation times or characteristic frequencies distributed as a power law (Balland et al., 2006), fails to provide significant information concerning cell de-adhesion. It seems that describing the multiscale nature of a cellular material by an infinite series of elementary Voigt models, implicitly assumes that the irreversibility of the cell response is uniquely due to its partial fluidic nature, and not to de-adhesion. For instance, cytoskeleton softening (see Figures Figure 40 F, Figure 42 F, Figure 46 F) is often associated to fluidization as shown by the discrete increase in the exponent α (see Figure 40 E, Figure 42 E, Figure 46 E). Since only the SV model provides significant evolutions of adhesion parameters consistent with the staining images of adhesion, we considered it as meaningful to describe the present biological evolutions. Based on the present corpus of data, obtained in a variety of biological conditions and in different pulmonary cells, the SV model has been able to provide data with an accuracy sufficient to detect sensitive cellular modifications, enabling to reveal a never reported PFC-induced cellular response.

Different physico-chemical factors related to the highly specific properties of PFC, might play a role in the cell response to PFC exposure. Amongst this characteristics we can exclude the role of the large density and dynamic viscosity (Wesseler et al., 1977), because AEC are tested in static conditions, relevant for reproducing the physiological conditions

experienced in alveolar territories (André Dias et al., 2015) so they experience no shear stress. Secondly, the large quantity of O_2 dissolved in PFC at normal atmospheric pressure could be seen as a mild hyperoxic condition and thus play a role in the modulation of functional, mechanical and adhesive properties (Sen, 2009). We thus performed the same evaluation of parameters in the condition of severe hypoxia (1% of O_2) and found that AEC properties were not modified (Figure 44 and Figure 45), suggesting that the larger amount of O_2 dissolved in PFC in standard experimental conditions does not account for the observed PFC-induced cell response.

Another PFC property that could be responsible for the reported cell response is the low surface tension of this liquid. Such assumption is consistent with the cellular results obtained when an exogenous surfactant layer is deposited at the apical cell surface. The presence of a surfactant layer appears to amplify the effects reported with PFC alone, especially for adhesion (Figure 46). Pulmonary surfactant, normally produced by type II alveolar cells but not by A549 cell line (Swain et al., 2010), is known to reduce surface tension at the interface between alveolar wall and air (Bernhard et al., 2000). Intercalating a surfactant layer at the interface between the cell surface and the fluid, e.g., (i) DMEM or (ii) PFC (Figure 46), induces a cellular response. In case (i) the cellular adaptation goes in the direction of PFC response herein characterized, and in case (ii) we obtain also the same response, but amplified for de-adhesion parameters.

Based on the above experimental considerations, the reduced surface tension which characterizes PFC and surfactant, constitutes a physical factor whose role in cell response, would be a triggering factor. The question is why and how such a passive physical property would act as an activator of the cell response. To answer these questions, it is important to consider the impact of a reduced surface tension on the energy balance at the cell surface.

V.2 The role of surface tension on the energy balance at the cell surface

The plasma membrane is composed by phospholipid bilayer in which glycoprotein and glycolypids are embedded. The membrane composition is about 45% protein, 45% lipids and 10% carbohydrate. In these membrane proteins there are two major classes: the hydrophobic (water-"scared") and hydrophilic (water-"friendly") proteins (André P., 1990; Bongrand, 1995; Bongrand, 1982; Bongrand, 1984). Membrane proteins occupy 25% of the cell surface (Bongrand, 1995), and the standard cell has a mass of 70% of water (Lehninger, 1973). There is permanent exchange and interaction, between the intra cellular and extracellular (aqueous) contents through ion channels, which are formed as assemblies of several individual proteins, closely packed around a water-filled pore through the plane of the membrane or lipid bilayer. Incidentally adhesion receptors are intrinsic membrane proteins with a specific shape and flexibility, which may protrude 10-20 nm above the lipid bilayer (Bongrand, 1995). The structures that extend above 20 nm of lipid bilayer include the glycosaminoglycans, namely glycocalyx. All these components contribute to the molecular complexity of the cell surface, which includes polar and non-polar components in an unknown and likely variable proportion.

For the presently studied epithelial cells, the cellular model is a continuous monolayer of confluent cells adherent on a substrate, with a liquid PFC or DMEM above. To describe the energetic equilibrium between the monolayer and the medium, we need an equation such as Equation 26 modified for the cell layer:

$$W = \sigma_{cell} + \sigma_{liquid} - \sigma_{cell-liquid} \qquad \textbf{Equation 35}$$

The interaction between the cell monolayer is dominated by the adhesion system. The description of the cell surface above tell us that σ_{cell} has both a polar and non-polar component, whose exact proportion is not precisely known. For the liquid above the cell

layer, namely DMEM and PFC, σ_{liquid} ,has two components for DMEM-polar and non-polar- $\sigma^{p}_{H_20} = 51\,\text{mN/m}$, $\sigma^{d}_{H_20} = 22\,\text{mN/m}$ (Comyn, 1992), and only one non-polar component for PFC $\sigma_{PFC} = \sigma^{d}_{PFC}$,because highly fluorinated species hold low polarity surfaces $\sigma^{p}_{PFC} = 0$ (Chhatre et al., 2010; Yakhshi-Tafti et al., 2011). We use the values of surface tension obtained for PFC in IV.4.1, $\sigma_{PFC} = 19\,\text{mN/m}$.

Taking a simplistic model for representing the cell, we use a polar solid (glass) and a polar liquid (water) with both polar and non-polar components. For the polar solid: $\sigma^{p}_{glass} = 80$ mN/m, $\sigma^{d}_{glass} = 32$ mN/m (Chibowski et al., 1989). To obtain the work of adhesion corresponding to this system, we use the equations Equation 29 and Equation 30 from III.3.2. The results are presented in Table 8. This table also presents the estimation of interfacial energy using Equation 35.

Results in Table 8 show that replacing PFC for water in our model of cell monolayer, considerably reduces the work of adhesion W, and thereby interfacial energy $\sigma_{cell-liquid}$ is expected to be considerably increased (Table 8). Assuming that cell surface properties are somewhere in between the solid and the liquid phases, it can be said that using a non-polar fluid with low surface energy such as PFC does not reduce the interfacial energy between fluid and "cell" surface but on the contrary increases the "cell" surface energy.

Table 8: Values of surface tension, work of adhesion and surface energy per unit area (mN/m). Values obtained with the Owens and Wendt model.

Interface	σ_A *(mN/m)*	σ_B *(mN/m)*	ψ	*W (mN/m)*	σ_{AB} *(mN/m)*
H_2O-PFC	73	19	0.55	41	51
Glass-PFC	112	19	0.53	49	82

Glass-H_2O	112	73	1	181	4

This reasoning holds independently on the precise amount of each polar and non-polar component. It is based on the fact that the non-polar PFC liquid, will never match the polar component of the cellular surface (Figure 52). Also besides being a non-polar liquid, PFC has also extremely low surface tension, which causes decreased work of adhesion and an increase in interfacial energy at the contact surface.

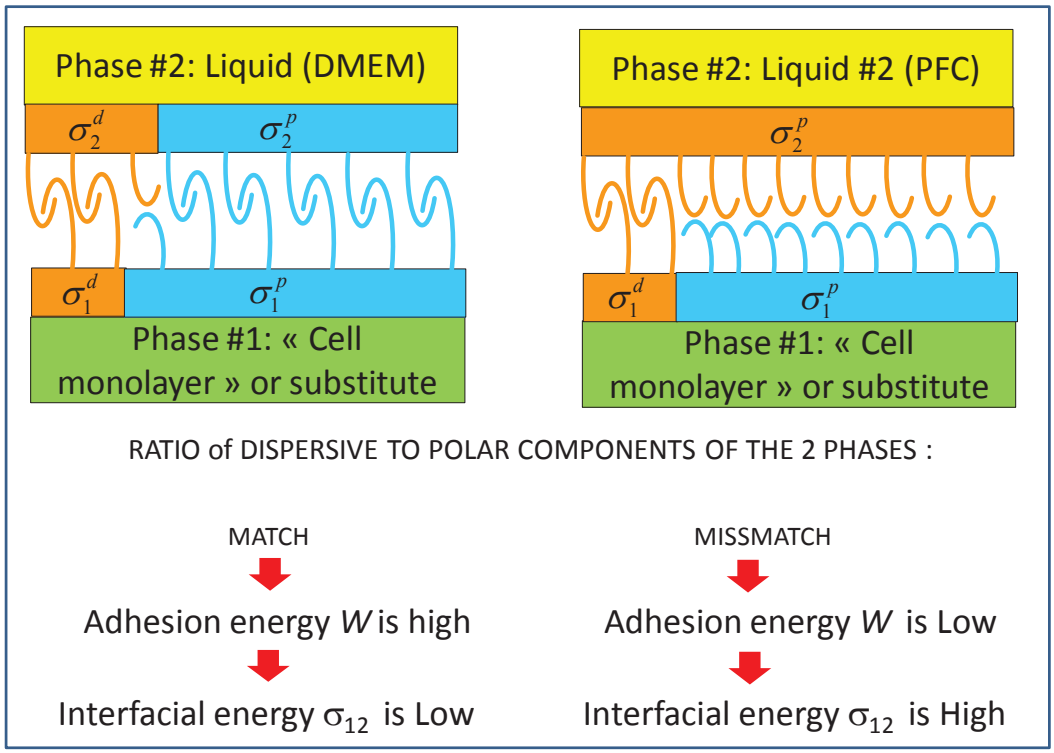

Figure 52 : Matching of polar and non-polar components of the liquid in interface with the cell layer.

This approach demonstrates that the use of the low surface tension liquid, such as PFC, necessarily causes an increase of the interfacial energy between the cell monolayer and that liquid, meaning that the cell surface energy changes dramatically when substituting PFC for DMEM. This change in energetic equilibrium at the cell surface is supposed to be at the origin of the cellular response along with adaptation to this new energy balance.

For the presently studied alveolar macrophages, the cellular response to PFC exposure was not found (see section IV.3.1). This result might be surprising if we consider the high sensitivity of macrophages to the substrate (Fereol et al., 2006; Fereol et al., 2009; Fereol et al., 2008), and even to surface tension of the bronchial wall (Bachofen and Schurch, 2001).

To try to explain this lack of response, we will consider the energetic equilibrium in the macrophage model. The assumption of a continuous monolayer is not applicable anymore, because macrophages are not at confluence. As a consequence, a new interface between the liquid and the substrate, must be taken into account, and a new energy balance has to be considered (Figure 53). Indeed, due to this new interface, the energy equation (Equation 35) has to be modified using Equation 6:

$$W_{cell\text{-}substrate}^{liquid} = \sigma_{cell\text{-}liquid} + \sigma_{substrate-liquid} - \sigma_{cell\text{-}substrate}$$ **Equation 36**

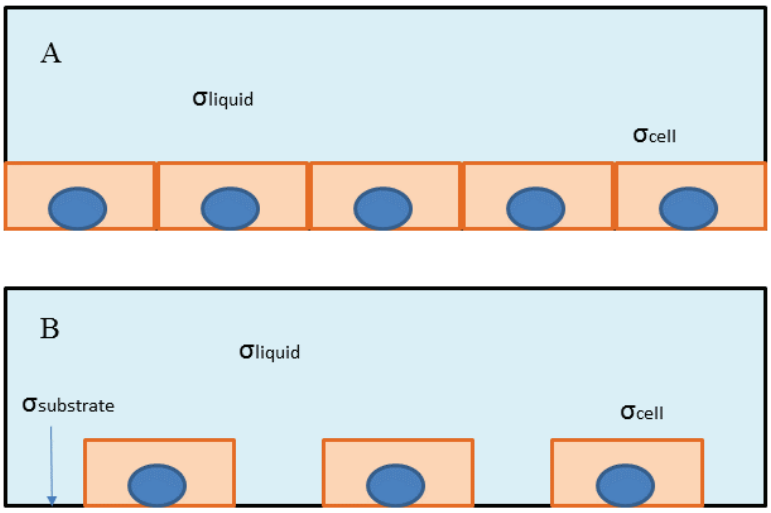

Figure 53 : Schematic representation of (A) a confluent epithelial monolayer (B) macrophage alveolar cells. The alveolar macrophages are unable to form a confluent monolayer, so the substrate is going to influence the energy balance.

Note that our macrophages are adherent on a plastic substrate (polystyrene) which has an almost negligible polar component, so it can be considered a non-polar solid (

$\sigma^{d}_{polyst} \approx \sigma_{polyst} \approx$34.5 mN/m) (DataPhysics). We will start by calculating $\sigma_{substrate-liquid}$ for the two different liquids: PFC and DMEM. Because polystyrene is a non-polar solid, using the equations from the Owens and Wendt model (Equation 29) we obtain a similar work of adhesion $W_{substrate\text{-}liquid}$ for the two liquids with the polystyrene substrate (Table 9). Using this value we will find the $\sigma_{substrate-liquid}$ for each liquid, that are respectively $\sigma_{substrate-liquid}$ = 2 mN/m for PFC, $\sigma_{substrate-liquid}$ = 55 mN/m for DMEM. Using the $\sigma_{cell\text{-}liquid}$ values calculated for the cell monolayer model, and knowing from the measures of de-adhesion in section IV.3.1, that macrophage adhesion is not changed by PFC exposure ($\sigma_{cell\text{-}substrate}$ is the same in the presence of both liquids). Therefore we can demonstrate using Equation 36 that $W^{DMEM}_{cell\text{-}substrate} \approx W^{PFC}_{cell\text{-}substrate}$, meaning that the energetic condition with the macrophage is such that the substrate interacts with the energy balance. In other words when there is a discontinuous cell layer, the energy equilibrium must take into account the interaction between the liquid and the substrate.

Table 9 : Values of surface tension, work of adhesion and surface energy per unit area (mN/m). Values obtained with the Owens and Wendt model.

Interface	σ_A *(mN/m)*	σ_B *(mN/m)*	ψ	*W (mN/m)*	σ_{AB} *(mN/m)*
Polystyrene-PFC	34	19	1	51	2
Polystyrene -H_2O	34	73	0.55	55	52

We recognize that these models are very crude compared to the complexity of cell structure. Cells have an adhesion system well represented by the integrin-ligand binding, that works either in complementary or competition, with the physical environment created by interfaces between the cell, and the different environments composing the cell neighborhood. An intriguing question is the huge differences in adhesion energy and surface energy. Usual

surface energies are of the order several tens of (mJ/m^2 or mN/m) (Table 6) while measurements of adhesion energy in A549 cells performed in AFM (Atomic Force Microscopy) (manuscript by Nguyen et al. under revision in *Biology of the cell, "Coupled evaluation of parallel integrin-matrix ligand binding and mechanics by force spectroscopy in alveolar epithelial cells"*) are of the order of hundredth of mJ/m^2 or mN/m. In other words, there is a ratio of two hundred between surface tension and adhesion energy. It means that the cells have an adhesion system which is able to sense the high energy of interfaces. By analogy the cell sensitivity to environmental stiffness occurring, through the low energy adhesion system, is capable to sense variations of orders of magnitude in Young modulus (see section II.4).

V.3 Pathophysiological consequences of the regulation by surface tension

This study shows the interest of decreasing the surface tension of the fluid in contact with epithelial cells, to modulate the interfacial energy and the work of adhesion at cellular wall, as well as to increase compliance at the lung level. We attempt in this applicative paragraph to theoretically estimate the evolution of the work of adhesion and interfacial energies that lung cells may experience during different pathophysiological conditions. Because the polar and dispersive components of surface tension of physiological liquids and cell surface are unknown, we cannot directly estimate W and σ_{AB}. Thus, we use the relationships obtained between surface tension and both W and σ_{AB} from some known solids and liquids: H_2O-PFC, Glass-PFC and Glass- H_2O (Table 8), to extrapolate the values of W and σ_{AB} for different values of surface tension. Using these 3 interfaces, we obtain the following relationships with surface tension (Figure 54).

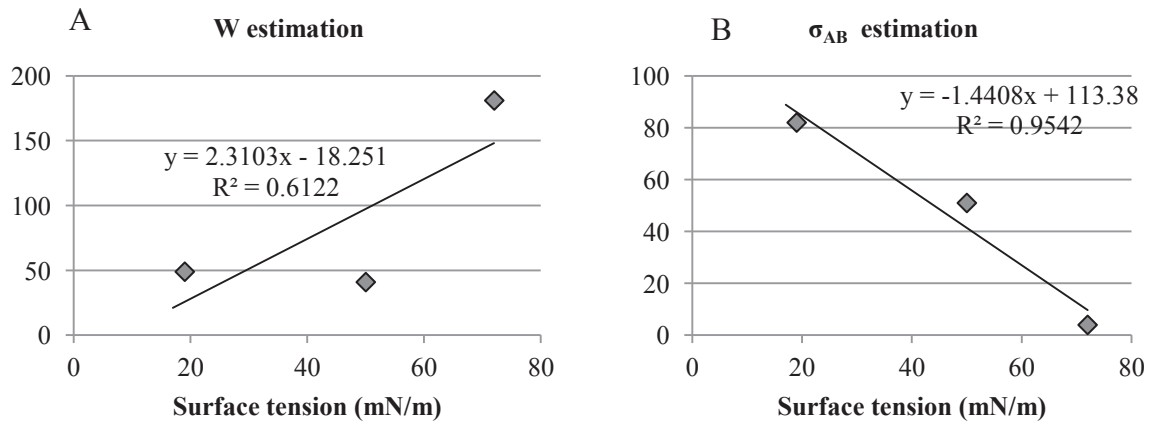

Figure 54: Relationships between work of adhesion, W in mN/m (and interfacial energy, σ_{AB}, in mN/m) and surface tension (in mN/m) obtained from 3 well-known interfaces: H_2O-PFC, Glass-PFC and Glass-H_2O .

Using the linear relationships obtained from the graphics in Figure 54 and knowing the values of surface tension for each condition, we can extrapolate the values for W and σ_{AB} in a variety of surface tensions (Figure 55).

- Water (control condition in cell culture, or edematous alveoli during, e.g., ARDS)
- Air with no surfactant (premature baby whit very diluted surfactant)
- DMEM + surfactant (cell culture with a surfactant layer)
- Water in interface with PFC (edematous alveoli during, e.g., ARDS ventilated with PFC)
- Air + surfactant (normal condition for a lung)
- PFC (lung ventilated with PFC or to a cell layer exposed to PFC)
- PFC + surfactant (lung ventilated with PFC with a surfactant layer or a cell culture with a surfactant layer and exposed to PFC)

In Figure 55 is represented a range of energetic situations potentially experienced by lung cells, due to change of the surface tension of the fluid in contact with the alveolar surface. Clearly the use of PFC enables an efficient decrease in the work of adhesion and an associated increase in interfacial energy to which epithelial cells were found to be sensitive.

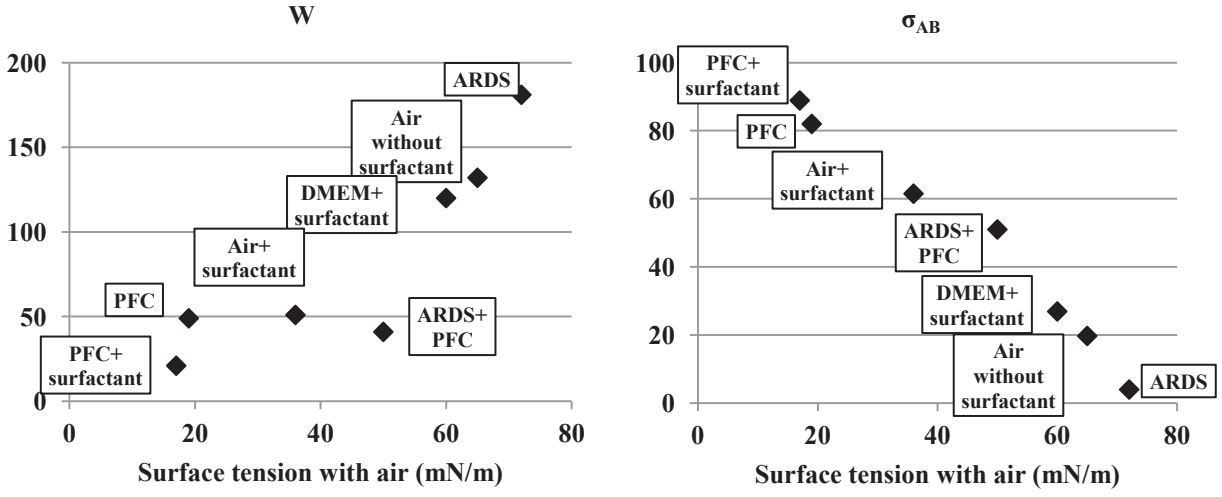

Figure 55: Evolution of the work of adhesion, W, in mN/m and interfacial energy, σ_{AB}, in mN/m with surface tension for different states of the lung.

The predictions in Figure 55 are especially important to understand how the surface tension evolves in a lung from normal to pathological conditions, and from air ventilation to PFC ventilation. Taking the case of an acutely injured lung (e.g., ARDS), a condition of acute edema, there is a dilution of surfactant accompanied by a decrease in compliance due to an increase in surface tension caused by the invasion of the lungs by blood plasma (Bersten et al., 1998). The evolution of surface tension with air for different concentrations of surfactant gives an idea of how fast this parameter changes as edema increases. As done above, the work of adhesion and the associated interfacial energy can be related to surface tension (section IV.4), for different surfactant dilutions in interfaces with air (Figure 56) and PFC (Figure 57). The interesting message is that PFC interface reduces the deleterious effect of diluting surfactant which is a favorable condition in case where plasma filtration begins and water starts filling the alveoli.

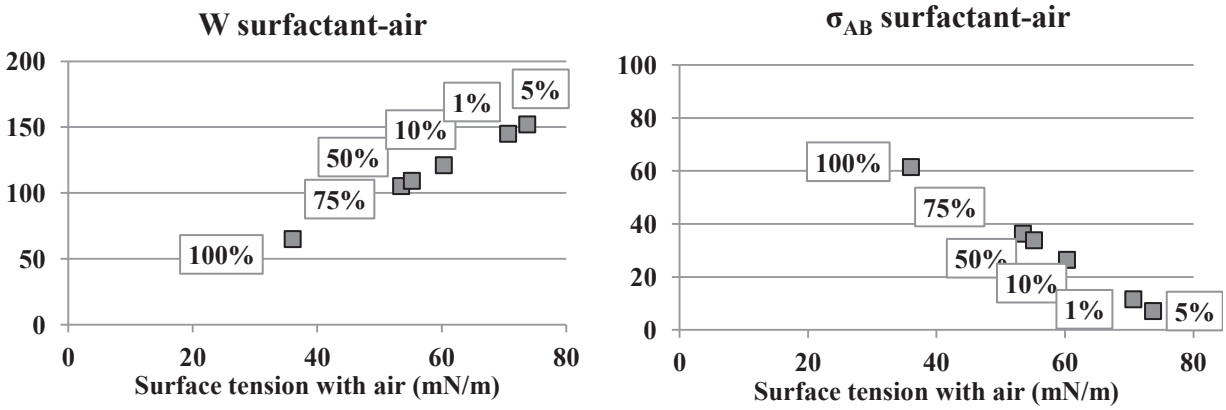

Figure 56: Evolution of the work of adhesion, W in mN/m and interfacial energy, σ_{AB}, in mN/m with surface tension for different percentages of surfactant with air.

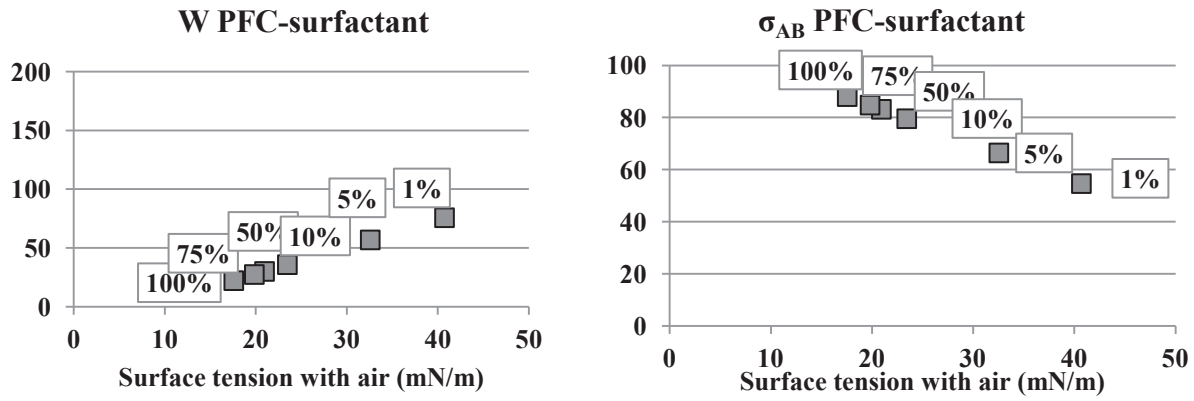

Figure 57: Evolution of the work of adhesion, W, in mN/m and interfacial energy, $\sigma_{AB,}$ in mN/m with surface tension for different percentages of surfactant with PFC.

V.4 Surface tension regulates lung compliance and cellular interfacial energy

The energetic considerations of the previous section are consistent with the results found for lung compliance in pigs ventilated in PFC, with and without cardiac arrest. In pigs without cardiac arrest (normal lungs) the found values of compliance during liquid ventilation are greater than the values found with air ventilation from literature (De Robertis et al., 2001; Kytta et al., 1995). These variations in lung compliance from air to PFC are also in agreement with a study performed in juvenile lambs in which the lung compliance in air increased from 12 ml/cm H_2O to 21 ml/cm H_2O during hypothermic liquid ventilation (Sage et al., 2016). In normal lungs, surfactant and PFC coexist, so the interfacial energy experienced by the lung is very high, due to the decrease in the work of adhesion, caused by the low surface tension of the PFC-surfactant interface. In pigs ventilated with TLV with abnormal lungs (cardiac arrest followed by cardiac massage), lung compliance is dramatically decreased. This situation is energetically close to an ARDS lung ventilated with PFC. The baro/volotraumatisms induced by the cardiac massage, most likely causes an invasion of the lung by blood plasma or even blood, severely diluting surfactant and increasing the polarity of the alveolar interface. As a consequence the work of adhesion was increased causing a drastic reduction of the interfacial energy experienced in the lung. In summary, we can relate the change of increase of interfacial energy with the decrease of surface tension, with the increase of compliance. So surface tension on lung cells, affects both cell response and lung compliance (Figure 58).

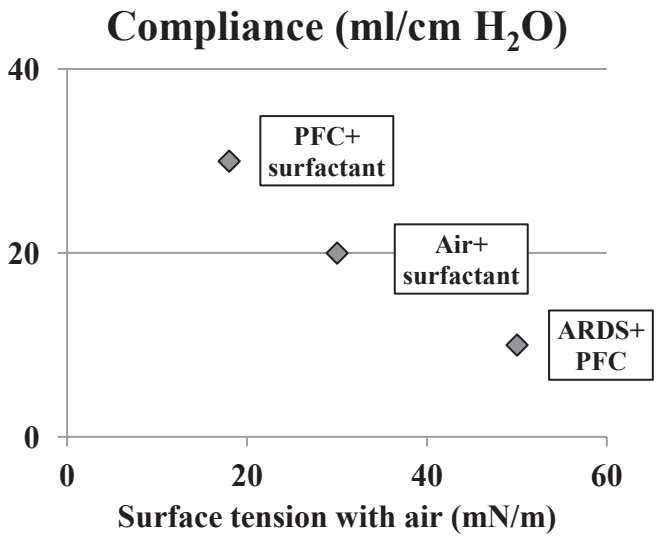

Figure 58 : Values obtained for pigs lung compliance in experimental and literature studies, and their supposed relation to the surface tension of the fluids present in the lungs.

VI. CONCLUSIONS AND PERSPECTIVES

When we started this work, we came across of a gap in the knowledge of the cell response to PFC exposure. This gap is particularly surprising due the wide possible applications of PFC, with different outcomes. Some of these applications are subject to ongoing validation: Total Liquid Ventilation (TLV) in neonates, for instance after meconium aspiration, and hypothermic TLV in adults for resuscitation after cardiac arrest, and organ preservation. Amongst the possible applications of PFC, the ventilation applications of PFC appear of major interest for new ventilatory methods and biomedical innovations. This is due to the particular PFC properties such as the great power of oxygen dissolution, that allow to obtain normal gas exchanges with liquid ventilation (TLV). So, studying the response of epithelial lung cells exposed to PFC became a priority to allow the lung applications of PFC.

In order to fill the lack of a systematic and transversal studies of the pulmonary cell response to PFC exposure, we designed a full evaluation of structural, mechanical and functional properties. To do so, we used appropriate tools, to reveal sensitive cellular and molecular modifications due to this unusual change of environment. The new proposed approach is the complementary evaluation of:

(i) the cell mechanical and adhesion properties,

(ii) the mechanical and structure properties by cell imaging,

(iii) the cell mechanical properties while changing environmental conditions from the apical cell face,

(iv) the surface tension properties measured by an adapted experimental method, and their impact on the work of adhesion and interfacial energy, at the cell surface,

(v) the surface tension effects on lung compliance, the latter being estimated from records in large animal ventilated by TLV.

From three well characterized lung cell models: alveolar epithelial cell, bronchial epithelial cell and alveolar macrophage, exposed to PFC, we obtain an assembly of experimental data, characterized by their biological and biomechanical consistency. A major finding obtained in this study is the discovery of cell sensitivity to PFC exposure in epithelial cells, while studied in exclusive static conditions, i.e., with no effect of density and dynamic viscosity. After eliminating the hypothesis of the effect of oxygen over cell response, a detailed analysis of the work of adhesion and interfacial energy, taking into account the non-polar nature of perfluorocarbon, has revealed a marked change in the energetic balance at cellular surface when changing DMEM for PFC.

There is a strong consistency between (i) the revelation of the cell response to PFC exposure, and (ii) the theoretical finding of the increase in interfacial energy. This connection was possible due to the acuteness of our cellular and molecular measurements and also to the non-polar nature of PFC, which makes this liquid ideal for the evaluation of the cell surface energy as it might be useful for any type of solid surface energy.

The surface energy serves as connection bridge between the different levels of lung scale, from the cell, to the respiratory system. The experimental study of fluid-fluid and of surface energies has evidenced the particular behavior of PFC at interface with mixtures of aqueous mediums, in which surfactant is diluted at different concentrations. This result has direct consequences during liquid ventilation. Our analysis of the respiratory compliance in pigs treated by total liquid ventilation, with and without acute lung injury, reveals at the same time the critical contribution of surface tension to the outcome of the ventilated animal. And also the cellular consequences associated to the change in interfacial energy.

In summary, the same phenomenon that controls lung compliance during air or liquid ventilation would be responsible at a smaller scale, for cellular adaptation of alveolar epithelial cells and to a change in surface energy. We find that a decreased surface tension is responsible for increasing altogether the cell interfacial energy, and for increasing lung compliance.

An interesting perspective to further evaluations, would be to follow the mechanical parameters of epithelial cells during air ventilation for different concentrations of surfactant covering the epithelium, as well as during total liquid ventilation. Another interesting step might by to study the effect of surface energy in real alveolar geometry, because the curvature magnifies the surface tension effects, and their reinforced impact on cells must be determined. A promising step forward study would be to reinvent the pioneering study of Bachofen and Schur (Bachofen and Schurch, 2001), by introducing a complete cellular evaluation, that would complement the predicted physiological evolutions. Reinventing this study would be of great interest, because it demonstrates the link between the surface tension, the lung architecture and the alveolar geometry, and going further in discovering the link with cell response, would by fascinating.

VII. RÉSUMÉ DE LA THÈSE

Les perfluorocarbures (PFC) sont des composés organiques fluorés ayant une grande capacité à dissoudre de fortes concentrations d'oxygène et de dioxyde de carbone, ce qui confère à ce liquide des qualités intéressantes pour le transport de ces gaz au sein de l'appareil respiratoire jusqu'aux alvéoles pulmonaires, permettant des échanges gazeux respiratoires liquidiens (Clark and Gollan, 1966). La Ventilation Liquidienne Totale (VLT) a été proposée pour son efficacité dans des applications telles que (i) le lavage bronchique après aspiration de méconium (Avoine et al., 2011), (ii) l'induction d'une hypothermie ultrarapide au décours d'un arrêt cardiaque réanimé, offrant ainsi un mode de protection des tissus cérébraux et cardiaques (Darbera et al., 2013; Hutin et al., 2015), et (iii) l'amélioration des échanges gazeux et de la compliance pulmonaire chez les adultes et les enfants souffrant de détresse respiratoire aiguë (Hirschl et al., 1995; Leach et al., 1996; Wolfson and Shaffer, 2005).

Le PFC présente d'autres propriétés physiques particulières, à savoir une tension de surface parmi les plus faibles des liquides standards, ainsi qu'une masse volumique et une viscosité dynamique élevées, de l'ordre de 2 fois plus grande que celles de l'eau. Ces deux dernières caractéristiques sont responsables de résistances hydrodynamiques élevées en VLT. Ceci est dû aux contraintes de cisaillement élevées à la paroi des voies aériennes comme nous l'avons montré dans le cadre d'un récent projet ANR intitulé «Hyperothermie thérapeutique par ventilation liquide totale pour mort subite par réanimation» (ABYSS) et d'une publication traitant de la chute de pression dans les différentes générations de voies respiratoires (André Dias et al., 2015). Pour aller plus loin dans l'évaluation de l'impact physiopathologique et biologique du PFC sur le poumon, et contribuer ainsi au processus de validation de la technique de Ventilation Liquide Totale nécessaire à un futur transfert clinique, Bertin Technologies s'est intéressé aux conséquences cellulaires de la VLT. Ainsi, une évaluation

exhaustive des propriétés physiques du PFC et de la relation avec les changements cellulaires et pulmonaires, a été effectuée dans le cadre d'une convention doctorale (CIFRE) dédiée à cette problématique..

L'architecture fortement divergente des voies aériennes fait que pendant la ventilation liquidienne, les cellules épithéliales alvéolaires ne sont pas soumises à des contraintes de cisaillement, car la vitesse devient négligeable dans les bronches distales, et ceci contrairement aux cellules épithéliales bronchiques. En revanche, les cellules épithéliales alvéolaires qui se trouvent à l'interface avec le fluide utilisé pour la ventilation, sont exposées à un fluide de tension de surface abaissée dans le cas de la VLT.

Les propriétés physiques particulières du PFC sont principalement dues au fluor. Pour cette raison, le PFC est hautement électronégatif et possède un faible niveau de polarisation avec un potentiel d'ionisation élevé (Karsa, 1995), ce qui signifie de faibles interactions de type van der Waals entre les chaînes fluorées ainsi que de faibles densités d'énergie cohésive (Chhatre et al., 2010). Ces interactions de bas niveau font du PFC un liquide non polaire de faible tension superficielle, ayant un coefficient d'étalement élevé et un grand pouvoir de solubilité des gaz (Riess and Krafft, 1997). Les connexions entre le fluor et les atomes de carbone (C-F) jouent également un rôle dans les propriétés du PFC. Ces liaisons sont très stables en raison du chevauchement de l'orbite électronique qui augmente la force de liaison. En conséquence, les fluorocarbones sont thermiquement et chimiquement très stables et n'ont pas de propriétés biologiques délétères connues, notamment, absence d'effets toxiques, cancérigènes ou mutagènes (Krafft, 2001). Du point de vue fluidique, la faible tension superficielle et le pouvoir d'étalement élevé du PFC permettent au fluide de se répartir uniformément dans tout le poumon et un déplacement liquide facile vers les territoires pulmonaires distaux, conduisant à une amélioration échanges gazeux et à de plus grandes

compliances pulmonaires que celles mesurées lors de la ventilation gazeuse (Tooley et al., 1996; Wolfson et al., 1996).

Pour les diverses applications pulmonaires du PFC citées plus haut, la réponse biologique des cellules épithéliales à l'exposition au PFC est une question centrale qui a rarement été étudiée. Certaines études suggèrent des effets cellulaires ou tissulaires anti-inflammatoires potentiels (Nakstad et al., 2001; Obraztsov et al., 2000; Varani et al., 1996), et des effets sur certaines fonctions cellulaires induit par un passage au travers la membrane lipidique (Obraztsov et al., 2000; Rüdiger et al., 2003; Wemhöner et al., 2010; Woods et al., 2000b). Cependant, à notre connaissance, aucune étude structurale et mécanique approfondie de la réponse cellulaire à l'exposition au PFC a été réalisée. Or de nombreuses études ont montré que des changements de propriétés chimiques et/ou mécaniques de l'environnement cellulaire modifient la réponse cellulaire, entrainant des modifications de la migration, de la structure et de la rigidité cellulaire (Fereol et al., 2006; Planus et al., 1999). L'une des principales questions soulevées par l'exposition des cellules pulmonaires au PFC est de savoir si un changement des conditions environnementales, au niveau de leur face apicale de ces cellules, affecte la structure cellulaire, la mécanique cellulaire et l'adhésion.

Nous avons donc conçu une étude sur modèles cellulaires *in vitro* dans laquelle des cellules épithéliales alvéolaires ou bronchiques sont exposées au PFC pendant des durées différentes ($\leq$ 2 heures), alors qu'une évaluation systématique des propriétés structurales, mécaniques et fonctionnelles est réalisée, et comparée à la réponse cellulaire obtenue avec un milieu de culture classique (DMEM). Cette dernière condition est définie dans cette étude comme la condition contrôle. Nous avons notamment testé les rôles du cytosquelette, de sa tension interne et de la répartition et de l'expression de la couche de glycocalyx qui sont des facteurs connus pour contribuer à la mécanotransduction ou signalisation physicochimique, permettant l'adaptation cellulaire aux contraintes mécaniques et conférant une sensibilité

transmembranaire à l'environnement mécanique (Martins and Abairos, 2002; Thi et al., 2004). Les modifications de la structure des F-actine, de l'adhésion focale et du glycocalyx ont été suivies et évaluées à l'aide d'images sur cellules fixes et vivantes, marquées après exposition au PFC (groupe cellulaire exposé au PFC) ou au milieu de culture (groupe témoin). La structure des F-actines, la répartition et l'expression du glycocalyx sont comparées entre les deux groupes faisant apparaitre des changements qualitatifs et quantitatifs entre le groupe exposé et le groupe contrôle, démontrant un remodelage du cytosquelette et une redistribution avec diminution de l'expression du glycocalyx induit par l'exposition au PFC. En outre, les changements dans l'adhésion sont comparés en comptabilisant le nombre moyen de points d'adhésion focale par cellule et le nombre d'adhésions focales par taille. Ces changements mettent en évidence un affaiblissement sensible de l'adhésion focale pour les cellules exposées. Enfin, nous utilisons la méthode dite de Magnétocymétrie (MTC), récemment modifiée pour évaluer simultanément la mécanique et l'adhésion cellulaire à partir des liaisons cellule-ligand avec des microbilles ferromagnétiques fonctionnalisées à la fibronectine pour être reconnues par les intégrines (Isabey et al., 2016). Les réponses moléculaires intracellulaire et interfaciale au couple magnétique exercé par les billes mises en rotation par des champs magnétiques ont été évaluées pour des durées limitées d'exposition au PFC (≤ 2 heures). Les évolutions de l'adhésion cellulaire et de la mécanique dans les cellules exposées et non exposées au PFC sont évaluées à l'aide d'un modèle probabiliste de dé-adhésion couplé à l'un des deux modèles microrhéologiques classiques suivants : un modèle de solide viscoélastique à un élément de Voigt -modèle SV- en bon accord avec le faible contenu fréquentiel du signal MTC (échelon de stress de 1 min suivi d'un temps de relaxation), ou une loi de puissance (modèle PL) décrit dans la littérature comme une série infinie d'éléments de Voigt ayant des constantes de temps viscoélastiques respectant une distribution sous forme de loi puissance. Les résultats sont analysés à partir des propriétés mécaniques (Module d'Young

et temps de relaxation viscoélastique pour le modèle SV ; exposant de la loi puissance et norme du module d'élasticité complexe à 1 Hz pour le modèle LP) et des paramètres d'adhésion (taux de dissociation naturel et contrainte de référence pour le modèle de dé-adhésion). Les cellules exposées au PFC abaissent leur module élastique avec les deux modèles testés alors que la dé-adhésion augmente, ce qui constitue une confirmation de la mise en évidence par cette étude d'une réponse cellulaire avec adaptation aux nouvelles conditions environnementales générées par l'exposition au PFC. En traitant les cellules d'une part par un agent bloquant la polymérisation des F-actines (donc affectant fortement la tension intracellulaire) et d'autre part une enzyme dégradant le glycocalyx (donc en supprimant l'effet régulateur du glycocalyx), il apparait que la tension interne ou tonus cellulaire, et que la couche de glycocalyx jouent des rôles clés dans la réponse cellulaire à l'exposition au PFC. Notamment les effets du PFC sur le module d'élasticité et les paramètres d'adhésion sont supprimés avec la cytoD. A noter que les diminutions de rigidité cellulaire et d'adhésion observées après exposition au PFC, ont des retentissements fonctionnels et notamment une amélioration significative de la migration et de la réparation cellulaires, observée sur des modèles de blessure de monocouches de cellules alvéolaires épithéliales. La réponse à l'exposition au PFC a été confirmée par des mesures similaires de mécaniques et de dé-adhésion effectuées sur des cellules épithéliales bronchiques aux mêmes temps de mise en culture (1 jour), avec toutefois un effet réponse au PFC atténué en raison de niveaux moindres de maturation sur ce type cellulaire. La stimulation mécanique étudiée sur ces mêmes cellules épithéliales bronchiques à l'aide de la Magnétostimulation (MTS), a permis d'étudier l'effet d'une contrainte cyclique durable (1 h) simulant ainsi un stress cyclique comme celui imposé par la VLT (Chen et al., 2001; Wang et al., 2012). En condition contrôle, une telle stimulation est censée entrainer un renforcement de la rigidité et de l'adhésion qui est ici atténuée en raison du caractère immature des cellules stimulées mécaniquement. Les essais réalisés après

exposition au PFC ont néanmoins démontré que l'exposition au PFC n'empêchait pas une fonction cellulaire importante, à savoir l'adaptation cellulaire à la stimulation mécanique. En revanche, l'exposition de macrophages alvéolaires au PFC ne provoque pas de modification cellulaire dans les conditions d'étude présentes.

Le rôle possible de l'oxygène plus concentré dans le PFC que dans le milieu aqueux de culture (28% versus 18%) a été éliminé en constatant l'identité des réponses cellulaires mécanique et fonctionnelle avec et chambre à hypoxie. Le facteur le plus probable à l'origine de l'adaptation cellulaire étant le changement de tension de surface causé par le PFC, nous avons d'une part mesuré cette tension de surface pour les fluides utilisés en adaptant une méthode de mesure de tension de surface dans des tubes capillaires. D'autre part, nous avons réalisé une estimation théorique de l'évolution du travail d'adhésion, et de l'énergie d'interface ressentie par les cellules en présence d'un PFC (non-polaire). Les résultats cellulaires en mécanique et adhésion effectués en ajoutant une couche moléculaire de surfactant entre la cellule et le PFC, ont montré que les basses énergies de surface entre PFC et surfactant potentialisaient la réponse cellulaire déjà trouvée sans surfactant. Les résultats expérimentaux et théoriques montrent que la réponse cellulaire aux changements de tension superficielle imposés par le liquide en contact sur la face apicale, tout en restant dans la gamme physiologique, sont en étroite corrélation entre les changements estimés du travail d'adhésion et de l'énergie interfaciale, A notre connaissance, cette adaptation cellulaire au changement des conditions énergétiques interfaciales n'avait jamais été décrite précédemment. De plus, en adaptant cette approche en énergie de surface au cas des macrophages non adhérents, nous avons pu expliquer pourquoi les macrophages n'ont pas été en mesure d'exprimer une sensibilité aux changements de conditions d'apicales et ceci en raison de l'interférence du substrat dans les équilibres énergétiques.

En corrélation avec l'effet cellulaire des changements d'énergie interfaciale, nous discutons finalement les conséquences au niveau pulmonaire de la faible tension superficielle du PFC sur les valeurs de compliance pulmonaires. Ces dernières ont été obtenues par une analyse rétrospective des paramètres mécaniques ventilatoires sur des cochons de 20kg ventilés en VLT. Les différences importantes de valeurs de compliance pulmonaire mesurées entre poumon normal et poumons œdémateux relevant de la réanimation cardiologique, ont été reliées aux effets des changements d'énergie de surface induits par la présence d'une couche aqueuse entre le PFC et la surface alvéolaire.

En résumé, le mécanisme qui contrôle les changements de compliance pulmonaire au passage ventilation en air et ventilation liquidienne totale par PFC, est en outre responsable à plus petite échelle de la réponse des cellules pulmonaires épithéliales au travers des changements d'énergie d'interface, laquelle est augmentée alors que la compliance pulmonaire est diminuée.

VIII. APPENDICES

VIII.1 Contribution of cellular membrane components to the energetic approach

The role of surface tension on (i) the regulation of cell response via the interfacial energy, and (ii) the lung compliance via the fractal nature of lung architecture, may be partially understood by looking at the ratio matching/mismatching of polar and non-polar components of, (1) the epithelial cell layer and (2) the fluid in contact with the cell layer. Using the wide panel of pathophysiological conditions represented in Figure 55, we describe schematically in Figure 59, the evolution of interfacial energy at cell surface. The schemas A to E correspond to situations where interfacial energy is increased from low to high levels, while work of adhesion is decreased from high to low and the surface tension is decreased. The polar components are represented in blue, and the non-polar (dispersive) ones in red. Glycocalyx is hydrophilic and lipid membrane molecules are essentially non-polar. Water in alveoli (originated from the filtering from blood plasma through the alveolo-capillary barrier) is an aqueous liquid with high surface tension and has great polar component. In the case of PFC alone, the sole component existing is the non-polar component, which is in any case quite small. Surfactant has a hydrophilic head and a hydrophobic tail, so it can make connections of both natures, either polar or non-polar.

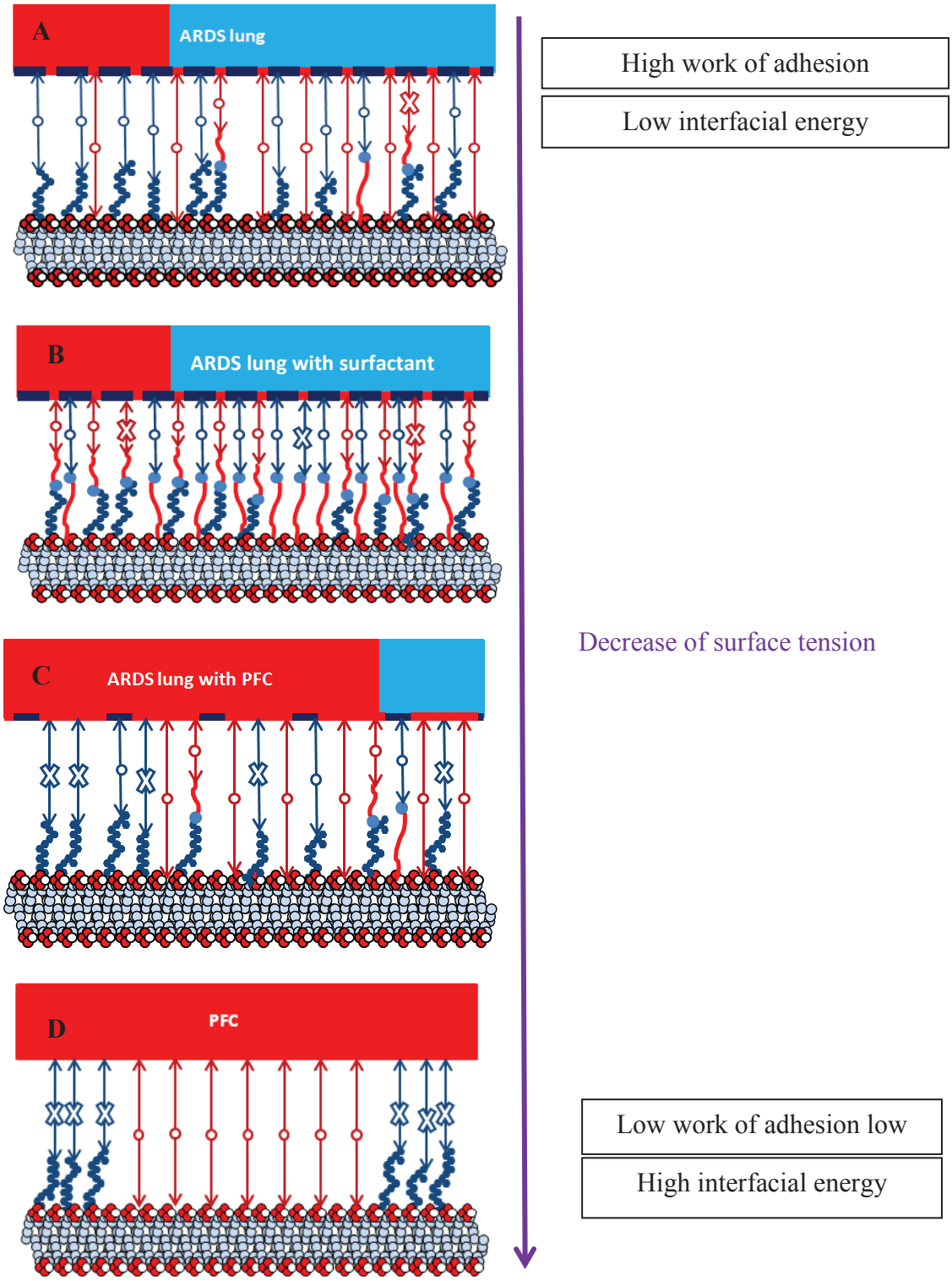
A
ARDS lung
B
ARDS lung with surfactant
C
ARDS lung with PFC
D
PFC
High work of adhesion
Low interfacial energy
Decrease of surface tension
Low work of adhesion low
High interfacial energy

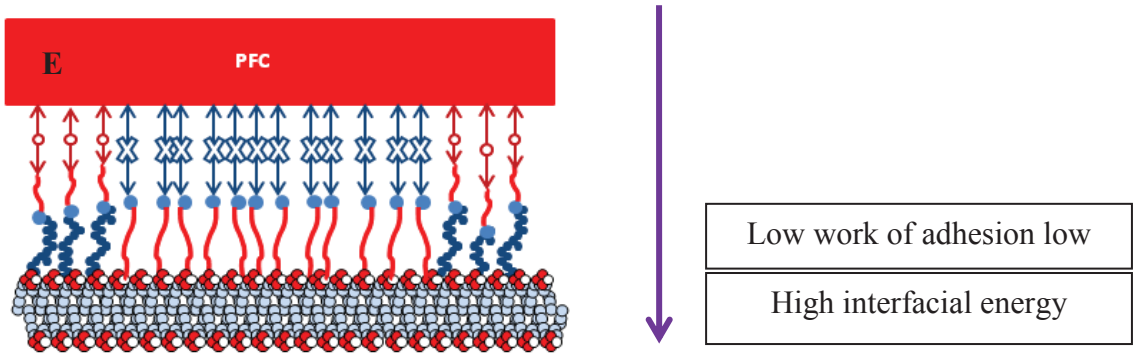

Figure 59: Energetic representation at the interface of epithelial cells with a liquid from an oedematous ARDS lung (A) to normal lung ventilated with PFC (E). The polar and non-polar connections are either effective (o) and ineffective (x). In blue are the polar components and in red the non-polar components. (A) Oedematous (ARDS) lung (with air mechanical ventilation or not) with water at epithelial cell surface and large dilution of surfactant (e.g., ARDS). (B) Oedematous (ARDS) lung with water at epithelial cell surface with surfactant treatment. (C) Oedematous (ARDS) lung with water at epithelial cell surface, surfactant diluted and PFC liquid ventilation. (D) PFC liquid ventilation without surfactant (before surfactant treatment or failure of surfactant treatment). (E) PFC liquid ventilation with a layer of surfactant (secreted) on the epithelial cell surface. The arrow shows the evolution (decrease) of surface tension.

In (A): In the edematous alveoli, surfactant is too diluted to play a significant role and thereby liquid surface tension is high (water). The large number of connections makes the work of adhesion great and thus interfacial energy is low. A similar situation exists in our cell culture in control condition, except that inflammatory factors are not present.

In (B): In the edematous alveoli and in case of successful surfactant treatment, the surfactant should help to decrease surface tension thus reducing slightly the work of adhesion due to the large number of remaining connections. Interfacial energy is a little increased secondary to the slight decrease in work of adhesion.

In (C): The edematous alveoli is ventilated with the insoluble PFC, surfactant is diluted in water. Adding PFC to a lung whose alveoli are covered with a water layer

substantially decreases surface tension from 72 to 49 mN/m (see Table 6) with an additional but limited decrease in work of adhesion and a subsequent increase in interfacial energy

Figure 59 (D): Liquid ventilation with PFC in the non edematous alveoli depleted in surfactant (e.g., using a preliminary washing with detergent (Tooley et al., 1996)). The exposure to PFC causes also a decrease in glycocalyx expression, and possibly a glycocalyx displacement toward the cell periphery (Figure 39, Figure 51). Very few polar connections can be made, leading to a decrease of the work of adhesion, surface tension is drastically decreased, and thus interfacial energy is increased . This is case of our cell cultures exposed to PFC without surfactant layer.

In (E): Liquid ventilation with PFC in the non edematous alveoli -PFC with a surfactant layer- (secreted or preliminary deposited on cell surface like in our cell culture with surfactant layer intercalated). The presence of surfactant utterly modifies the connections between the cell layer and PFC: the non-polar cell layer is covered with surfactant letting their polar head non recognized by the apolar PFC, and because glycocalyx is highly decreased due to PFC exposure, the number of connections will be even smaller, surface tension will be decreased, yielding to the highest levels of interfacial energy and the lowest work of adhesion.

VIII.2 Magnetic Twisting Cytometry device and signal treatment

VIII.2.1 Comparison of our MTC device with other devices of similar types

The magnetic torque depends on (i) the perpendicular magnetic field, (ii) the magnetic moments of beads proper to each technique, and (iii) the arccosine of the bead rotation angle, meaning that torques is slightly reduced as beads rotate. The maximum value of perpendicular magnetic field for our device is 63 Gausss or 6.3mT (Fereol et al., 2008; Laurent et al., 2003; Ohayon et al., 2004) while it is 70 Gauss or 7mT for OMTC (Optical Magnetic Twisting Cytometry) by Fabry et al. (Fabry et al., 2003).

The torque per unit bead volume (i.e., a stress) per gauss, *c*, also called bead calibration coefficient, characterizes the type of bead used (bead geometry and ferromagnetic material content). Our ferromagnetic beads are made of polystyrene and covered by a thin layer of chromium oxide. In most studies, *c* is calibrated from the friction of a large population of beads rotating in a medium of known dynamic viscosity (Wang and Ingber, 1995). For the same type spherical polystyrene beads coated with chromium oxide of 4.5 mm of diameter, *c* was earlier found to be about 0.05 Pa/Gauss, i.e., 0.5 Pa/mT (Wang and Ingber, 1995). In previous studies in which our device was used (Fereol et al., 2008; Laurent et al., 2003; Ohayon et al., 2004) bead magnetic moment *m* was obtained after measurement of bead magnetization in a bead sample using the Föner method (Laurent et al., 2002). The magnitude of the bead magnetic moment (*m)* is a parameter that requires to be calibrated since it depends on the ferromagnetic beads specifically used. It can be estimated from: $m = M \times V$ (where M is the bead magnetization ~4700 A/m, and V is the bead volume, the bead diameter is 4.5 mm). A typically found value for m is: $m \approx 2.3 \times 10^{-13}$ A.m^2. The parameter *c* corresponding to our bead samples can be estimated from: $c = \frac{\mu_0 \times m}{\kappa \times V}$, (μ_0 is the μ_0 : permeability constant, κ

(=6 for a sphere) is a particle shape factor related with the hydrodynamic drag), i.e., $c \approx 0.08$ Pa/Gauss or 0.8 Pa/mT. By comparison, for ferromagnetic Fe_3O_4 beads full of ferromagnetic material (diameter of 4.5 mm) as used in (Fabry et al., 2003), c reaches 1.86 Pa/Gauss or 18.6 Pa/mT which is 25 greater.

For the bead displacement obtained in epithelial cells and in alveolar macrophages, a range of curvilinear bead displacement between 500 nm and a maximum of 2500 nm was found in response to a range of torques: 400 - 1200pN×µm (Fereol et al., 2008; Laurent et al., 2003). This range of deformation corresponds to bead rotation angles in the range 15°–60°, and corresponds to a relatively large range of cellular deformations. For comparison, during OMTC measurements in Human Airway Smooth Muscle (HASM) cells, the median displacement amplitude was only 57 nm (Fabry et al., 2001) and reached a maximum of 259 nm during OMTC (Fabry et al., 2003). In such small ranges of deformations, the nonlinear behavior of cellular material is not obvious while in the range of deformation obtained with our device, a stress or strain hardening response can be observed as a characteristic of the cellular adaptation to stress (Fereol et al., 2009).

VIII.2.2 Measurement of the remnant magnetic field

The magnetometer (Magnetoscop 1.068 Forster) is mounted with a pair of low noise probes for field and gradient (type 1.009-4512). These probes make it possible to measure static magnetic fields and slow dynamic fields (up to 180 Hz) as well as field gradients for B values between 10^{-2} µT and 100 µT. Each probe is mounted in a plastic block of 10×10×60 mm and is connected to the magnetometer. In order to achieve the optimum sensitivity of the magnetometer, a special attention is paid to magnetically protect the connection circuit using a magnetic shielding sleeve. Under these conditions, the noise of the probes is 0.14 nT peak to peak.

VIII.2.3 Principle of Lock-in Amplifier for MTC

The synchronous detection (Lock-in Amplifier, SR 830 DSP Stanford Research Systems), enables to extract a signal with a known carrier wave from an extremely noisy environment. Right after magnetization, the remnant magnetic field resulting from the 10^5 ferromagnetic beads embedded in the cell culture, is as low as 1 nT or 10^{-9} T. The latter must be measured while a huge component of permanent magnetic field that is generated over the 1 min-duration of the perpendicular field. This constant magnetic field component is about 10 million times higher than the remnant magnetic field. Thus, the lock-in amplification is quite appropriate to the treatment of MTC signal. By rotating the culture well at around 10 Hz (see figure bellow), the lock-in amplifier process enables to extract the amplitude of the MTC signal with great accuracy, considerably improving the signal-to-noise ratio independently of the origin of the noise.

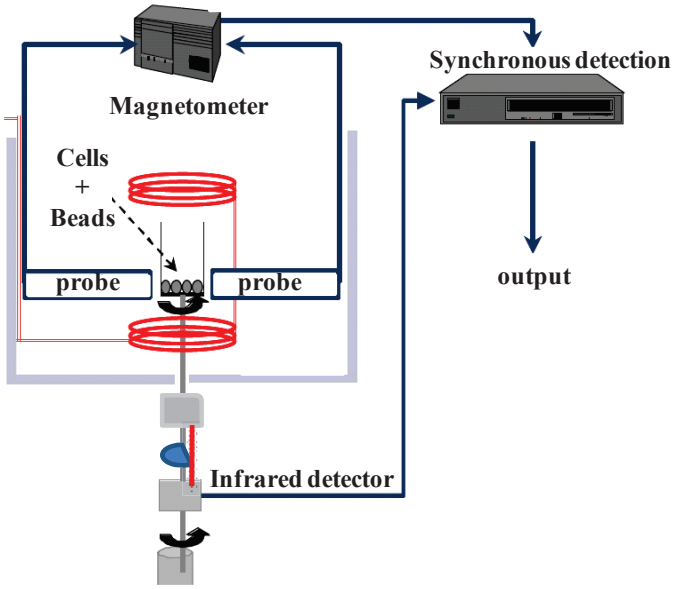

Figure 60: Extraction of the MTC signal

Synchronous detection is used to detect the signal component of the magnetometer at the reference frequency of the system (namely 10 Hz). To carry out this operation, two signals are used: the signal from the magnetometer and the signal from the infrared detector. Due to rotation of the culture well, the remnant magnetic field signal is detected by the magnetometer as:

$$S_{mag}=V_{mag}\{t\}\times\sin(\omega_{mag}t+\theta_{mag})+\text{Noise}$$

$V_{mag}\{t\}$ is the wanted amplitude of the signal, ω_{mag} is the signal pulse (rotation velocity of the well) and θ_{mag} is the phase of the signal. The reference signal issued from the command of the well rotation is given by the infrared detector and has a squared form. Its fundamental harmonic is $S_{ref}=V_{ref}\times\sin(\omega_{mag}t+\theta_{ref})$, V_{ref} is the amplitude of the reference signal, and θ_{ref} is the phase of the reference signal.. The various steps for carrying out the operation are the following:

i) The synchronous detection amplifies the signal from the magnetometer and multiplies it to the reference signal using a PSD (Phase-sensitive detector). The result is:

$$S_{mag}\times S_{ref}=V_{mag}\{t\}\times V_{ref}\sin(\omega_{mag}t+\theta_{mag})\sin(\omega_{mag}t+\theta_{ref})+\text{Noise}\times V_{ref}\sin(\omega_{ref}t+\theta_{ref}).$$

This result can be arranged in another form using classical trigonometric treatment:

$$S_{mag}\times S_{ref}=\frac{1}{2}V_{mag}\{t\}\times V_{ref}\cos\left(\theta_{mag}-\theta_{ref}\right)+\text{Noise}\times V_{ref}\sin(\omega_{ref}t+\theta_{ref})$$
$$-\frac{1}{2}V_{mag}\{t\}\times V_{ref}\cos\left(\left[2\omega_{mag}\right]t+\left(\theta_{mag}+\theta_{ref}\right)\right)$$

Thus the output of the multiplier corresponds to two sinusoids, (one at the frequency $2\omega_{mag}$ and the other at the frequency ω_{mag}) and a steady component.

ii) This signal is then filtered by a low-pass filter (first-order filter of the RC type). All the alternating signals are eliminated but the continuous component of the signal remains. The alternating signals eliminated are: the frequency sinusoid ω_{mag} and $2\omega_{mag}$. As a result, the low pass filter eliminates most of the parasites. The filtered output of the multiplier is a continuous signal of the form:

$$f_{lp}\left\{S_{mag}\times S_{ref}\right\}=\frac{1}{2}V_{mag}\left\{t\right\}\times V_{ref}\cos\left(\theta_{mag}-\theta_{ref}\right).$$

Such a process assumes that the frequencies components of the wanted signal ($V_{mag}\{t\}$) are bellow the cut-off frequency of the low-pass filter.

iii) This continuous signal is proportional to the amplitude of the signal of interest (the amplitude of the remnant field measured by the magnetometer) and depends on the phase difference Θ, between the signal of the magnetometer and the reference signal: $\theta_{mag}-\theta_{ref}$. This phase dependence can be eliminated by performing a second multiplication (using a second phase-sensitive detector): the signal from the magnetometer must be multiplied by the reference signal shifted by 90° (i.e., $V_{ref}\times\sin(\omega_{mag}t+\theta_{ref}+90^0)$).This signal is then filtered by the low-pass filter and the output of the multiplier is:

$$f_{lp}\left\{\left(S_{mag}\times S_{ref}\right)_{bis}\right\}=\frac{1}{2}V_{mag}\left\{t\right\}\times V_{ref}\sin\left(\left[\theta_{mag}-\theta_{ref}\right]\right).$$

iv) There are two signals at the outputs of the multipliers, one is proportional to $\cos\theta$ and the other is proportional to $\sin\theta$. If $\frac{1}{2}V_{mag}\left\{t\right\}\times V_{ref}\cos\theta=X$ and $\frac{1}{2}V_{mag}\left\{t\right\}\times V_{ref}\sin\theta=Y$, the amplitude of the signal of interest can be calculated from: $V_{mag}\left\{t\right\}=\left(X^2+Y^2\right)^{1/2}$ and the difference of phase between the two signals is such that: $\theta=\tan^{-1}\left(\frac{Y}{X}\right)$.

Finally, the output of the synchronous detection on is composed of two signals: the amplitude of the remnant field of the microbeads detected by the magnetometer in a horizontal direction, and the phase difference between the signal of the microbeads and the reference signal.

VIII.2.4 Filters of the detection system

The time constant which defines the cut-off frequency of the low-pass filter is given by $\tau c = 1/2\pi f$, f is the cut-off frequency of filter. In order to obtain a well-filtered signal, it is necessary to have a very low cut-off frequency, so a very large time constant in order to keep only the continuous signals (and have a correct signal-to-noise ratio). The chosen time constant is of 300 ms and the frequency of the detection is 50 Hz.

VIII.2.5 Acquisition system

The two signals issued from the lock-in are collected on a PC using an Acqknowledge acquisition card (Biopac, USA). The Acqknowledge software associated with this acquisition card makes it possible to visualize the variations of these signals over time and to process these signals using the Matlab program developed in the lab to obtain the mechanical properties and adhesion parameters by best curve fitting.

VIII.3 Optical correction for measuring the contact angle of the capillary meniscus with an inverted microscope

The capillary is positioned horizontally on the stage of the inverted microscope. The capillary axis (z) is the plane of the stage, and an accurate measurement of the contact angle of the meniscus θ_e, requires an optical correction. This optical correction is essential, because the two walls of the capillary behave as double dioptre (refraction index of glass differs from that of air), thus generate an optical distortions according to both the optical (vertical) axis (x) and the transversal (horizontal) axis (y) (Figure 61). The largest meniscus is observed in the medium capillary plane (zy), and therefore the contact angle must be determined in this plane. We verified experimentally that there is no distortion according to the capillary axis (no magnification effect).

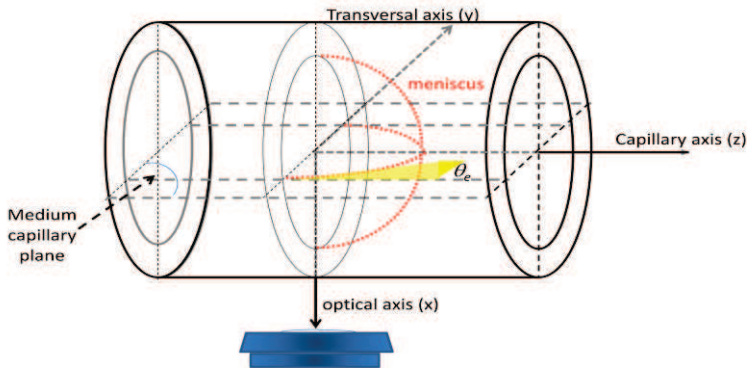

Figure 61: The 3 main axis of the capillary tube: optical axis (x), transversal axis (y), capillary axis (z). The plane yz is located on the stage of the inverted microscope. The meniscus is observed (focused) in the plane yz of the medium capillary plane, by the objective of the inverted microscope located on the optical axis (x). The contact angle θe is formed between the meniscus and the inner glass wall of the capillary. θe is measured in the medium capillary plane of the image, and corrected for the effect of the double concentric dioptres described in this paragraph.

The Gullstrand formula was initially proposed by a Swedish ophthalmologist and optician, Allvar Gullstrand (1862-1930), Nobel Prize of Physiology and Medicine in 1911, for his research on the eye as a light-refracting apparatus. The Gullstand's formula predicts that the association of two centered spherical dioptres (noted 1 and 2) separated by a distance, e (called interstice or optical distance) in which there is a medium with a unique refraction index noted n_2, can be treated as an equivalent dioptre with a total vergence called V_{12} (in m^{-1}) given by:

$$V_{12}=V_1+V_2-\frac{e}{n_2}V_1V_2$$ **Equation 37**

V_1 is the vergence of dioptre #1 (formed by the inner circular wall of the capillary), which separates the fluid inside the capillary with a refraction index noted n_1, from the glass forming the wall of the capillary of refraction index n_2 (= 1.5), leading to the vergence #1:

$$V_1=\frac{n_2-n_1}{-R_{int.}}$$ **Equation 38**

V_2 is the vergence of dioptre #2 (formed by the outer circular wall of the capillary), which separates the glass of the capillary wall with a refraction n_2 (= 1.5), from the fluid around the outer capillary wall which, in our case, is always air n_3 (= 1), #2 leading to the vergence #2:

$$V_2=\frac{n_3-n_2}{-R_{ext.}}$$ **Equation 39**

Refraction index for water and PFC are the same, namely $n_1 \approx 1.33$ while $n_1 \approx 1$ for air. As a consequence: $n_2-n_1>0$ and $n_3-n_2<0$. Thus, the vergence signs is as follows: $V_1<0$ and $V_2>0$, meaning that although the 2 spherical dioptres are concave, dioptre #1 is always divergent and dioptre #2 is always convergent. The total vergence V_{12}, can be either positive or negative, meaning that the equivalent dioptre separating mediums # 1 and #3 may

be convergent or divergent, depending on the fluid tested. Schemas in Figure 62 and Figure 63 show the total vergence values for water (or PFC) and air inside.

Table 10: Geometrical dimensions (Inner radius $R_{int.}$ and outer radius $R_{ext.}$, interstice distance, e) of small et large glass capillaries and total vergence for water (or PFC) and air.

	Fluid inside	***R_{int} (mm)***	***R_{ext} (mm)***	***e (mm)***	V_{12} (m^{-1})	***Property***
Small	Water or PFC	0.25	0.7	0.45	+179	convergent
capillary	Air	0.25	0.7	0.45	–858	divergent
Large	Water or PFC	0.5	0.7	0.2	+406	convergent
capillary	Air	0.5	0.7	0.2	–190	divergent

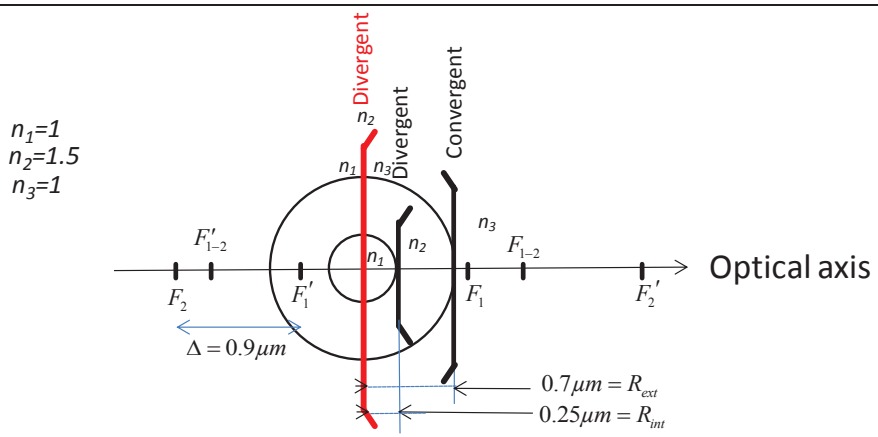

Figure 62: Case of small capillary with air on the inside and the outside. The application of the Gullstrand's principle enables to associate two centered spherical dioptres constituted by the inner, (divergent) and the outer (convergent), circular walls of the smaller capillary glass tube. The equivalent spherical dioptre (in red) is divergent and located at the tube center, if the inner part of the capillary is filled with air.

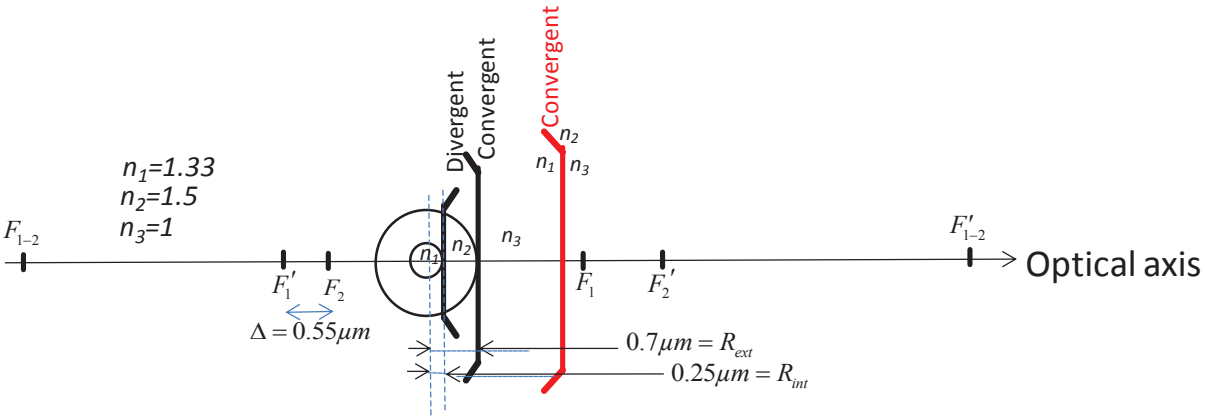

Figure 63: Case of small capillary with water or PFC inside and air outside. The application of the Gullstrand's principle enables to associate two centered spherical dioptres, constituted by the inner (divergent) and the outer (convergent), circular walls of the smaller capillary glass tube (scale is half compared to Figure 62). The equivalent spherical dioptre (in red) is convergent and centered outside of the capillary when water or PFC fills the inner part of the capillary

A major interest of this coupling approach is to enable an easy calculation of the magnifications:

(i) According to the transversal axis y (see Figure 61), the so-called transversal magnification : γ_t which can be calculated as explicated below,

(ii) According to the optical axis x (see Figure 62), the so-called axial or longitudinal magnification: $\gamma_a = \frac{n_3}{n_1}\gamma_t^2$

(iii) According to curvilinear axis, the so-called angular magnification: $G = \frac{\gamma_t}{\gamma_a}$.

The calculation of γ_t is obtained from a solution of the following equation system. p and p' are the distances measured on the optical axis between the dioptre and the objet or the dioptre, and its image: $\gamma_t = \frac{n_1}{n_3}\frac{p'}{p}$, $\frac{n_3}{p'} - \frac{n_1}{p} = V_{12}$ (Descartes formula).

x is an algebraic abscissa measured on optical axis x, and is a normalized distance using the inner capillary radius $R_{int.}$ as unit. At the inner capillary wall, x=0, at the capillary center, x=−1, and at the opposed inner wall, x=−2. The following table present the values of magnification coefficients, i.e., or correcting factors, obtained for the different cases studied.

Table 11: Magnifications calculated for the 2 capillary glass tubes used and for both the transversal axis y and the optical axis x. Note that $\gamma_t = \gamma_a$ at the center of the capillary (x=−1).

x (abscissa on optical axis)			**0**	**-0.5**	**-1**	**-1.5**	**-2**
Small capillary glass tube $R_{int.} = 0.25mm$	***Water or PFC***	γ_t	1.27	1.3	1.33	1.35	1.39
		γ_a	1.21	1.27	1.33	1.38	1.46
	Air	γ_t	1.27	1.12	1.00	0.90	0.82
		γ_a	1.61	1.26	1.00	0.83	0.67
	Surfactant 100%	γ_t	1.27	1.34	1.42	1.51	1.61
		γ_a	1.13	1.26	1.41	1.61	1.83
Large capillary glass tube $R_{int.} = 0.5mm$	***Water or PFC***	γ_t	1.10	1.21	1.33	1.48	1.67
		γ_a	0.92	1.10	1.33	1.64	2.08
	Air	γ_t	1.10	1.05	1.00	0.95	0.91
		γ_a	1.21	1.10	1.00	0.91	0.83
	Surfactant 100%	γ_t	1.13	1.27	1.45	1.68	2.00
		γ_a	0.89	1.13	1.48	1.99	2.82

The image of the meniscus in the medium plane (plane of axis y and z) of the capillary namely for x=−1, is the most easily and accurately detectable, due to the of maximum contrast on transmission or fluorescent images. Thus, the image distortion existing in the direction perpendicular to this plane, namely along the optical axis namely γ_a, does not count for our evaluation. Recalling the method used to determine the contact angle, i.e., Equation: $2\theta_e = \arctan\left(H/R_{cap}\right)$ (see paragraph III.3.1.2, Equation 26 and Figure 31), it happens that the meniscus height H has to be measured along the capillary axis which suffers no distortion

and thus H does not require any correction. By contrast, the radius of the meniscus R_{cap} is measured in the direction of the transversal axis, and needs to be corrected. Since it is magnified, the image of the radius distance has to be reduced by the value of γ_t. Theoretical results obtained in Table 10 for water and air demonstrate that the magnification γ_t is actually equal to the refraction index of the fluid inside the capillary, i.e., $\gamma_t = n_2$ because we consider the correction in the medium capillary plane. This results provides a method to measure refraction index in liquid where this index is unknown, e.g., for pure surfactant, n_2=1.4. Note also that, with air inside the capillary, it is possible to have accurate measurements of the inner capillary radius since no correction is needed.

In summary, the present optical correction method in capillary tubes enables: (i) to measure the refraction index of the fluid inside the tube, (ii) to correct the measured ratio H/R_{cap} by a multiplication factor equal to n_2: i.e., , $H \times n_2/R_{cap}$ leading to the best possible estimation of the contact angle θ_e using the microscopic image.

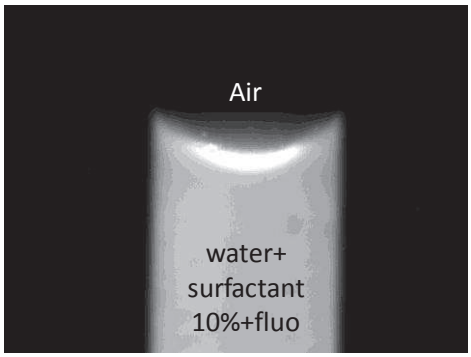

Interface surfactant 10%+fluo
and air in a small capillary

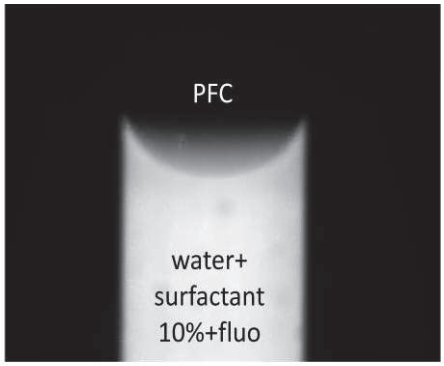

Interface surfactant 10%+fluo
and PFC in a small capillary

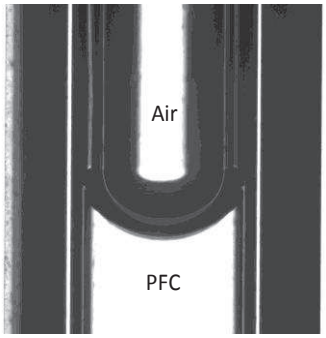

Interface air and PFC
in a small capillary

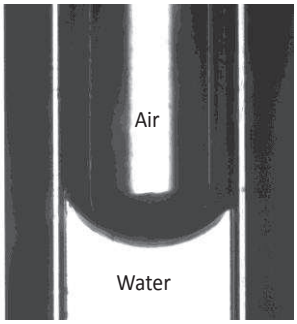

Interface air and water
in a small capillary

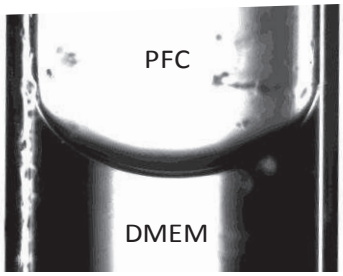

Interface PFC and DMEM
in a large capillary

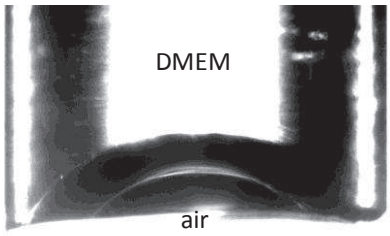

Interface air and DMEM
at the bottom end of a large capillary

Figure 64: Images of meniscus obtained for different interfaces in the small and the large capillary tubes without optical correction.

IX. REFERENCES

Abbondanzieri, E. A., Greenleaf, W. J., Shaevitz, J. W., Landick, R. and Block, S. M. (2005). Direct observation of base-pair stepping by RNA polymerase. *Nature* **438**, 460-5.

Absolom, D. R., Zingg, W., Thomson, C., Policova, Z., Van Oss, C. J. and Neumann, A. W. (1985). Erythrocyte adhesion to polymer surfaces. *Journal of Colloid and Interface Science* **104**, 51-59.

Adams, F. H., Towers, B., Osher, A. B., Ikegami, M., Fujiwara, T. and Nozaki, M. (1978). Effects of tracheal instillation of natural surfactant in premature lambs. I. Clinical and autopsy findings. *Pediatr Res* **12**, 841-8.

André Dias, S., Berdeaux, A., Darrasse, L., Demanesse, M., de Rochefort, L., Filoche, M., Ghaleh, B., Hutin, A., Isabey, D., Kunc, T. et al. (2015). ABYSS: Therapeutic hypothermia by total liquid ventilation following cardiac arrest and resuscitation. *IRBM* **36**, 110-117.

André P., B. P. (1990). Cell-cell contacts. In *Biophysics of the Cell Surface*, (ed. R. G. a. D. Gingell), pp. 287–322. Berlin: Springer.

Anzueto, A., Baughman, R. P., Guntupalli, K. K., Weg, J. G., Wiedemann, H. P., Raventos, A. A., Lemaire, F., Long, W., Zaccardelli, D. S. and Pattishall, E. N. (1996). Aerosolized surfactant in adults with sepsis-induced acute respiratory distress syndrome. Exosurf Acute Respiratory Distress Syndrome Sepsis Study Group. *N Engl J Med* **334**, 1417-21.

Arnaout, M. A., Goodman, S. L. and Xiong, J. P. (2007). Structure and mechanics of integrin-based cell adhesion. *Curr Opin Cell Biol* **19**, 495-507.

Ashbaugh, D. G., Bigelow, D. B., Petty, T. L. and Levine, B. E. (1967). Acute respiratory distress in adults. *Lancet* **2**, 319-23.

Asparuhova, M. B., Gelman, L. and Chiquet, M. (2009). Role of the actin cytoskeleton in tuning cellular responses to external mechanical stress. *Scand J Med Sci Sports* **19**, 490-9.

Avery, M. E. and Mead, J. (1959). Surface properties in relation to atelectasis and hyaline membrane disease. *AMA J Dis Child* **97**, 517-23.

Avoine, O., Bosse, D., Beaudry, B., Beaulieu, A., Albadine, R., Praud, J. P., Robert, R., Micheau, P. and Walti, H. (2011). Total liquid ventilation efficacy in an ovine model of severe meconium aspiration syndrome. *Crit Care Med* **39**, 1097-103.

Bachofen, H. and Schurch, S. (2001). Alveolar surface forces and lung architecture. *Comp Biochem Physiol A Mol Integr Physiol* **129**, 183-93.

Bachofen, M. and Weibel, E. R. (1982). Structural alterations of lung parenchyma in the adult respiratory distress syndrome. *Clin Chest Med* **3**, 35-56.

Balaban, N. Q., Schwarz, U. S., Riveline, D., Goichberg, P., Tzur, G., Sabanay, I., Mahalu, D., Safran, S., Bershadsky, A., Addadi, L. et al. (2001). Force and focal adhesion assembly: a close relationship studied using elastic micropatterned substrates. *Nat Cell Biol* **3**, 466-72.

Balland, M., Desprat, N., Icard, D., Fereol, S., Asnacios, A., Browaeys, J., Henon, S. and Gallet, F. (2006). Power laws in microrheology experiments on living cells: Comparative analysis and modeling. *Phys Rev E Stat Nonlin Soft Matter Phys* **74**, 021911.

Bayas, M. V., Leung, A., Evans, E. and Leckband, D. (2006). Lifetime measurements reveal kinetic differences between homophilic cadherin bonds. *Biophys J* **90**, 1385-95.

Beaulieu, A., Bosse, D., Micheau, P., Avoine, O., Praud, J. P. and Walti, H. (2012). Measurement of fractional order model parameters of respiratory mechanical impedance in total liquid ventilation. *IEEE Trans Biomed Eng* **59**, 323-31.

Bell, G. I. (1978). Models for the specific adhesion of cells to cells. *Science* **200**, 618-27.

Bernhard, W., Mottaghian, J., Gebert, A., Rau, G. A., von Der, H. H. and Poets, C. F. (2000). Commercial versus native surfactants. Surface activity, molecular components, and the effect of calcium. *Am J Respir Crit Care Med* **162**, 1524-33.

Bershadsky, A., Kozlov, M. and Geiger, B. (2006). Adhesion-mediated mechanosensitivity: a time to experiment, and a time to theorize. *Curr Opin Cell Biol* **18**, 472-81.

Bersten, A. D., Davidson, K., Nicholas, T. E. and Doyle, I. R. (1998). Respiratory mechanics and surfactant in the acute respiratory distress syndrome. *Clin Exp Pharmacol Physiol* **25**, 955-63.

Bhavanandan, V. P., and Furukawa. (1995). Biology and oncology of sialoglycoproteins. New York.

Bico, J. (2000). Mécanismes d'imprégnation : Surfaces texturées, Bigouttes, Poreux. In *Matière Condensée, Chimie & Organisation*, vol. Docteur de l'Université de Paris VI: Université de Paris VI.

Bico, J. and Quéré, D. (2000). Liquid trains in a tube. *Europhys. Lett.* **51**, 546-550.

Bongrand, P. (1995). Adhesion of cells. In *Handbook of Biological Physics*, vol. 1: Elsevier Science B.V.

Bongrand, P., C. Capo and R. Depieds. (1982). Physics of cell adhesion. *Prog. Surf. Sci* **12**, 217–286.

Bongrand, P. a. G. I. B. (1984). Cell-cell adhesion: Parameters and possible mechanisms. In *Cell Surface Dynamics: Concepts and Models*, (ed. C. D. a. F. W. W. A.S. Perelson), pp. 459–493. New York: Marcel Dekker.

Bourrillon, R. and Aubery, M. (1989). Cell surface glycoproteins in embryonic development. *Int Rev Cytol* **116**, 257-338.

Brochard, L. and Mancebo, J. (1994). Ventilation artificielle Principes et applications. Paris, France: ARNETTE S.A.

Bruinsma, R. (2005). Theory of force regulation by nascent adhesion sites. *Biophys J* **89**, 87-94.

Burridge, K. and Wennerberg, K. (2004). Rho and Rac take center stage. *Cell* **116**, 167-79.

Butler, J. P., Brown, R. E., Stamenovic, D., Morris, J. P. and Topulos, G. P. (2002). Effect of surface tension on alveolar surface area. *J Appl Physiol (1985)* **93**, 1015-22.

Buxbaum, K., Evans, E. and Brooks, D. E. (1982). Quantitation of surface affinities of red blood cells in dextran solutions and plasma. *Biochemistry* **21**, 3235-9.

Canadas, P., Wendling-Mansuy, S. and Isabey, D. (2006). Frequency response of a viscoelastic tensegrity model: Structural rearrangement contribution to cell dynamics. *J Biomech Eng* **128**, 487-95.

Carreau, A., El Hafny-Rahbi, B., Matejuk, A., Grillon, C. and Kieda, C. (2011). Why is the partial oxygen pressure of human tissues a crucial parameter? Small molecules and hypoxia. *J Cell Mol Med* **15**, 1239-53.

Chen, J., Fabry, B., Schiffrin, E. L. and Wang, N. (2001). Twisting integrin receptors increases endothelin-1 gene expression in endothelial cells. *Am J Physiol Cell Physiol* **280**, C1475-84.

Chenoune, M., De Rochefort, L., Bruneval, P., Lidouren, F., Kohlhauer, M., Seemann, A., Ghaleh, B., Korn, M., Dubuisson, R. M., Ben Yahmed, A. et al. (2014). Evaluation of lung recovery after static administration of three different perfluorocarbons in pigs. *BMC Pharmacol Toxicol* **15**, 53.

Chhatre, S. S., Guardado, J. O., Moore, B. M., Haddad, T. S., Mabry, J. M., McKinley, G. H. and Cohen, R. E. (2010). Fluoroalkylated silicon-containing surfaces-estimation of solid-surface energy. *ACS Appl Mater Interfaces* **2**, 3544-54.

Chibowski, E., Ho?ysz, L., Kip, G. A. M., Silfhout, A. v. and Busscher, H. J. (1989). Surface free energy components of glass from ellipsometry and zeta potential measurements. *Journal of Colloid and Interface Science* **132**, 54-61.

Choquet, D., Felsenfeld, D. P. and Sheetz, M. P. (1997). Extracellular matrix rigidity causes strengthening of integrin-cytoskeleton linkages. *Cell* **88**, 39-48.

Chowdhury, F., Li, Y., Poh, Y. C., Yokohama-Tamaki, T., Wang, N. and Tanaka, T. S. (2010). Soft substrates promote homogeneous self-renewal of embryonic stem cells via downregulating cell-matrix tractions. *PLoS One* **5**, e15655.

Clark, L. C., Jr. and Gollan, F. (1966). Survival of mammals breathing organic liquids equilibrated with oxygen at atmospheric pressure. *Science* **152**, 1755-6.

Clements, J. A., Platzker, A. C., Tierney, D. F., Hobel, C. J., Creasy, R. K., Margolis, A. J., Thibeault, D. W., Tooley, W. H. and Oh, W. (1972). Assessment of the risk of the respiratory-distress syndrome by a rapid test for surfactant in amniotic fluid. *N Engl J Med* **286**, 1077-81.

Comyn, J. (1992). Contact angles and adhesive bonding. *International Journal of Adhesion and Adhesives* **12**, 145-149.

Cozens-Roberts, C., Lauffenburger, D. A. and Quinn, J. A. (1990). Receptor-mediated cell attachment and detachment kinetics. I. Probabilistic model and analysis. *Biophys J* **58**, 841-56.

Darbera, L., Chenoune, M., Lidouren, F., Kohlhauer, M., Adam, C., Bruneval, P., Ghaleb, B., Dubois-Rande, J. L., Carli, P., Vivien, B. et al. (2013). Hypothermic liquid ventilation prevents early hemodynamic dysfunction and cardiovascular mortality after coronary artery occlusion complicated by cardiac arrest in rabbits. *Crit Care Med* **41**, e457-65.

de Gennes, P. G. (1985). Wetting: statics and dynamics. *Reviews of Modern Physics* **57**, 827-863.

De Robertis, E., Liu, J. M., Blomquist, S., Dahm, P. L., Thorne, J. and Jonson, B. (2001). Elastic properties of the lung and the chest wall in young and adult healthy pigs. *Eur Respir J* **17**, 703-11.

Discher, D. E., Janmey, P. and Wang, Y. L. (2005). Tissue cells feel and respond to the stiffness of their substrate. *Science* **310**, 1139-43.

Doornaert, B., Leblond, V., Planus, E., Galiacy, S., Laurent, V. M., Gras, G., Isabey, D. and Lafuma, C. (2003). Time course of actin cytoskeleton stiffness and matrix adhesion molecules in human bronchial epithelial cell cultures. *Exp Cell Res* **287**, 199-208.

Doyle, R. L., Szaflarski, N., Modin, G. W., Wiener-Kronish, J. P. and Matthay, M. A. (1995). Identification of patients with acute lung injury. Predictors of mortality. *Am J Respir Crit Care Med* **152**, 1818-24.

Dreyfuss, D., Soler, P., Basset, G. and Saumon, G. (1988). High inflation pressure pulmonary edema. Respective effects of high airway pressure, high tidal volume, and positive end-expiratory pressure. *Am Rev Respir Dis* **137**, 1159-64.

Engler, A. J., Griffin, M. A., Sen, S., Bonnemann, C. G., Sweeney, H. L. and Discher, D. E. (2004). Myotubes differentiate optimally on substrates with tissue-like stiffness: pathological implications for soft or stiff microenvironments. *J Cell Biol* **166**, 877-87.

Enhorning, G. and Robertson, B. (1972). Lung expansion in the premature rabbit fetus after tracheal deposition of surfactant. *Pediatrics* **50**, 58-66.

Evans, E., Berk, D. and Leung, A. (1991). Detachment of agglutinin-bonded red blood cells. I. Forces to rupture molecular-point attachments. *Biophysical Journal* **59**, 838-848.

Evans, E., Heinrich, V., Leung, A. and Kinoshita, K. (2005). Nano- to microscale dynamics of P-selectin detachment from leukocyte interfaces. I. Membrane separation from the cytoskeleton. *Biophys J* **88**, 2288-98.

Evans, E., Heinrich, V., Ludwig, F. and Rawicz, W. (2003). Dynamic tension spectroscopy and strength of biomembranes. *Biophys J* **85**, 2342-50.

Evans, E. and Kinoshita, K. (2007). Using force to probe single-molecule receptor-cytoskeletal anchoring beneath the surface of a living cell. *Methods Cell Biol* **83**, 373-96.

Fabry, B., Maksym, G. N., Butler, J. P., Glogauer, M., Navajas, D. and Fredberg, J. J. (2001). Scaling the microrheology of living cells. *Phys Rev Lett* **87**, 148102.

Fabry, B., Maksym, G. N., Butler, J. P., Glogauer, M., Navajas, D., Taback, N. A., Millet, E. J. and Fredberg, J. J. (2003). Time scale and other invariants of integrative mechanical behavior in living cells. *Phys Rev E Stat Nonlin Soft Matter Phys* **68**, 041914.

Fauroux, B., Leroux, K., Desmarais, G., Isabey, D., Clément, A., Lofaso, F. and Louis, B. (2008). Performance of ventilators for noninvasive positive-pressure ventilation in children. *European Respiratory Journal* **31**, 1300-1307.

Fereol, S., Fodil, R., Labat, B., Galiacy, S., Laurent, V. M., Louis, B., Isabey, D. and Planus, E. (2006). Sensitivity of alveolar macrophages to substrate mechanical and adhesive properties. *Cell Motil Cytoskeleton* **63**, 321-40.

Fereol, S., Fodil, R., Laurent, V. M., Balland, M., Louis, B., Pelle, G., Henon, S., Planus, E. and Isabey, D. (2009). Prestress and adhesion site dynamics control cell sensitivity to extracellular stiffness. *Biophys J* **96**, 2009-22.

Fereol, S., Fodil, R., Pelle, G., Louis, B. and Isabey, D. (2008). Cell mechanics of alveolar epithelial cells (AECs) and macrophages (AMs). *Respir Physiol Neurobiol* **163**, 3-16.

Fernandez, P., Pullarkat, P. A. and Ott, A. (2006). A master relation defines the nonlinear viscoelasticity of single fibroblasts. *Biophys J* **90**, 3796-805.

Filoche, M., Tai, C. F. and Grotberg, J. B. (2015). Three-dimensional model of surfactant replacement therapy. *Proc Natl Acad Sci U S A* **112**, 9287-92.

Foster, K. A., Oster, C. G., Mayer, M. M., Avery, M. L. and Audus, K. L. (1998). Characterization of the A549 Cell Line as a Type II Pulmonary Epithelial Cell Model for Drug Metabolism. *Experimental Cell Research* **243**, 359-366.

Foty, R. A. and Steinberg, M. S. (2005). The differential adhesion hypothesis: a direct evaluation. *Dev Biol* **278**, 255-63.

Fukuda, M. (1996). Possible roles of tumor-associated carbohydrate antigens. *Cancer Res* **56**, 2237-44.

Fulkerson, W. J., MacIntyre, N., Stamler, J. and Crapo, J. D. (1996). Pathogenesis and treatment of the adult respiratory distress syndrome. *Arch Intern Med* **156**, 29-38.

Galbraith, C. G., Yamada, K. M. and Sheetz, M. P. (2002). The relationship between force and focal complex development. *J Cell Biol* **159**, 695-705.

Gasparski, A. N. and Beningo, K. A. (2015). Mechanoreception at the cell membrane: More than the integrins. *Arch Biochem Biophys* **586**, 20-6.

Geiger, B. and Bershadsky, A. (2001). Assembly and mechanosensory function of focal contacts. *Current Opinion in Cell Biology* **13**, 584-592.

Glynn, K. P. and Gale, N. A. (1990). Exogenous lipoid pneumonia due to inhalation of spray lubricant (WD-40 lung). *Chest* **97**, 1265-6.

Goerke, J. and Clements, J. A. (1986). Alveolar Surface Tension and Lung Surfactant. In *Handbook of Physiology, The Respiratory System, Mechanics of Breathing*, pp. 247-261.

Good, R. J. (1977). Surface free energy of solids and liquids: Thermodynamics, molecular forces, and structure. *Journal of Colloid and Interface Science* **59**, 398-419.

Gruenwald, P., Johnson, R. P., Hustead, R. F. and Clements, J. A. (1962). Correlation of Mechanical Properties of Infant Lungs with Surface Activity of Extracts. *Experimental Biology and Medicine* **109**, 369-371.

Guerin, C. and Richard, J. C. (2007). Measurement of respiratory system resistance during mechanical ventilation. *Intensive Care Med* **33**, 1046-9.

Gunther, A., Siebert, C., Schmidt, R., Ziegler, S., Grimminger, F., Yabut, M., Temmesfeld, B., Walmrath, D., Morr, H. and Seeger, W. (1996). Surfactant alterations in severe pneumonia, acute respiratory distress syndrome, and cardiogenic lung edema. *Am J Respir Crit Care Med* **153**, 176-84.

Herzenberg, L. A. and Herzenberg, L. A. (2013). Our NIH Years: A Confluence of Beginnings. *Journal of Biological Chemistry* **288**, 687-702.

Hirschl, R. B., Pranikoff, T., Gauger, P., Schreiner, R. J., Dechert, R. and Bartlett, R. H. (1995). Liquid ventilation in adults, children, and full-term neonates. *Lancet* **346**, 1201-2.

Hirschl, R. B., Tooley, R., Parent, A., Johnson, K. and Bartlett, R. H. (1996). Evaluation of gas exchange, pulmonary compliance, and lung injury during total and partial liquid ventilation in the acute respiratory distress syndrome. *Crit Care Med* **24**, 1001-8.

Huang, S. and Ingber, D. E. (1999). The structural and mechanical complexity of cell-growth control. *Nat Cell Biol* **1**, E131-8.

Hutin, A., Lidouren, F., Kohlhauer, M., Lotteau, L., Seemann, A., Mongardon, N., Renaud, B., Isabey, D., Carli, P., Vivien, B. et al. (2015). Total liquid ventilation offers ultra-fast and whole-body cooling in large animals in physiological conditions and during cardiac arrest. *Resuscitation* **93**, 69-73.

Ingber, D. E. (2008). Tensegrity-based mechanosensing from macro to micro. *Prog Biophys Mol Biol* **97**, 163-79.

Ingber, D. E., Prusty, D., Sun, Z., Betensky, H. and Wang, N. (1995). Cell shape, cytoskeletal mechanics, and cell cycle control in angiogenesis. *J Biomech* **28**, 1471-84.

Isabey, D., Féréol, S., Caluch, A., Fodil, R., Louis, B. and Pelle, G. (2013). Force distribution on multiple bonds controls the kinetics of adhesion in stretched cells. *Journal of Biomechanics* **46**, 307-313.

Isabey, D., Pelle, G., Andre Dias, S., Bottier, M., Nguyen, N. M., Filoche, M. and Louis, B. (2016). Multiscale evaluation of cellular adhesion alteration and cytoskeleton remodeling by magnetic bead twisting. *Biomech Model Mechanobiol* **15**, 947-63.

Israelachvili, J. N. (2015). Intermolecular and Surface Forces: Elsevier Science.

Janmey, P. A. (1998). The cytoskeleton and cell signaling: component localization and mechanical coupling. *Physiol Rev* **78**, 763-81.

Joanny, J.-F. (1985). LE MOUILLAGE: QUELQUES PROBLEMES STATIQUES ET DYNAMIQUES: Université Pierre et Marie Curie.

Kacmarek, R. M., Wiedemann, H. P., Lavin, P. T., Wedel, M. K., Tutuncu, A. S. and Slutsky, A. S. (2006). Partial liquid ventilation in adult patients with acute respiratory distress syndrome. *Am J Respir Crit Care Med* **173**, 882-9.

Kalifat, S. R., Dupuy-Coin, A. M. and Delarue, J. (1970). Démonstration ultrastructurale de polysaccharides dont certains acides dans le Film de surface de l'alvéole pulmonaire. *Journal of Ultrastructure Research* **32**, 572-589.

Kang, H., Fan, Y. and Deng, X. (2011). Vascular smooth muscle cell glycocalyx modulates shear-induced proliferation, migration, and NO production responses. *American Journal of Physiology - Heart and Circulatory Physiology* **300**, H76-H83.

Karsa, D. R. (1995). Fluorinated surfactants: synthesis properties applications, by Erik Kissa. Marcel Dekker Inc., New York, 1994, pp. vii + 469, price US$165.00. ISBN 0-8247-9011-1. *Polymer International* **36**, 101-101.

Kawkitinarong, K., Linz-McGillem, L., Birukov, K. G. and Garcia, J. G. N. (2004). Differential Regulation of Human Lung Epithelial and Endothelial Barrier Function by Thrombin. *American Journal of Respiratory Cell and Molecular Biology* **31**, 517-527.

Ko, K. S., Arora, P. D. and McCulloch, C. A. (2001). Cadherins mediate intercellular mechanical signaling in fibroblasts by activation of stretch-sensitive calcium-permeable channels. *J Biol Chem* **276**, 35967-77.

Krafft, M. P. (2001). Fluorocarbons and fluorinated amphiphiles in drug delivery and biomedical research. *Adv Drug Deliv Rev* **47**, 209-28.

Kuo, S. C. and Sheetz, M. P. (1993). Force of single kinesin molecules measured with optical tweezers. *Science* **260**, 232-4.

Kytta, J., Randell, T., Tanskanen, P., Kajimoto, Y. and Rosenberg, P. H. (1995). Monitoring lung compliance and end-tidal oxygen content for the detection of venous air embolism. *Br J Anaesth* **75**, 447-51.

Lamour, G., Soues, S. and Hamraoui, A. (2011). Interplay between long- and short-range interactions drives neuritogenesis on stiff surfaces. *J Biomed Mater Res A* **99**, 598-606.

Laurent, V. M., Fodil, R., Canadas, P., Fereol, S., Louis, B., Planus, E. and Isabey, D. (2003). Partitioning of cortical and deep cytoskeleton responses from transient magnetic bead twisting. *Ann Biomed Eng* **31**, 1263-78.

Laurent, V. M., Henon, S., Planus, E., Fodil, R., Balland, M., Isabey, D. and Gallet, F. (2002). Assessment of mechanical properties of adherent living cells by bead micromanipulation: comparison of magnetic twisting cytometry vs optical tweezers. *J Biomech Eng* **124**, 408-21.

Leach, C. L., Greenspan, J. S., Rubenstein, S. D., Shaffer, T. H., Wolfson, M. R., Jackson, J. C., DeLemos, R. and Fuhrman, B. P. (1996). Partial liquid ventilation with perflubron in premature infants with severe respiratory distress syndrome. The LiquiVent Study Group. *N Engl J Med* **335**, 761-7.

Lee, C.-K., Wang, Y.-M., Huang, L.-S. and Lin, S. (2007). Atomic force microscopy: Determination of unbinding force, off rate and energy barrier for protein–ligand interaction. *Micron* **38**, 446-461.

Lehninger, A. (1973). Biochimie. Paris: Flammarion.

Lieber, M., Todaro, G., Smith, B., Szakal, A. and Nelson-Rees, W. (1976). A continuous tumor-cell line from a human lung carcinoma with properties of type II alveolar epithelial cells. *International Journal of Cancer* **17**, 62-70.

Lo, C. M., Wang, H. B., Dembo, M. and Wang, Y. L. (2000). Cell movement is guided by the rigidity of the substrate. *Biophys J* **79**, 144-52.

Long, W., Thompson, T., Sundell, H., Schumacher, R., Volberg, F. and Guthrie, R. (1991). Effects of two rescue doses of a synthetic surfactant on mortality rate and survival without bronchopulmonary dysplasia in 700- to 1350-gram infants with respiratory distress syndrome. The American Exosurf Neonatal Study Group I. *J Pediatr* **118**, 595-605.

Maniotis, A. J., Chen, C. S. and Ingber, D. E. (1997). Demonstration of mechanical connections between integrins, cytoskeletal filaments, and nucleoplasm that stabilize nuclear structure. *Proc Natl Acad Sci U S A* **94**, 849-54.

Martins, M. d. F. and Abairos, V. (2002). Glycocalyx of lung epithelial cells. In *International Review of Cytology*, vol. Volume 216, pp. 131-173: Academic Press.

Mege, J. L., Capo, C., Benoliel, A. M. and Bongrand, P. (1987). Use of cell contour analysis to evaluate the affinity between macrophages and glutaraldehyde-treated erythrocytes. *Biophysical Journal* **52**, 177-186.

Modell, J. H., Gollan, F., Giammona, S. T. and Parker, D. (1970). Effect of fluorocarbon liquid on surface tension properties of pulmonary surfactant. *Chest* **57**, 263-5.

Nakstad, B., Wolfson, M. R., Shaffer, T. H., Kahler, H., Lindemann, R., Fugelseth, D. and Lyberg, T. (2001). Perfluorochemical liquids modulate cell-mediated inflammatory responses. *Crit Care Med* **29**, 1731-7.

Neumann, A. W., Absolom, D. R., van Oss, C. J. and Zingg, W. (1979). Surface thermodynamics of leukocyte and platelet adhesion to polymer surfaces. *Cell Biophys* **1**, 79-92.

Nishikido, N., Mahler, W. and Mukerjee, P. (1989). Interfacial tensions of perfluorohexane and perfluorodecalin against water. *Langmuir* **5**, 227-229.

Noy, A. and Friddle, R. W. (2013). Practical single molecule force spectroscopy: how to determine fundamental thermodynamic parameters of intermolecular bonds with an atomic force microscope. *Methods* **60**, 142-50.

Obraztsov, V. V., Neslund, G., Kornbrust, E., Flaim, S. and Woods, C. M. (2000). In vitro cellular effects of perfluorochemicals correlate with their lipid solubility. *Am J Physiol* **278**.

Ohayon, J., Tracqui, P., Fodil, R., Fereol, S., Laurent, V. M., Planus, E. and Isabey, D. (2004). Analysis of nonlinear responses of adherent epithelial cells probed by magnetic bead twisting: A finite element model based on a homogenization approach. *J Biomech Eng* **126**, 685-98.

Owens, D. K. and Wendt, R. C. (1969). Estimation of the surface free energy of polymers. *Journal of Applied Polymer Science* **13**, 1741-1747.

Pahakis, M. Y., Kosky, J. R., Dull, R. O. and Tarbell, J. M. (2007). The role of endothelial glycocalyx components in mechanotransduction of fluid shear stress. *Biochemical and Biophysical Research Communications* **355**, 228-233.

Planus, E., Galiacy, S., Fereol, S., Fodil, R., Laurent, V. M., d'Ortho, M. P. and Isabey, D. (2005). Apical rigidity of an epithelial cell monolayer evaluated by magnetic twisting cytometry: ICAM-1 versus integrin linkages to F-actin structure. *Clin Hemorheol Microcirc* **33**, 277-91.

Planus, E., Galiacy, S., Matthay, M., Laurent, V., Gavrilovic, J., Murphy, G., Clerici, C., Isabey, D., Lafuma, C. and d'Ortho, M. P. (1999). Role of collagenase in mediating in vitro alveolar epithelial wound repair. *J Cell Sci* **112 (Pt 2)**, 243-52.

Potard, U. S., Butler, J. P. and Wang, N. (1997). Cytoskeletal mechanics in confluent epithelial cells probed through integrins and E-cadherins. *Am J Physiol* **272**, C1654-63.

Pratt, P. C., Vollmer, R. T., Shelburne, J. D. and Crapo, J. D. (1979). Pulmonary morphology in a multihospital collaborative extracorporeal membrane oxygenation project. I. Light microscopy. *Am J Pathol* **95**, 191-214.

Pries, A. R., Secomb, T. W. and Gaehtgens, P. (2000). The endothelial surface layer. *Pflügers Archiv* **440**, 653-666.

Rai, S., Nejadhamzeeigilani, Z., Gutowski, N. J. and Whatmore, J. L. (2015). Loss of the endothelial glycocalyx is associated with increased E-selectin mediated adhesion of lung tumour cells to the brain microvascular endothelium. *J Exp Clin Cancer Res* **34**, 105.

Riess, J. G. (1994). Highly fluorinated systems for oxygen transport, diagnosis and drug delivery. *Colloids and Surfaces A: Physicochemical and Engineering Aspects* **84**, 33-48.

Riess, J. G. and Krafft, M. P. (1997). Advanced fluorocarbon-based systems for oxygen and drug delivery, and diagnosis. *Artif Cells Blood Substit Immobil Biotechnol* **25**, 43-52.

Rüdiger, M., Wissel, H., Ochs, M., Burkhardt, W., Proquitté, H., Wauer, R. R., Stevens, P. and Rüstow, B. (2003). Perfluorocarbons are taken up by isolated type II pneumocytes and influence its lipid synthesis and secretion. *Crit Care Med* **31**.

Sage, M., Nadeau, M., Kohlhauer, M., Praud, J. P., Tissier, R., Robert, R., Walti, H. and Micheau, P. (2016). Effect of ultra-fast mild hypothermia using total liquid ventilation on hemodynamics and respiratory mechanics. *Cryobiology* **73**, 99-101.

Schakenraad, J. M., Busscher, H. J., Wildevuur, C. R. and Arends, J. (1988). Thermodynamic aspects of cell spreading on solid substrata. *Cell Biophys* **13**, 75-91.

Schoenwaelder, S. M. and Burridge, K. (1999). Bidirectional signaling between the cytoskeleton and integrins. *Curr Opin Cell Biol* **11**, 274-86.

Schwartz, M. A. and Assoian, R. K. (2001). Integrins and cell proliferation: regulation of cyclin-dependent kinases via cytoplasmic signaling pathways. *J Cell Sci* **114**, 2553-60.

Sen, C. K. (2009). Wound Healing Essentials: Let There Be Oxygen. *Wound repair and regeneration : official publication of the Wound Healing Society [and] the European Tissue Repair Society* **17**, 1-18.

Sill, H. W., Chang, Y. S., Artman, J. R., Frangos, J. A., Hollis, T. M. and Tarbell, J. M. (1995). Shear stress increases hydraulic conductivity of cultured endothelial monolayers. *Am J Physiol* **268**, H535-43.

Simmons, R. M., Finer, J. T., Chu, S. and Spudich, J. A. (1996). Quantitative measurements of force and displacement using an optical trap. *Biophys J* **70**, 1813-22.

Squire, J. M., Chew, M., Nneji, G., Neal, C., Barry, J. and Michel, C. (2001). Quasi-periodic substructure in the microvessel endothelial glycocalyx: a possible explanation for molecular filtering? *J Struct Biol* **136**, 239-55.

Stamenovic, D., Mijailovich, S. M., Tolic-Norrelykke, I. M., Chen, J. and Wang, N. (2002). Cell prestress. II. Contribution of microtubules. *Am J Physiol Cell Physiol* **282**, C617-24.

Steinberg, M. S. (1962). Mechanism of tissue reconstruction by dissociated cells. II. Time-course of events. *Science* **137**, 762-3.

Stroetz, R. W., Vlahakis, N. E., Walters, B. J., Schroeder, M. A. and Hubmayr, R. D. (2001). Validation of a new live cell strain system: characterization of plasma membrane stress failure. *Journal of Applied Physiology* **90**, 2361-2370.

Swain, R. J., Kemp, S. J., Goldstraw, P., Tetley, T. D. and Stevens, M. M. (2010). Assessment of cell line models of primary human cells by Raman spectral phenotyping. *Biophys J* **98**, 1703-11.

Tallawi, M., Rai, R., Boccaccini, A. R. and Aifantis, K. E. (2015). Effect of substrate mechanics on cardiomyocyte maturation and growth. *Tissue Eng Part B Rev* **21**, 157-65.

Tan, J. L., Tien, J., Pirone, D. M., Gray, D. S., Bhadriraju, K. and Chen, C. S. (2003). Cells lying on a bed of microneedles: an approach to isolate mechanical force. *Proc Natl Acad Sci U S A* **100**, 1484-9.

Tank, D. W., Wu, E. S. and Webb, W. W. (1982). Enhanced molecular diffusibility in muscle membrane blebs: release of lateral constraints. *J Cell Biol* **92**, 207-12.

Tashiro, K., Matsumoto, Y., Nishizuka, K., Shibata, K., Yamamoto, K., Yamashita, M. and Kobayashi, T. (1998). Mechanism of acute lung injury caused by inhalation of fabric protector and the effect of surfactant replacement. *Intensive Care Med* **24**, 55-60.

Tha, S. P., Shuster, J. and Goldsmith, H. L. (1986). Interaction forces between red cells agglutinated by antibody. II. Measurement of hydrodynamic force of breakup. *Biophysical Journal* **50**, 1117-1126.

Thi, M. M., Tarbell, J. M., Weinbaum, S. and Spray, D. C. (2004). The role of the glycocalyx in reorganization of the actin cytoskeleton under fluid shear stress: A "bumper-car" model. *Proceedings of the National Academy of Sciences of the United States of America* **101**, 16483-16488.

Tooley, R., Hirschl, R. B., Parent, A. and Bartlett, R. H. (1996). Total liquid ventilation with perfluorocarbons increases pulmonary end-expiratory volume and compliance in the setting of lung atelectasis. *Crit Care Med* **24**, 268-73.

Topulos, G. P., Brown, R. E. and Butler, J. P. (2002). Increased surface tension decreases pulmonary capillary volume and compliance. *J Appl Physiol (1985)* **93**, 1023-9.

Trinkaus, J. P. and Lentz, J. P. (1964). Direct Observation of Type-Specific Segregation in Mixed Cell Aggregates. *Dev Biol* **9**, 115-36.

van Oss, C. J. (1991). Interaction forces between biological and other polar entities in water: How many different primary forces are there? *J. Disp. Sci. Technol.* **12**, 201-220.

Varani, J., Hirschl, R. B., Dame, M. and Johnson, K. (1996). Perfluorocarbon protects lung epithelial cells from neutrophil-mediated injury in an in vitro model of liquid ventilation therapy. *Shock* **6**, 339-44.

Vlahakis, N. E. and Hubmayr, R. D. (2000). Invited review: plasma membrane stress failure in alveolar epithelial cells. *J Appl Physiol (1985)* **89**, 2490-6;discussion 2497.

Vogel, V. and Sheetz, M. (2006). Local force and geometry sensing regulate cell functions. *Nat Rev Mol Cell Biol* **7**, 265-75.

Wang, B., Caluch, A., Fodil, R., Fereol, S., Zadigue, P., Pelle, G., Louis, B. and Isabey, D. (2012). Force control of endothelium permeability in mechanically stressed pulmonary micro-vascular endothelial cells. *Biomed Mater Eng* **22**, 163-70.

Wang, N., Butler, J. and Ingber, D. (1993). Mechanotransduction across the cell surface and through the cytoskeleton. *Science* **260**, 1124-1127.

Wang, N. and Ingber, D. E. (1994). Control of cytoskeletal mechanics by extracellular matrix, cell shape, and mechanical tension. *Biophys J* **66**, 2181-9.

Wang, N. and Ingber, D. E. (1995). Probing transmembrane mechanical coupling and cytomechanics using magnetic twisting cytometry. *Biochem Cell Biol* **73**, 327-35.

Wang, N., Tolic-Norrelykke, I. M., Chen, J., Mijailovich, S. M., Butler, J. P., Fredberg, J. J. and Stamenovic, D. (2002). Cell prestress. I. Stiffness and prestress are closely associated in adherent contractile cells. *Am J Physiol Cell Physiol* **282**, C606-16.

Ware, L. B. and Matthay, M. A. (2000). The acute respiratory distress syndrome. *N Engl J Med* **342**, 1334-49.

Weibel, E. R. (2011). Functional Morphology of Lung Parenchyma. In *Comprehensive Physiology*: John Wiley & Sons, Inc.

Wemhöner, A., Hackspiel, I., Hobi, N., Ravasio, A., Haller, T. and Rüdiger, M. (2010). Effects of Perfluorocarbons on surfactant exocytosis and membrane properties in isolated alveolar type II cells. *Respiratory Research* **11**, 1-12.

Wendling, S., Planus, E., Laurent, V. M., Barbe, L., Mary, A., Oddou, C. and Isabey, D. (2000). Role of cellular tone and microenvironmental conditions on cytoskeleton stiffness assessed by tensegrity model. *Eur. Phys. J. AP* **9**, 51-62.

Wenzel, V., Idris, A. H., Banner, M. J., Kubilis, P. S., Band, R., Williams, J. L., Jr. and Lindner, K. H. (1998). Respiratory system compliance decreases after cardiopulmonary resuscitation and stomach inflation: impact of large and small tidal volumes on calculated peak airway pressure. *Resuscitation* **38**, 113-8.

Wesseler, E. P., Iltis, R. and Clark, L. C. (1977). The solubility of oxygen in highly fluorinated liquids. *Journal of Fluorine Chemistry* **9**, 137-146.

West, J. B. (2000). Invited review: pulmonary capillary stress failure. *J Appl Physiol (1985)* **89**, 2483-9;discussion 2497.

West, J. B., Tsukimoto, K., Mathieu-Costello, O. and Prediletto, R. (1991). Stress failure in pulmonary capillaries. *J Appl Physiol (1985)* **70**, 1731-42.

Wickman, G. R., Julian, L., Mardilovich, K., Schumacher, S., Munro, J., Rath, N., Zander, S. A., Mleczak, A., Sumpton, D., Morrice, N. et al. (2013). Blebs produced by actin-myosin contraction during apoptosis release damage-associated molecular pattern proteins before secondary necrosis occurs. *Cell Death Differ* **20**, 1293-1305.

Williams, P. M. (2003). Analytical descriptions of dynamic force spectroscopy: behaviour of multiple connections. *Analytica Chimica Acta* **479**, 107-115.

Wolfson, M. R., Greenspan, J. S. and Shaffer, T. H. (1996). Pulmonary administration of vasoactive substances by perfluorochemical ventilation. *Pediatrics* **97**, 449-55.

Wolfson, M. R. and Shaffer, T. H. (2004). Liquid ventilation: an adjunct for respiratory management. *Paediatr Anaesth* **14**, 15-23.

Wolfson, M. R. and Shaffer, T. H. (2005). Pulmonary applications of perfluorochemical liquids: ventilation and beyond. *Paediatr Respir Rev* **6**, 117-27.

Wong, J. Y., Leach, J. B. and Brown, X. Q. (2004). Balance of chemistry, topography, and mechanics at the cell–biomaterial interface: Issues and challenges for assessing the role of substrate mechanics on cell response. *Surface Science* **570**, 119-133.

Woods, C. M., Neslund, G., Kornbrust, E. and Flaim, S. F. (2000a). Perflubron attenuates neutrophil adhesion to activated endothelial cells in vitro. *American Journal of Physiology - Lung Cellular and Molecular Physiology* **278**, L1008-L1017.

Woods, C. M., Neslund, G., Kornbrust, E. and Flaim, S. F. (2000b). Perflubron attenuates neutrophil adhesion to activated endothelial cells in vitro. *Am J Physiol* **278**.

Wu, S. (1973). Polar and Nonpolar Interactions in Adhesion. *The Journal of Adhesion* **5**, 39-55.

Yakhshi-Tafti, E., Kumar, R. and Cho, H. J. (2011). Measurement of Surface Interfacial Tension as a Function of Temperature Using Pendant Drop Images. *International Journal of Optomechatronics* **5**, 393-403.

Yao, Y., Rabodzey, A. and Dewey, C. F. (2007). Glycocalyx modulates the motility and proliferative response of vascular endothelium to fluid shear stress. *American Journal of Physiology - Heart and Circulatory Physiology* **293**, H1023-H1030.

Yeung, T., Georges, P. C., Flanagan, L. A., Marg, B., Ortiz, M., Funaki, M., Zahir, N., Ming, W., Weaver, V. and Janmey, P. A. (2005). Effects of substrate stiffness on cell morphology, cytoskeletal structure, and adhesion. *Cell Motil Cytoskeleton* **60**, 24-34.

Young, K. G. and Copeland, J. W. (2010). Formins in cell signaling. *Biochim Biophys Acta* **1803**, 183-90.

Young, T. (1805). An Essay on the Cohesion of Fluids. *Philosophical Transactions of the Royal Society of London* **95**, 65-87.

Zaidel-Bar, R., Itzkovitz, S., Ma'ayan, A., Iyengar, R. and Geiger, B. (2007). Functional atlas of the integrin adhesome. *Nat Cell Biol* **9**, 858-67.

Zhang, X. and Moy, V. T. (2003). Cooperative adhesion of ligand-receptor bonds. *Biophys Chem* **104**, 271-8.

Zhu, C., Bao, G. and Wang, N. (2000). Cell mechanics: mechanical response, cell adhesion, and molecular deformation. *Annu Rev Biomed Eng* **2**, 189-226.

Zilberberg, M. D. and Epstein, S. K. (1998). Acute lung injury in the medical ICU: comorbid conditions, age, etiology, and hospital outcome. *Am J Respir Crit Care Med* **157**, 1159-64.

Zisman, W. A. (1964). Relation of the Equilibrium Contact Angle to Liquid and Solid Constitution. In *Contact Angle, Wettability, and Adhesion*, vol. 43, pp. 1-51: AMERICAN CHEMICAL SOCIETY.

Zurkhov, S. N. (1965). Kinetic concept of the strength of solids. *Int. J. Fract. Mech.*, 311-323.

X. ABSTRACT

During Total Liquid Ventilation (TLV), lung cells are exposed to perfluorocarbon (PFC) whose physical properties highly differ from aqueous medium (DMEM) standardly used for cell culture and farther air properties. In this thesis, we study the effects of PFC exposure on the response of pulmonary epithelial cell by performing a thorough assessment of their structural, mechanical and functional properties. The response of A549 cells (alveolar), HBE (bronchial), and AM (alveolar macrophages) exposed to PFC is studied by comparison to DMEM. Changes in F-actin structure, focal adhesion size and density and glycocalyx expression are evaluated by fluorescence. Changes in cell mechanics and adhesion parameters are measured by a multiscale Magnetic Twisting Cytometry (MTC) method. Cell mechanics is analyzed by two microrheological models reflecting two possible cytoskeleton features. Cell-matrix adhesion is analyzed by a stochastic multibond de-adhesion model describing the non-reversible component of the cell response by MTC. The key roles of F-actin structure and glycocalyx layer are established by respectively depolymerising F-actin and degrading glycocalyx. Results show that PFC exposure induces F-actin remodeling, cytoskeleton softening and adhesion weakening. They demonstrate that PFC triggers an epithelial cell response which is characterized by decay in intracellular tension, adhesion weakening and glycocalyx redistribution. The origin of this cellular adaptations is physical and most likely related to the increase in interfacial energy, associated to the low surface tension of the non polar perflurorocarbon, The low surface tension of PFC is also responsible for an increase in lung compliance during TLV and has deep impacts during ventilation parallel to the modification of cell response.

Au cours de la ventilation liquide totale (VLT), les cellules pulmonaires sont exposées à des perfluorocarbones (PFC) dont les propriétés physiques diffèrent fortement du milieu standard de culture cellulaire (DMEM) et encore plus des propriétés de l'air. Dans cette thèse nous étudions les effets d'une exposition au PFC sur la réponse des cellules épithéliales pulmonaires, en effectuant une étude approfondie des propriétés structurales, mécaniques et fonctionnelles. La réponse des cellules A549 (alvéolaire), HBE (bronchique) et AM (Macrophage alvéolaire) exposées au PFC est étudiée par comparaison au DMEM. Les variations de la structure de F-actine, de la densité d'adhésion focale et de la distribution du glycocalyx sont évaluées par fluorescence. Les changements de propriétés mécaniques et de paramètres d'adhésion sont mesurés par la Magnétocymétrie (MTC) étendue à l'analyse multiéchelle. La mécanique cellulaire est caractérisée par deux modèles microrhéologiques reflétant deux types de comportement possibles du cytosquelette (CSK). L'adhésion à la matrice cellulaire est analysée par un modèle stochastique de dé-adhésion, décrivant la composante non-réversible de la réponse cellulaire. Les rôles fondamentaux de la structure de F-actine et de la couche de glycocalyx sont respectivement évalués par dépolymérisation de F-actine et en dégradant le glycocalyx. Les résultats montrent que l'exposition au PFC induit un remodelage de la structure de F-actine, un affaiblissement du CSK et une diminution de l'adhésion. Ces résultats démontrent que le PFC déclenche une réponse particulière des cellules épithéliales caractérisée par une diminution de la tension intracellulaire, l'affaiblissement de l'adhésion et la redistribution du glycocalyx. L'origine de cette adaptation cellulaire est physique et très probablement reliée à l'augmentation de l'énergie interfaciale associée à la basse tension de surface d'un PFC chimiquement apolaire. La faible tension de surface du PFC est également responsable d'une augmentation de la compliance pulmonaire pendant VLT et a des impacts profonds dans les paramètres respiratoires, parallèlement à la modification de la réponse cellulaire.